5 FRAGILITY METHODOLOGY

5.1 Role of Fragility in Probabilistic Safety Assessment

A probabilistic safety assessment (PSA) is a structured framework for evaluating uncertainty, performance, and reliability of an engineered facility. It is distinguished from traditional deterministic approaches to safety assurance by its focus on why and how the facility might fail and by its explicit treatment of uncertainties, both in the phenomena and in the analytical tools used to model them. A PSA provides basis for decision-making in the face of uncertainty that can be audited independently by a regulatory authority and updated periodically as circumstances warrant. The move toward quantitative risk assessment began in the nuclear industry in the mid-1970's, and has accelerated since then as the benefits of quantitative risk analysis have become apparent in many fields (Ellingwood, 1994).

One begins the PSA process by identifying limit states (LS), or conditions in which the structural system ceases to perform its intended functions in some way. For structural components and systems in NPPs, such limit states may be either strength or deformation-related (as discussed subsequently), as large (inelastic) deformations affect the integrity or operability of mechanical or electrical systems that are attached to or otherwise interface with the structure. Limit state identification requires a thorough understanding of the behavior of the safety-related systems within the plant and the role of structural components and systems in ensuring acceptable behavior of such systems.

With the limit states identified, the limit state probability can be expressed as,

$$P[LS] = \sum_{x} P[LS|D = x]\, P[D = x] \tag{5.1}$$

in which D is a random variable (or random vector) describing the intensity of demand on the system, and $P[LS|D = x]$ is the conditional limit state probability, given that $D = x$. The probability $P[D = x]$ is sometimes denoted the hazard, and variable x is the "control" or "interface" variable. The conditional probability, $P[LS|D = x] = F_R(x)$, is the fragility.

It is clear that a fragility analysis is an essential ingredient of the fully coupled risk analysis embodied in Eq. 5.1. It also can be used to determine probabilistic safety margins against specific identified events for decision and regulatory purposes. Identification of probabilistic safety margins is central to modern facility risk management. Although providing a less informative measure of safety than that obtained from a fully coupled risk analysis, risk-informed decision-making based on the results of a structural fragility assessment has several advantages:

(1) The probabilistic system analysis is effectively uncoupled from the hazard analysis. Thus, while knowledge of the hazard is useful in identifying appropriate review-level events (e.g., a 2,500-yr mean recurrence interval earthquake), such knowledge is not essential. Absent credible data on review-level events, one might simply inquire as to the fragility were the design-basis event to be exceeded by some arbitrary margin, say 50 percent.

(2) The need to interpret and defend very small limit state probabilities (on the order of 10^{-5}/yr or less) is avoided. There are limited data to support probabilities of this level, and such estimates are highly dependent on the probabilistic models selected. At the current state-of-the-art, (conditional) fragilities are more robust than unconditional limit state probabilities.

(3) A properly conducted fragility analysis is less complex, less costly, and involves fewer disciplines than a fully coupled risk analysis. Accordingly, there is less likelihood of

miscommunication among members of the risk analysis team and the results are more easily understood by a nonspecialist decision-maker or regulator.

Fragility modeling of reinforced concrete structural components and systems found in NPPs is the focus of the safety analysis methods presented in this report.

5.2 Fragility Modeling Concepts

Fragility analysis is a technique for assessing and displaying, in probabilistic terms, the capability of an engineered component or system to withstand a specified event (sometimes referred to as a review-level event), one that often is well in excess of the design-basis event. Fragility modeling requires a focus on the behavior of the system as a whole and, specifically, on things that can go wrong with the system. The fragility modeling process leads to a median-centered estimate of system performance, coupled with an estimate of the uncertainty in performance. This focus is different from typical deterministic analysis, where conservative estimates of structural parameters are used, and the conservatism propagates through the safety analysis in an unpredictable manner. The fragility concept has found widespread usage in the nuclear industry, where it has been used in seismic probabilistic safety and/or margin assessments of safety-related plant systems (Kennedy and Ravindra, 1984). In a seismic margins study, the control variable usually is the effective peak ground acceleration or spectral acceleration at the fundamental period of the structure.

The fragility of a structure commonly is modeled by a lognormal cumulative distribution function (CDF). If the structural capacity can be described as the product of numerous statistically independent random variables, the central limit theorem provides some justification for this choice of CDF. The lognormal CDF is described by,

$$F_R(x) = \Phi [\ln(x/m_R)/ \beta_R] \tag{5.2}$$

in which $F_R(x)$ is the probability of failure for an applied load equal to x, Φ [ ] = standard normal probability integral, m_R = median capacity (expressed in units that are dimensionally consistent with the demand parameter, x, in Eq. 5.1), and β_R = logarithmic standard deviation, approximately equal to the coefficient of variation (COV), V_R, when $V_R < 0.3$.

Equation 5.2 depicts the conditional limit state probability of the system when the state of knowledge is essentially perfect (within the bounds of normal engineering mechanics). In this case, parameters m_R and β_R measure inherent randomness (or aleatory uncertainty). Such uncertainties are essentially irreducible under current engineering analysis procedures. As an example, the yield strength of ASTM A615/60 reinforcing bars tested in accordance with standard ASTM procedures is a random variable that can be modeled by a lognormal distribution, with a mean of 490 MPa (71 ksi) and COV of 0.10. These statistical estimates are relatively stable from dataset to dataset, assuming that the sample size is not too small. Sampling from a different lot of A615/60 bars (or different bar sizes) will yield essentially the same statistics. This is characteristic of aleatory uncertainty; additional data or other information does not change the probabilistic models in any significant way. Similarly, compression or tension strength of concrete and dimensions of structural components fabricated and inspected according to ACI standards are inherently random.

Thus, if the state of knowledge is essentially perfect, the 5-percent exclusion limit for capacity, defined as,

$$R_{0.05} = m_R \exp(-1.645\, \beta_R) \tag{5.3}$$

might be selected as a basis for checking safety. If the review-level demand selected were less than $R_{0.05}$, then the probability of acceptable performance of that structural component at that level would be at least 95%.

However, additional sources of uncertainty in capacity arise from assumptions made in the analysis of the system and from limitations in the supporting databases. In contrast to aleatory uncertainties, these knowledge-based (or epistemic) uncertainties depend on the quality of the analysis and supporting databases, and generally can be reduced, at the expense of more comprehensive (and costly) analysis. Sources of epistemic uncertainty in reinforced concrete structures would include two-dimensional models of three-dimensional structures, support conditions that are neither fully rigid nor simple, neglect of shear deformations in structural analysis, treatment of cracking by "smeared" models, and limitations in the supporting databases.

The presence of epistemic uncertainty means that the fragility actually is described by a family of curves, reflecting incomplete knowledge regarding the parameters used to model the structural fragility: in the median, COV, and the CDF itself. To first order, these uncertainties can be assumed to be vested in the estimate of the median capacity, m_R, in Eqs. 5.2 and 5.3. Under this assumption, m_R is replaced by a random variable, M_R, which is assumed to be modeled by a lognormal distribution with median m_R and logarithmic standard deviation β_U. Then, the family of lognormal CDFs, defined by parameters (m_R, β_R, β_U), displays the overall uncertainty in capacity. The 5-percent exclusion limit in Eq. 5.3 thus becomes a random variable as a result of the uncertainty in M_R, modeled by β_U. The lower 5-percent confidence interval on $R_{0.05}$ is defined by,

$$R_k = m_R \exp[-1.645(\beta_R + \beta_U)] \tag{5.4}$$

One might say (with a Bayesian interpretation) that the probability of surviving an event with intensity R_k is 95% with 95% confidence. In some previous seismic margin studies, R_k has been called the HCLPF, or "high-confidence, low probability of failure" capacity.

In many applications, it is desirable to have one overall estimate of fragility for review purposes that reflects both aleatory and epistemic uncertainty. Such an estimate is provided by the mean fragility, defined as (Ellingwood, 1994)

$$E[F_R(x)] = \Phi [\ln(x/m_R)/\beta_C] \tag{5.5}$$

in which

$$\beta_C = (\beta_R^2 + \beta_U^2)^{1/2} \tag{5.6}$$

At the usual levels of aleatory and epistemic uncertainty found in the assessment of reinforced concrete structures, R_k in Eq. 5.4 corresponds to approximately the 1 to 2-percentile of $E[F_R(x)]$.

5.3 Limit States for Structural Performance Evaluation and Their Analysis

Two common reinforced concrete structures were selected for the structural fragility assessments in this study: a propped cantilever beam subjected to uniform load and a low-rise shear wall subjected to in-plane forces. The beam was under-reinforced, and is typical of relatively common indeterminate structures (beams and one-way slabs) subjected to flexure. The solutions for the undegraded case could be compared to previous results (MacGregor et al., 1983), the effects of degradation due to reinforcement

corrosion and concrete spalling on strength, stiffness and ductility could be visualized easily, and the results could be used to validate the finite element analysis used in later phases of the study. The low-rise shear wall (height/length of approximately 1.0) is typical of those found in safety-related (noncontainment) buildings in nuclear power plants. Such shear walls provide the primary earthquake-resisting system for such buildings, and often appear as critical components in plant logic models developed in seismic PRAs of NPPs (e.g., Zion, 1981; Ellingwood and Song, 1996).

Limit state(s) of structural performance must be identified around which the fragility model(s) can be constructed. Such limit states depend on the functional requirements and performance goals of the system in which they must function. Performance goals usually are qualitative in nature, e.g.: the system must remain functional under operating conditions; the system must be controllable/recoverable under extreme environmental conditions; etc. Such goals must be transformed into structural limit states that can be verified by analysis or test. Although the focus in conventional reinforced concrete design according to ACI Standard 318 (and ACI 349) has been on ultimate strength, the structural strength limit state may be of lesser importance than a deformation-related limit state when the structure is an integrated component of a complex system in which structural, mechanical and electrical systems all must interface properly. Key safety-related mechanical or electrical components often are mounted on or interface with the structure. Properly designed reinforced concrete structures, particularly those that are highly redundant, may behave in a ductile manner under extreme loads, and damage to appurtenant systems may occur at structural deformations well below those at incipient structural collapse. This is particularly true of structures that resist lateral forces, such as those due to earthquake ground motion.

Fragility analysis of a concrete structure in a NPP requires a thorough understanding of the mechanics of structural response to challenges over a wide range, including those at and beyond the design basis. At such levels, the behavior of the structure usually is highly nonlinear in nature. The strength limit state of a reinforced concrete structure, while certainly important, may not be sufficient to evaluate the integrity and safety of a plant system in which that component plays a role in safety. Moreover, the equations for strength of shear walls found in the ACI Standards do not apply to the low-rise walls that are typical of nuclear plant construction. Indeed, because of the complexity of the structural components and systems, closed-form models of structural behavior may not be sufficient to describe their response to extreme operating or environmental events, and one must resort to finite element analysis.

In this study, the commercially available finite element analysis computer program ANSYS has been chosen to perform the structural analyses because of its ability to model the significant nonlinear action expected to occur in the concrete structures analyzed. The program was validated using structural models of the indeterminate beam, which could be checked relatively easily by other methods, and subsequently was used extensively to support fragility modeling of the low-rise concrete shear walls. The general procedure followed was to construct a load-deflection (or moment-curvature) relation for the structure of interest. The limit state of the propped cantilever beam was associated with the point at which the maximum uniform load was reached, just prior to the formation of the final plastic hinge near midspan. The limit state of the low-rise shear wall was defined as occurring at a deformation equal to 4 times the deformation at first yielding, making the assumption that appurtenant safety-related mechanical or electrical equipment would malfunction at approximately these deformation levels. Similar limiting deformation levels have been assumed in previous seismic PRAs and margin studies of nuclear plants (e.g., Wesley and Hashimoto, 1981). Modern approaches to earthquake-resistant design of buildings and other structures also are based on deformation capacity rather than on strength (e.g., FEMA 273).

5.4 Databases to Support Fragility Assessment

A fragility analysis must be supported by a database to describe the statistical nature of all parameters known to affect the capacity of the structure. Probabilistic models and statistics are required for all

parameters that play a significant role in performance and safety of reinforced concrete structural components and systems.

Some fragility parameters can be identified through a review of the literature. Other parameters may have to be identified and estimated through expert opinion. Within any group of experts, there is experiential knowledge regarding engineering behavior and parameters that can be elicited through careful questioning. Proper construction of a consensus estimation survey (sometimes called a Delphi) and careful analysis of the results can lead to statistical models that subsequently can be updated using Bayesian techniques, if and when further information becomes available. It is emphasized that fragility modeling of existing systems requires best (mean or median) estimates of strength; otherwise, the conservatisms attached to traditional design parameters are propagated throughout the analysis in an unpredictable way. Furthermore, all sources of uncertainty must be included in the fragility analysis to predict the likely variability in performance of the structure in service.

A summary of statistical data to describe the strength of reinforced concrete flexural members (beams and slabs) and low-rise concrete shear wall structures subjected to static forces is provided in Table 5.1. This summary is based on a comprehensive review of published literature (Ellingwood and Hwang, 1983; MacGregor et al., 1983) and additional data from specific NPPs.

The steel and concrete strengths presented in Table 5.1 are "static" strengths in-situ, i.e., application of load to determine strength occurs over a period of approximately one hour. Mill tests of steel and concrete cylinder tests are conducted at a higher strain rate than is typical for static structural loading. The mill test data for steel are adjusted to static conditions by the approximate relation, $f_{y,stat} = f_{y,mill} - 27.6$ MPa (4 ksi). Although some studies have indicated that reinforcement strength decreases with increasing bar diameter, the data reviewed in this study indicate that this effect is negligible.

Standard-cured concrete cylinder tests are adjusted for static rate of load effects by multiplying by 0.89. The in-situ strength of concrete requires additional corrections to account for differences between standard-cure cylinder strengths and field strength that arise from field placement, consolidation, and curing conditions (MacGregor, Mirza and Ellingwood, 1983; Ellingwood, 1983). The concrete strength statistics and samples in Column 2 of Table 5.1 reflect 28-day in-situ strength under "static" load conditions. There is a significant gain in concrete strength beyond the 28-day strength used as the basis for design. For example, results obtained from NPP-related facilities indicate that after 25 years the concrete strength can increase by over 50% relative to the 28-day strength (Naus et al., 1996). Such increases may have only a nominal effect on flexural strength of the under-reinforced beam, but may have a substantial impact on shear wall behavior, where the concrete strength is more important.

The ANSYS finite element program utilizes the compressive stress-strain curve for the concrete. The limiting compressive strain is a random variable, as indicated in Table 5.1; it has little effect on flexural capacity (i.e., one obtains about the same M_u using 0.003 vs 0.004), but it may affect the apparent ductility of the beam. The tensile strength of concrete is utilized for the analysis of cracking or shear strength in the beam. The tensile strength of concrete, f_t, is based on split-cylinder strength. Both f_t and initial tangent modulus, E_c, are correlated with compressive strength; the nominal correlation coefficient is assumed to be 0.7 in both cases. The dependence of both f_t and E_c on $(f_c)^{1/2}$ arises from regression analysis. There is also a standard error of regression which must be considered; otherwise, one arrives at the conclusion that the COV of f_t (or E_c) is 50% that of f_c, which is incorrect. Unfortunately, this error went unrecognized in a number of early seismic fragility studies.

The effective depth, d, is a random variable due to variability in bar placement during construction. The COV in d is 0.5/d; for the beam analyzed, this is 0.024, a very small number, which will have little impact of fragility. On the other hand, the uncertainty in d is more important in the analysis of slabs. Overall

dimensional variabilities have a negligible contribution to fragility and can be ignored. The reinforcement cover, c, is required to determine strength changes that may arise from spalling of the concrete as a result of in-service deterioration, and is a random variable. Studies have shown that the reinforcement cover tends to be slightly greater than the nominal 37 mm (1-1/2 in.) specified for protected concrete in all structural components. The bar placement error and the variability in placement are somewhat greater in slabs than in columns or beams. Placement error also tends to be larger for top bars than for bottom bars due to the construction process. However, there is enough noise in the data reported that it is not necessary to distinguish between these cases. Accordingly, the bar cover, c, is assumed to have a normal distribution, with mean (distance from concrete surface to center of the outer layer of reinforcement) equal to the nominal cover plus 6 mm (1/4 in.) and a standard deviation of 16 mm (5/8 in.) in all cases. This assumption is conservative but not unduly so.

The factors B_f and B_{sh} in Table 5.1 account for uncertainty in the analysis itself, and are epistemic in nature. This uncertainty arises from idealizations of behavior in any analytical model of a structure. The easiest way to visualize B_f is to: (1) imagine that all properties of a beam are known, perhaps by companion tests or independent measurement; (2) use these properties to analyze the ultimate capacity of the beam; (3) test the beam to failure; and (4) compare the results. The calculated and measured strengths will not be the same, and the ratio of Test/Calc is the modeling factor B_f. Parameter B_{sh} plays a similar role for shear walls. Refined structural models (e.g., nonlinear FEA) tend to be closer to reality than design code models, and in such cases the means of B_f or B_{sh} will be close to 1.0 (unbiased). As noted above, the fragility of the beam should be based on actual parameters, as best they can be determined.

When the structural component or system is subjected to dynamic forces, the statistical properties of strength of concrete and steel for use in developing fragility curves for shear walls must be adjusted for the increased rate of load. These increased values are summarized in Table 5.2. The steel and concrete "dynamic" strengths presented correspond to loading to failure in approximately 1 - 5 seconds. Mill tests of steel and concrete cylinder tests are conducted at a strain rate that falls somewhere between "static" and "dynamic" rates of application of structural actions.

Deterioration in reinforced concrete beams or shear walls due to corrosion is measured in this study by percentage loss of weight in reinforcement. Percentage losses of 10% and 20% are assumed, since these percentages might be related to surficial concrete cracking observed during a plant walkdown. Corrosion is a highly variable process; the corrosion test data reviewed in connection with the Structural Aging Program (Naus et al., 1996) indicates that the COV in corrosion penetration is on the order of 40 to 50 percent. Accordingly, it has been assumed that the corrosion penetration has a normal distribution, with mean penetration determined from the specified 10% or 20% weight loss, and COV of 0.45. Accordingly, the mean area of one No. 8 bar is 458 mm^2 (.71 $in.^2$) for 10% loss in weight and 406 mm^2 (.63 $in.^2$) for 20% loss in weight.

Closed-form expressions for the conditional limit state probabilities of indeterminate beams, slabs, and low-rise shear walls cannot be obtained using any other than idealized models of ultimate capacity. Thus, the uncertainties in structural capacity were estimated by a Monte Carlo procedure involving repeated finite element analyses, rather than in closed form. Because of the cost of performing nonlinear finite element analysis, the number of simulations, N, necessary to model the uncertainties and to construct the fragility must be kept to a minimum. Random sampling plans aimed at achieving efficiency in numerical experimentation (variance reduction techniques) are available (Rubenstein, 1981). Latin Hypercube (LHC) sampling has been found to be very useful in system reliability problems involving complex systems (Imam and Conover, 1980). Estimators that are obtained by LHC sampling are unbiased, and the standard error in the estimator is less than in most other methods with the same number of samples.

LHC sampling was used in conjunction with the ANSYS finite element program in the current study to generate the force-deformation curves for each structure sampled and to determine the fragilities. Each fragility curve is based on the analysis of 19 structures, in which the material strengths, dimensions, and modeling errors are consistent with the statistical data presented in Tables 5.1, 5.2 and the discussion above. The sample size of 19 was selected as a practical upper limit, given the time and effort required to generate load-deformation curves for the shear walls analyzed by ANSYS. The results of these finite element analyses are rank-ordered and plotted at rank mean positions between the 5-percentile and 95-percentiles. A lognormal distribution then is fit to these data and the fragility parameters m_R and β_C in Eqs. 5.5 and 5.6 are determined.

All random variables in Tables 5.1 and 5.2 are assumed to be statistically independent, with the exception of (f_c, f_t) and (f_c, E_c) both of which are assumed to have a correlation of 0.7. When a finite number of independent samples are simulated, however, some correlation in the samples may be evident. To illustrate this problem, the sample correlation coefficients for f_y and A_s (with corrosion) are listed in the following table:

No. 8 bars, 10% loss: -0.158
No. 8 bars, 20% loss: +0.007
No. 5 bars, 10% loss: +0.158
No. 5 bars, 20% loss: -0.138

This nonzero sample correlation is inherent in working with samples of this size; in fact, correlation coefficients, r, computed for samples of 19 variates (x, y) simulated from independent populations X and Y will generally be nonzero. If X and Y are independent, the sampling density of r is centered on 0, but small positive or negative values can occur when individual samples are taken. A closed-form expression for this sampling density does not exist for non-normal X and Y, but can be computed numerically. The 95-percent confidence interval on the sample correlation coefficient for samples of 19 when X is lognormal and Y is normal (as with f_y and A_s) is (-0.43, 0.45). In other words, sample correlation coefficients between -0.43 and 0.45 based on 19 samples give no cause to reject the null hypothesis that the true correlation coefficient is zero. If the sample size is increased from 19 to 49, the confidence interval decreases to (-0.27, 0.29), at the expense of more finite element structural analyses in the simulation process. While there are mathematical techniques for reducing (but not eliminating) such correlations (Imam and Conover, 1980), these strategies were not employed in this study. The effect of these small correlations on the fragility models constructed by LHC/ANSYS is small.

Table 5.1

Structural Resistance Statistics for
Reinforced Concrete Components Subjected to Static Forces

Property	Mean		COV	CDF
Concrete (4000-psi)				
Compression strength	3,552	psi	0.16	N
Tensile (splitting) strength	358	psi	0.18	N
Initial tangent modulus	3,800	ksi	0.18	N
Limiting compression strain	0.004		0.20	N
Grade 60 reinforcement				
Yield strength	66	ksi	0.10	LN
Modulus of Elasticity	29,000	ksi	na	na
Placement of reinforcement				
Effective depth, d	d	in.	0.5/d	N
Bar cover	c+1/4	in.	0.625/c	N
Structural analysis				
Flexure (B_f)	1.04		0.07	N
Shear (B_{sh})	1.00		0.14	N

Note: 1 in. = 25.4 mm; 1 psi = 6.895 kPa; 1 ksi = 6.895 MPa;
N = Normal Distribution; LN = Lognormal Distribution

Table 5.2

Steel and Concrete Strength Statistics for
Components Subjected to Dynamic Forces

Property	Mean		COV	CDF
(1) Concrete (nominal 4000 psi)				
Compression strength in-situ	4,400	psi	0.16	N
Tensile (splitting) strength	475	psi	0.18	N
Initial tangent modulus (150 pcf)	3,834	ksi	0.18	N
(2) ASTM A615/Grade 60 reinforcement				
Yield strength	71	ksi	0.10	LN
Modulus of elasticity	29,000	ksi	na	na

Note: 1 psi = 6.895 kPa; 1 ksi = 6.895 MPa; 1 pcf = 16.02 kg/m^3;
N = Normal Distribution; LN = Lognormal Distribution

6 EVALUATION OF REINFORCED CONCRETE FLEXURAL MEMBERS

The effects of degradation on the behavior of reinforced concrete flexural members (beams and one way slabs) are discussed in this section of the report. A specific example of a propped cantilever beam is used to evaluate fragility curves for both an undegraded beam and a beam with degraded properties. Lognormal distributions for the important beam properties are developed both for the undegraded and degraded conditions. These properties are then used to evaluate the probability of failure for the beam. Extensive calculations are performed with an analytical model of the beam (as recommended in ACI 318) and these results are verified with a finite element model of the beam. After the results for the specific example are found, analyses are performed to generalize the conclusions for beam properties other than those used in the specific example.

Several assumptions are made to simplify the problem. First, the strength of the beam measured in terms of uniform load capacity is used to define the limit state. Deformation-based limit states (peak displacement, maximum rotations, or ductility) usually are not the limiting conditions for typical flexural members in nuclear power stations. Second, dynamic effects are not considered for the beams. Most of the loads acting on flexural members in power plants are static gravity loads with dynamic seismic loads constituting a small portion of the total load. It should be noted that the objective here is to evaluate the change in fragility curves from the undegraded to the degraded cases.

The specific example used in the analyses is first discussed together with the methodology used to perform the response calculations. The finite element model of the beam is then developed and solutions compared with those obtained from the analytical model. The degradation mechanisms are then discussed and fragility curves are developed for both the undegraded and degraded beams. Finally, comparisons of the fragility curves are made and the significance of the difference to risk at nuclear power stations is discussed. These results are generalized to other beam shapes and material properties.

It should be noted that this section utilizes some equations and coefficients in accordance with the ACI 318 Code which are only valid in English units (i.e., not SI units). Therefore, for these situations, only English units are provided. Where appropriate, SI units are provided in parenthesis following the English units.

6.1 Sample Problem and Analytical Model

The design is first developed followed with a description of the methodology used to evaluate the beam's load-deflection response to an increasing uniform load.

6.1.1 Beam Design

A propped cantilever beam with a twenty-foot span is designed using the procedures in ACI 318-99. The beam is designed for a dead load of w_d = 1 kip/ft (14.6 kN/m) and a live load of w_l = 3 kips/ft (43.8 kN/m). The required strength of the beam (w_u), including load factors is:

$$w_u = 1.4\, w_d + 1.7\, w_l = 6.5 \text{ kips/ft (94.9 kN/m)} \tag{6.1}$$

The elastic shear and bending moment diagrams for the beam are shown in Figure 6.1. The peak elastic bending moment occurs in the negative moment region at the fixed support. The peak negative and positive moments are:

$$M_u^- = w_u L^2 / 8 = 325 \text{ ft-kips (441 kN-m)}; \quad M_u^+ = 9\, w_u L^2 / 128 = 183 \text{ ft-kips (248 kN-m)} \tag{6.2}$$

The beam is designed using concrete with a compressive strength f'_c = 4 ksi (27.6 MPa) and A615 Grade 60 reinforcement having a yield strength equal to 60 ksi (414 MPa). Young's modulus for the concrete is 3,605 ksi (24.9GPa). The balanced reinforcement ratio (ρ_b) for these materials is:

$$\rho_b = 0.85\ \beta_1\ (f'_c / f_y)[\varepsilon_u / (\varepsilon_u + f_y / E_s)] = 0.0285 \qquad (6.3)$$

where, β_1 = 0.85 for 4 ksi concrete
ε_u = failure strain in concrete = 0.003 for design
E_s = Steel modulus of elasticity = 29,000 ksi

The design is shown in Figure 6.2. The reinforcement ratios in the negative and positive moment regions are 0.0145 and 0.0087 respectively, both less than the maximum permitted by the ACI code (0.75 ρ_b = 0.0214). The moment capacity in the negative and positive moment regions are evaluated using Whitney's uniform stress block as prescribed in the code. The following equation gives the design strength (ϕM_n) of the beam:

$$\phi\ M_n = \phi\ A_s\ f_y\ (d - a/2) \qquad (6.4)$$

where, A_s = area of the tensile reinforcement
d = depth to the tensile reinforcement
ϕ = capacity reduction factor
a = depth of stress block = $A_s\ f_y / 0.85\ f'_c\ b$
b = width of beam

The design strengths of the beam shown in Figure 6.2 for negative and positive moments are:

$$\phi\ M_n^- = 325 \text{ ft-kips (441 kN-m)}; \quad \phi\ M_n^+ = 207 \text{ ft-kips (281 kN-m) and} \qquad (6.5)$$

ACI 318 requires the design strength to be equal to or greater than the required strength ($\phi\ M_n \geq M_u$). By comparison to the peak negative and positive moments given in Eq. 6.2 above, this requirement is met.

The effects of shear are considered next. The maximum shear occurs at the fixed support and is equal to 5 w_u L /8 = 81.3 kips (362 kN) (see Figure 6.1). The code permits the maximum shear to be evaluated at a distance d from the support where the shear is 69.9 kips (311 kN). The design strength in shear of the section shown in Figure 6.2 is:

$$\phi\ V_n = \phi\ [2\ (f'_c)^{1/2}\ b\ d + A_v\ f_y\ d / s] \qquad (6.6)$$
$$= 0.85\ [2\ (4000)^{1/2}\ (13*21)/\ 1000 + 0.4 * 60 * 21 / 10.5] = 70.1 \text{ kips (312 kN)}$$

where, s = spacing of shear reinforcement
A_v = area of shear reinforcement within a distance s

This is greater than the required strength in shear, V_u = 69.9 kips (311 kN), at the fixed support, and much greater than the demand in other portions of the beam where the demand is smaller.

6.1.2 Load-Deflection Response

The load-deflection behavior of the beam is evaluated using the procedures defined in ACI 318-99. The relationship between the applied loading and the beam moment strengths is first considered. For small

loadings the beam is uncracked and this range extends up to the point where the maximum bending moment (at the fixed support $M = w L^2 / 8$) equals the cracking moment (M_{cr}). The bending moment causing cracking is given as:

$$f_r = 7.5 [f'c]^{1/2} = 474 \text{ psi } (3.27 \text{ MPa}) \quad (6.7)$$

$M_{cr} = f_r I_g / c = 474 * (13 * 243 / 12) * 6 = 591{,}600$ in.-lbs = 49.3 ft-kips (66.8 kN-m)
where, I_g = gross section (uncracked) moment of inertia
c = distance from the neutral axis to extreme fiber of beam

Equating this moment to the peak moment results in the cracking load of $w_{cr} = 0.986$ kips/ft (14.4 kN/m). This represents the uniform load at which time cracking initiates in the beam at the fixed support.

The beam remains elastic (with decreasing stiffness as discussed below) until the bending moment at either the fixed support or at the region of maximum positive moment reaches the ultimate moments as given in the second line of Eq. 6.5. Since the maximum negative moment equals ($w L^2 / 8$) and the maximum positive moment equals ($9 w L^2 / 128$), the negative moment reaches ultimate first, and the first plastic hinge forms at the support. Equating the capacity to the applied moment determines that the load (w_{p1}) required to cause the first hinge to form is:

$$w_{p1} = 8 M_n^- / L^2 = 7.22 \text{ kips/ft } (105 \text{ kN/m}) \quad (6.8)$$

The beam remains elastic as the loading is increased beyond this value with plastic rotations occurring at the fixed support and the support moment remaining constant at 361 ft-kips (489 kN-m). A plastic limit analysis is performed to find the load at which the second hinge forms (w_{p2}) as shown in Figure 6.3. The external work (W_e) done for the virtual displacement (δ) is:

$$W_e = \delta w_{p2} [x/2 + (L - x)/2] \quad (6.9)$$
where, x is the distance from the fixed support to the second plastic hinge.

The internal work (W_i) done by the virtual displacement is:

$$W_i = \delta [M_n^- / x + M_n^+ (1/x + 1/\{L-x\})] \quad (6.10)$$

Equating the internal and external work results in the following prediction of the collapse load:

$$w_{p2} = 2[M_n^- + M_n^+ L / (L - x)] / L x \quad (6.11)$$

The value of x minimizing the collapse load is:

$w_{p2} = 7.79$ kips/ft (114 kN/m) at $x = 12.5$ ft (3.81 m)

The two plastic hinges form a mechanism so that no additional loading can be placed on the beam.

The stiffness characteristics of the beam are discussed next. These characteristics depend on the gross section moment of inertia (I_g) and the cracked section moment of inertia in the negative (I_{cr}^-) and positive (I_{cr}^+) moment regions. These are:

$$I_g = 14{,}976 \text{ in.}^4 (623{,}350 \text{ cm}^4); \; I_{cr}^- = 7{,}586 \text{ in.}^4 (315{,}750 \text{ cm}^4); \; I_{cr}^+ = 5{,}195 \text{ in.}^4 (216{,}230 \text{ cm}^4) \quad (6.12)$$

When the loading is small and before concrete cracking occurs, the stiffness of the beam is controlled by the gross section with negligible contribution from the reinforcement. The elastic deflected shape of the propped cantilever is:

$$\Delta = w\,x\,(L^3 - 3\,L\,x^2 + 2\,x^3) / 48\,E\,I \qquad (6.13)$$

where, x = distance from fixed end

The deflection is calculated at x = 12.5 ft (3.81 m) (where the second hinge forms) as:

$$\Delta = 316.0\,w / I$$

where, the deflection is in inches, load is in kips/ft and I is in in.^{4} units

Therefore the deflection at cracking is:

$$\Delta_{cr} = 316 * 0.986 / 14976 = 0.021\text{in. } (0.533\text{ mm}) \qquad (6.14)$$

The beam stiffness (based on I) gradually changes from the (I_g) to (I_{cr}) during the next phase of loading [from the cracking load = 0.986 kips/ft (14.4 kN/m) to the formation of the first plastic hinge at a load = 7.22 kips/ft (105 kN/m)]. An effective moment of inertia (I_e) is used from ACI 318-99:

$$I_e = (M_{cr} / M_a)^3\,I_g + [1 - (M_{cr} / M_a)^3]\,I_{cr} \qquad (6.15)$$

where, M_a is the peak bending moment

Effective moments of inertia are evaluated in both the negative and positive moment regions and an average value used to determine the beam deflections:

$$I_e = (I_e^+ + I_e^-) / 2 \qquad (6.16)$$

where, $I_e^+ = 14{,}976\,(49.3 / 28.1\,w)^3 + 5{,}195\,[1 - (49.3 / 28.1\,w)^3]$

$I_e^- = 14{,}976\,(49.3 / 50\,w)^3 + 7{,}586\,[1 - (49.3 / 50\,w)^3]$

For loads between the formation of the first and second hinges [7.22 kips/ft (105 kN/m) to 7.79 kips/ft (114 kN/m)], the moment at the fixed support remains constant at $M_n^- = 361$ ft-kips (489 kN-m) resulting in a deflected shape of:

$$\Delta = [4\,M_n^-\,(x^3 / L - L\,x) + w\,x\,(L^3 + x^3 - 2\,L\,x^2)] / 24\,E\,I \qquad (6.17)$$

The effective moment of inertia (Eq. 6.16) is used in Eq. 6.17 but the definitions of I_e^+ and I_e^- change to:

$$I_e^+ = 14{,}976\,(49.3 / 46.9\,w - 135.4)^3 + 5{,}195\,[1 - (49.3 / 46.9\,w - 135.4)^3]$$
$$I_e^- = 14{,}976\,(49.3 / 361.1)^3 + 7{,}586\,[1 - (49.3 / 361.1)^3] \qquad (6.18)$$

Of course for loads greater than 7.79 kips/ft (114 kN/m) the deflection increases without bound and the beam cannot carry additional load. Load-deflection plots are presented in the following section.

6.2 Finite Element Model

A finite element model of the sample beam problem is developed to verify the results of the analytical solution discussed in the previous section. The ANSYS, Version 5.4, computer code is used to develop the load-deflection characteristics of the beam. Modeling considerations are discussed first, followed by a

comparison of the results with those obtained from the analytical solution discussed in the previous section.

6.2.1 Modeling Considerations

The results from the closed-form solutions presented in Section 6.1 are verified with a finite element model of the beam with solutions obtained using the ANSYS computer code. The model used for the beam is shown in Figure 6.4. There are 46 elements along the length and 8 elements over the depth. Due to symmetry, one half of the beam is modeled in the 13 in. (33 cm) width direction with each concrete element having dimensions of 5.21 in. (13.2 cm) long x 3 in. (7.62 cm) deep by 6.5 in. (16.5 cm) wide. The axial and vertical deflections are restrained at the fixed end of the beam, the vertical deflections are restrained at the simple support, and the "through the thickness" deflections are restrained at the plane of symmetry. The reinforcement is placed on the outer surface of the beam at 3 in. (7.62 cm) down from the top for the negative reinforcement and at 3 in. (7.62 cm) up from the bottom for the positive reinforcement. Shear reinforcement is placed along the first set of nodes in from each support and then along every other vertical set of nodes except in those central portions of the beam where no shear reinforcement is required.

The concrete is modeled with element type "SOLID65" of ANSYS. This element is a three-dimensional solid that can model cracking in tension, crushing in compression, and plastic deformation. For a definition of the stress-strain relationship, the uniaxial stress strain law, based on Hognestad's formulation (Park and Paulay, 1975), is prescribed for the concrete as follows:

$$f_c = f'_c \left[2 \varepsilon_c / \varepsilon_o - (\varepsilon_c / \varepsilon_o)^2\right] \text{ for } \varepsilon_c \le \varepsilon_o \qquad (6.19)$$
$$f_c = f'_c \quad \text{for } \varepsilon_c > \varepsilon_o$$
where, $\varepsilon_o = 2 f'_c / E_{it}$ and E_{it} = initial tangent modulus

A tensile strength and failure compressive strain is also prescribed for the concrete. Cracking (at the tensile strength) and crushing (at the failure compressive strain) behavior of the concrete is considered in the solutions. The ANSYS model also allows the user of the program to prescribe shear transfer coefficients for open and closed cracks that may develop during the analysis. These shear transfer coefficients correspond to the stiffness along cracks and are represented as a fraction of the stiffness in the uncracked material (between 0.0 to 1.0). For this analysis the shear transfer coefficient was set to 0.5 (50% shear stiffness) for an open crack and 1.0 (100% shear stiffness) for a closed crack. No tensile stress can be transmitted across cracks, but compressive stresses can be transmitted after cracks close.

The steel reinforcement is modeled discretely with spar elements having elastic-perfectly plastic material properties.

6.2.2 Comparison of Results from ANSYS and Analytical Model Solutions

Uniform load intensity is increased on the beam until convergence of the ANSYS solutions can no longer be achieved. Crack patterns are shown in Figure 6.5 for onset of cracking, formation of the first plastic hinge, and formation of the second hinge. The hinge formation is defined at the time of first yielding of the reinforcement. Cracking was found to occur at a load of 1.65 kips/ft (24.1 kN/m), the first plastic hinge forms at 7.05 kips/ft (103 kN/m), and the second plastic hinge forms at 7.88 kips/ft (115 kN/m). It should be recalled that the ACI code calculated values (see Section 6.1.2) are 0.986 kips/ft (14.4 kN/m), 7.22 kips/ft (105 kN/m), and 7.79 kips/ft (114 kN/m). The ANSYS results are 167%, 98%, and 101% of the three analytical results.

Load-deflection plots for the analytical and ANSYS results are shown in Figure 6.6 for both the finite element and hand calculation models. It can be seen that the agreement between the two is quite good for calculation of ultimate strength, which is important for fragility calculations. For the region in the curves where cracking occurs, there are some differences. This is partly due to the use of the effective moment of inertia for the section (as given in ACI 318-99) to predict the deflection of the beam. The relationship in ACI 318-99 is empirically based and may not exactly represent the conditions for the beam considered. There is a second reason why the ANSYS model predicts somewhat softer behavior (larger deflections) than the analytical model. The modulus of elasticity used in the analytical solution is as given in ACI 318-99 and is equal to 3,605 ksi (24.9 GPa). This is representative of the secant modulus, but the same modulus is used in the ANSYS model as an initial tangent modulus, which decreases in accordance with the stress-strain relationship described in Eq. 6.19.

Based on the good comparison between the ANSYS FEM results and the analytical closed-form solutions, the latter solutions in Section 6.1 were used to generate the fragility curves for the various beam conditions to be studied.

6.3 Fragility Curves for Undegraded and Degraded Beams

Fragility of the propped cantilever beam is based on an ultimate load limit state. The load capacity of the beam is defined by Eq. 6.11. The random variables considered in Eq. 6.11 for the case of the undegraded beam are summarized in Table 5.1. They include: the concrete compressive strength, the yield strength of the steel reinforcement, and the effective depth (d) of the beam. Other random variables include the tensile strength of the concrete and the concrete failure strain, which are used to ensure that the flexural failure mode does not change from yield of the steel to crushing of the concrete. The modeling uncertainty in the flexural analysis is also included. Equation 6.3 is used to verify that the reinforcement ratio remains less than the balanced reinforcement ratio.

Nineteen samples of the random variables in Section 5 are developed using a Latin Hypercube sampling plan and are used to evaluate the beam fragility in the undegraded state. Fragility data for the undegraded beam is shown in Table 6.1 (generated using the EXCEL software). The first 7 columns in the table represent the values of the random variables discussed in Section 5. The parameters B_f and B_{sh} model the uncertainty in the flexural and shear prediction models used in the analysis. The next to last column (w_f) is the calculated ultimate capacity of the beam based on Eq. 6.11 and the last column in the table represent the balanced steel area calculated from Eq. 6.3 (multiplied by b d). As may be seen, the reinforcement in the beam is less than the balanced steel area for all 19 samples, so that the failure mode does not change from yielding of the reinforcement to crushing of the concrete.

The resulting mean strength is found to be 8.66 kips/ft (126 kN/m) [as compared to deterministic prediction of collapse equal to 7.79 kips/ft (114 kN/m)]. The coefficient of variation (COV) is found to be 0.11. A plot of the nineteen samples is shown on lognormal probability paper in Figure 6.7. The linear variation of the computed data verifies that the lognormal distribution is appropriate for the beam. The mean and standard deviation data are used to develop the fragility curve. The fragility curve for the undegraded beam is shown in Figure 6.8. It is interesting to note that these data indicate that the probability of failure for a load equal to the beam's design strength of 6.5 kips/ft (94.9 kN/m) is about 0.5%. The probability of failure at the collapse load predicted from the deterministic analysis with nominal values of all parameters [7.79 kips/ft (114 kN/m)] is about 18%.

The age-related degradation effects (discussed in Section 2) considered during this study are: decrease in compressive strength, loss of steel cross-sectional area, reduction in bond strength, and reduction in concrete area (cracking and/or spalling). Loss of concrete compressive strength is dismissed as a significant mechanism because it has a very small impact on the beam's flexural strength, and the normal

increase of compressive strength with age is likely to offset any strength loss resulting from degradation effects. Loss of steel area is a significant degradation mechanism and results from corrosive action caused by carbonation and/or chloride intrusion. Amleh and Mirza (1999) performed an experimental study relating loss of steel area and reduction in bond strength to corrosive action. Several levels of corrosion are identified based on the crack widths observed in the concrete. It was found that crack (parallel to the reinforcement) widths on the order of 0.15 mm (0.00591 in.) corresponded to the first stage of corrosion with essentially no reduction in steel cross-sectional area or bond strength while crack widths on the order of 9 mm (0.354 in.) are associated with 20% loss in steel (cross-sectional) area and significant loss of bond strength. Since the 9 mm (0.354 in.) crack is readily observable and would afford the opportunity to make repairs, it was decided to consider steel area losses of 20% and 10% (treated as random variables). The 20% reduction in steel area was modeled with a mean steel area of 405 mm^2 (0.628 $in.^2$) [the original area of the #8 bar is 510 mm^2 (0.79 $in.^2$)] with a coefficient of variation equal to 0.11, while the 10% reduction in steel area was modeled with a mean steel area equal to 455 mm^2 (0.705 $in.^2$) and a coefficient of variation equal to 0.05.

Reductions in bond strength would affect the stiffness of the beam throughout (because the steel could slip relative to the adjacent concrete) and would affect the strength of the beam if the rebars are not adequately anchored in critical regions (such as the fixed support of the propped cantilever). The change in stiffness should not have a significant impact on the strength limit state being considered. The change in strength would depend on the details of the anchorage (provided development length, use of hooks, confinement of reinforcement). With sufficient anchorage, it is expected that the loss of steel area would govern, and therefore, bond loss is not considered here. The experimental data indicated that corrosion did not result in a reduction in the yield strength of the uncorroded portion of the reinforcing bar.

Finally, concrete spalling (resulting from either freeze thaw problems or steel corrosion) is considered as a degradation mechanism. Spalling in concrete beams usually occurs outside of the steel cage. This is modeled by reducing the effective depth of the beam section by subtracting the cover from the depth. In the finite element model the loss of concrete cover was assumed to occur over the entire width and length of the beam. It should be noted that the loss of concrete cover is only critical at the location of maximum moments where the two plastic hinges form. The cover was defined with a mean depth of 1.75 in. (44.5 mm) with a coefficient of variation equal to 0.355. Since corrosion can result in loss of steel and concrete spalling, the combined case of both effects is considered in addition to the individual effects.

A tabulation of the degraded cases considered is given in Table 6.2 together with their means and coefficients of variation in capacity. The tables on which the calculations are based and the figures showing the fragility curves are referenced in this table. The specific data used to model the random variables defining the steel area and concrete cover are also presented. It can be seen in Table 6.2 that the maximum reduction in mean strength from 8.66 kips/ft (126 kN/m) to 7.11 kips/ft (104 kN/m) (18%) occurs for the 20% loss of bottom steel plus a bottom spall. It should be noted that this mechanism is associated with rather severe cracking of the concrete section which could be readily observed during an inspection. It is believed that inspections of the facility would identify such problem areas before significant degradation of strength would occur. The coefficient of variation in flexural capacity is about the same for all cases, varying from 0.109 for the undegraded case to 0.127 for the 20% loss of top and bottom steel. The load intensities associated with a 2% probability of failure are also shown in Table 6.2. The 20% loss of bottom steel and bottom spall is the critical case and results in a 20% reduction in the 2% probability of failure load. A lognormal probability plot of the fragility data for the 20% loss of steel top and bottom is shown in Figure 6.16. It can be seen that the data can be represented by the lognormal distribution.

A summary plot of all the fragility curves is shown in Figure 6.17. It is apparent that, in first approximation, the various assumed modes of degradation cause the median (or mean) flexural capacity

to decrease, but have little impact on the coefficient of variation in capacity. The fact that the fragility curves appear to remain parallel to one another under various states of degradation has some important implications for in-service fragility evaluation, updating, and condition assessment, which will be discussed in more detail in Section 8.

6.4 Generalization of Results

The results presented in the previous section apply to the propped cantilever considered in the study. The results of that study are generalized to other flexural members (beams and one-way slabs) in this section. Since it is shown in Figure 6.17 that the fragility curves are essentially parallel, the margin between degraded and undegraded capacities remains constant regardless of the probability of failure being considered. The results in this section are generated by evaluating the ratio of moment capacity for the beam with degraded properties to that without degradation.

The effects of concrete spalls are considered first. For a singly reinforced concrete beam or one-way slab, the moment capacity can be written as:

$$M = A_s f_y \ (d - q\, d) \qquad (6.20)$$
$$\text{where, } q = \rho f_y / 1.7 f'_c$$

Concrete spall reduces the depth d by the amount of cover (c). The ratio of the two moment capacities is:

$$M_{degrad} / M_{undegrad} = (1 - c/d - q) / (1 - q) \qquad (6.21)$$

This ratio is plotted in Figures 6.18, 6.19, and 6.20 for the three cases of concrete cover: 3/4 in. (19.1 mm), 1-1/2 in. (38.1 mm), and 3 in. (76.2 mm) respectively. The 3/4 in. (19.1 mm) is typical of a slab and it can be seen from Figure 6.18 that the cover spall can result in reductions of moment capacity greater than 20% when the slab thickness is less than about 5 in. (12.7 cm). These slab thicknesses are not likely to be found in NPPs. The degradation for 1-1/2 in. (38.1 mm) cover, typical of what would be found for interior beams, is shown in Figure 6.19. It can be seen that for beams with depths greater than 10 in. (25.4 cm) the degradation is less than 20%. The degradation for 3 in. (76.2 mm) cover, typical of what would be found for exterior beams, is shown in Figure 6.20. It can be seen that the degradation is greater than 20% for beams less than 18 in. (45.7 cm) depth. Most exterior beams in NPPs are likely to be deeper than this but some flexural members in intake structures or cooling towers may be shallower. Degradation of these members may be significant and should be considered carefully. It is also interesting to note from the figures that the degradation is not very sensitive to the design value of q.

Degradation of steel cross-sectional area and concrete compressive strength is considered next. If the ratio of degraded to undegraded concrete strength is designated as ζ, the ratio of moment capacities can be written as:

$$M_{degrad} / M_{undegrad} = (1 - q / \zeta) / (1 - q) \qquad (6.22)$$

The results of this case are shown in Figure 6.21. It can be seen that the degradation approaches 20% for the heavily reinforced beam when the degraded concrete strength is less than 70% of the design strength. In view of the concrete strength gain with age this is unlikely to occur.

If the ratio of degraded to undegraded steel area is designated as ξ, the ratio of moment capacities can be written as:

$$M_{degrad} / M_{undegrad} = \xi (1 - q \xi) / (1 - q) \quad (6.23)$$

The results of this case are shown in Figure 6.22. It can be seen that the degradation can exceed 20% for the lightly reinforced beam when the degraded steel area is less than about 80% of the design area. As discussed above, steel degradation in this range results in staining and cracking of the concrete that is readily observable.

Combined degradation of steel area loss and concrete spalling are considered next. Using the same notation as defined above, the ratio of degraded to undegraded moment capacity is:

$$M_{degrad} / M_{undegrad} = \xi (1 - c/d - \xi q) / (1 - q) \quad (6.24)$$

If the ratio of degraded to undegraded moment capacity is to be greater than 80% then the (c/d) ratio for the beam must be:

$$c/d > 1 - \xi q - 0.8 (1 - q) / \xi \quad (6.25)$$

This is used in Section 8 to establish acceptance criteria for flexural members.

A change in failure mode from that assumed for design purposes might be a source of concern. The failure mode of a flexural member changes from yielding of the reinforcement to crushing of the concrete when the steel reinforcement ratio exceeds the balanced ratio as given in Eq. 6.3. Degradation of the concrete compressive strength and/or the concrete failure strain would result in a lower balanced reinforcement ratio. A beam designed according to ACI 318-99, however, is restricted to have a reinforcement ratio less than 75% of the balanced ratio. It is unlikely that the combined effects of the failure strain and compressive strength would cause the failure mode to change from yielding of the steel to crushing of the concrete. Degradation of the steel area decreases the reinforcement ratio and makes it less likely that the failure mode would change.

The failure mode could also change from flexure to shear; although the design procedures, for flexural members, contained in ACI 318-99 are intended to produce flexural failures rather than the more brittle shear failures. The Code requires that the capacity reduction factor for shear be set at a more conservative value of 0.85 as compared to 0.9 for flexure. This accounts for the larger variabilities found for shear strength than for flexural strength. However, spalling of the concrete cover and corrosion of the stirrups may, in some instances, induce a shear failure. This is considered in Section 8.2 in developing acceptance criteria for flexural members.

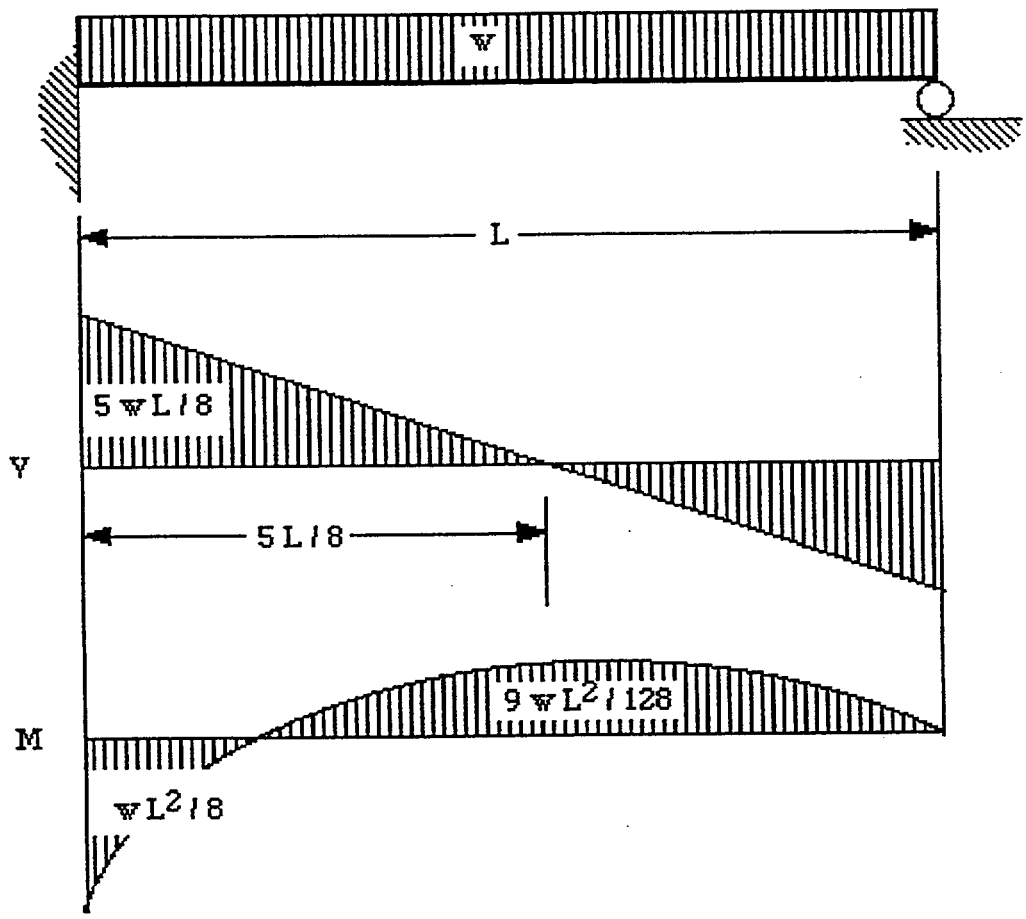

Figure 6.1 Shear and Moment Diagram for Propped Cantilever

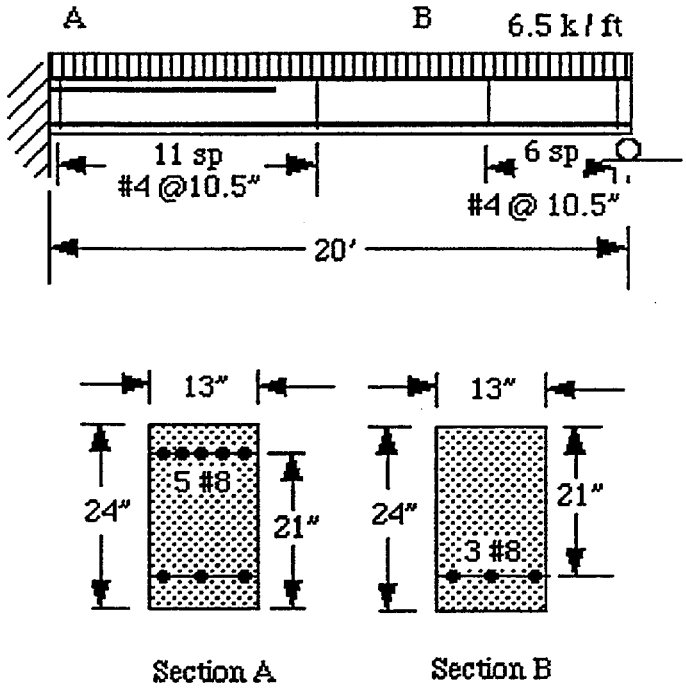

Note: 1 in. = 25.4 mm

Figure 6.2 Sample Beam Problem

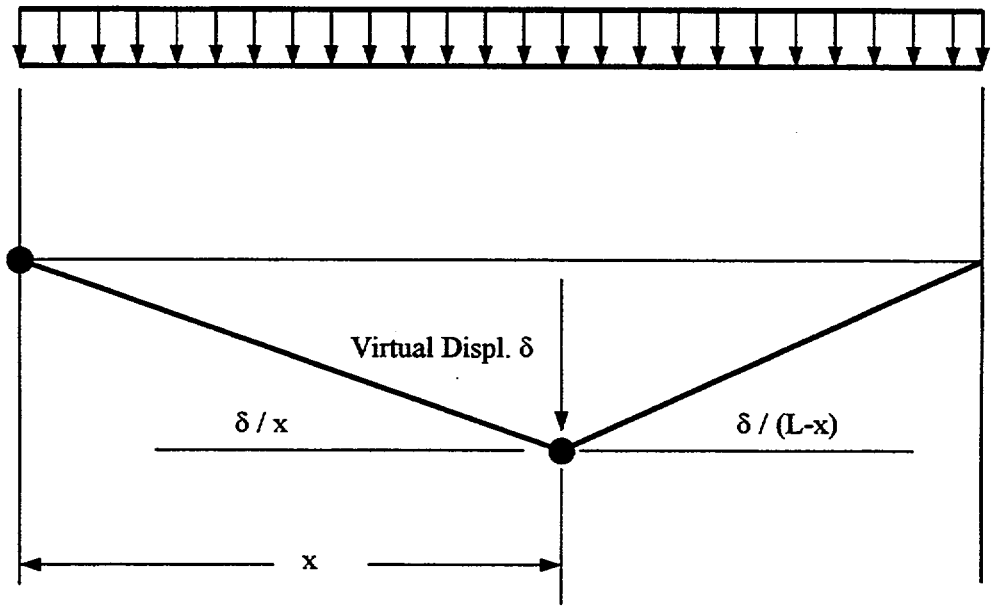

Figure 6.3 Limit Analysis of Propped Cantilever

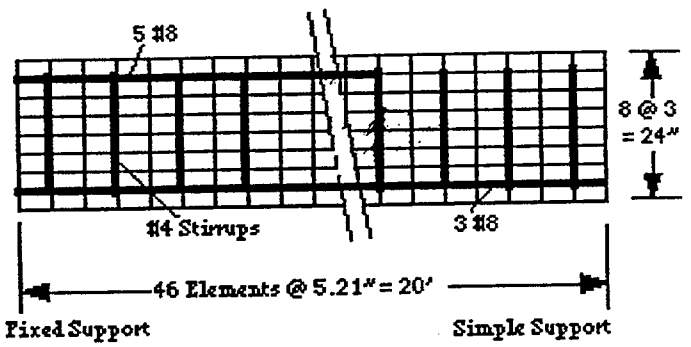

Note: 1 in. = 25.4 mm

Figure 6.4 ANSYS Beam Model

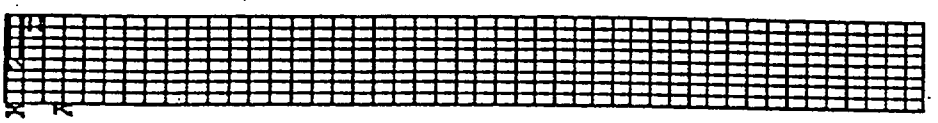

(a) First Cracking

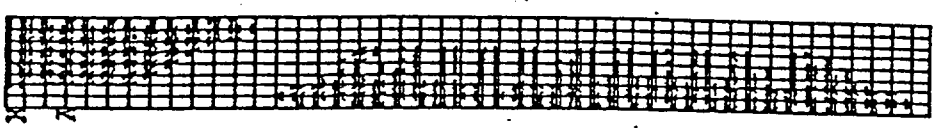

(b) Formation of Hinge at Fixed Support

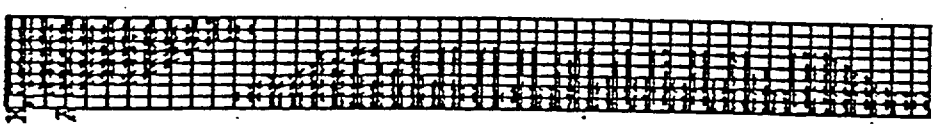

(c) Formation of Hinge in M^+ Region

Figure 6.5 Crack Patterns Predicted with ANSYS

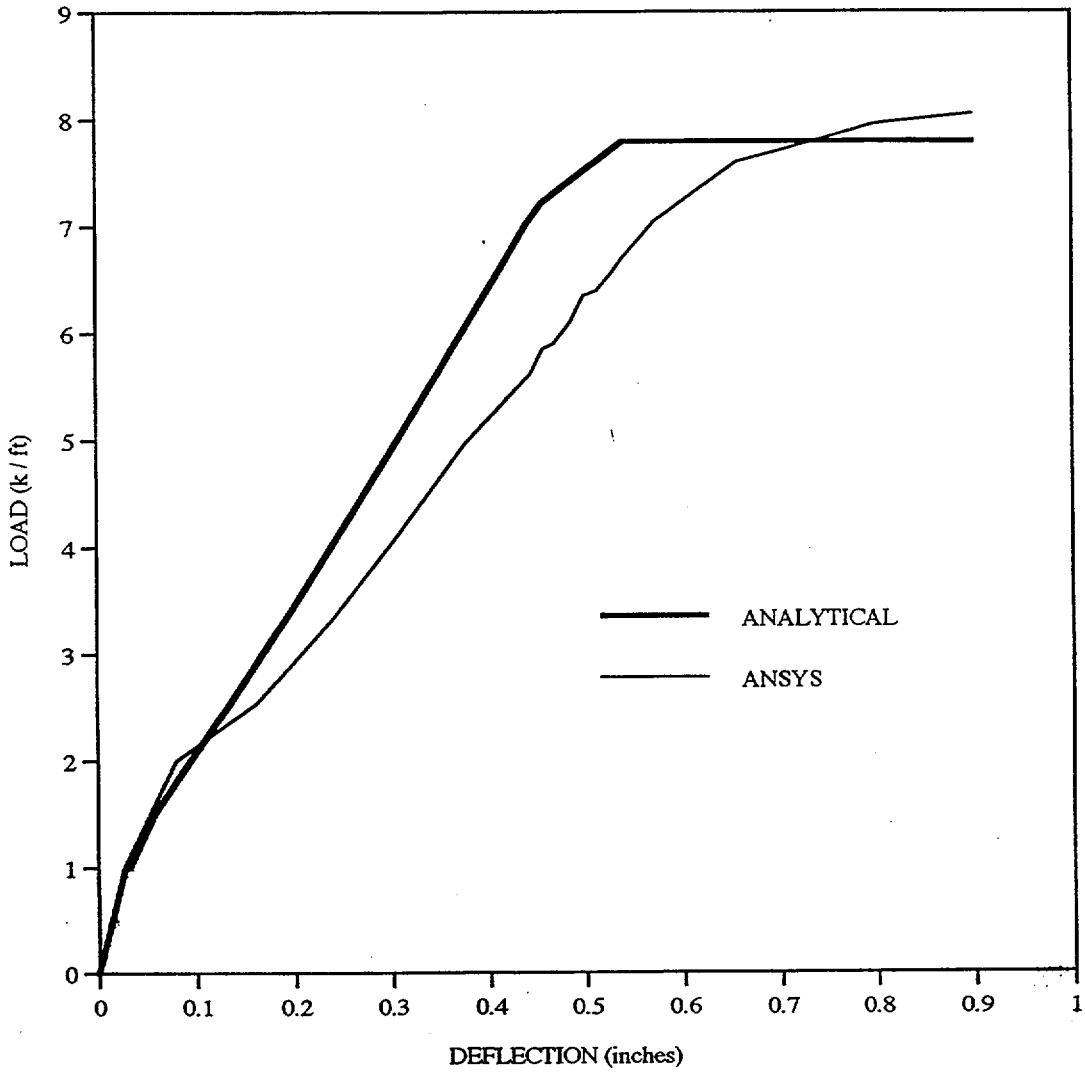

Note: 1 in. = 25.4 mm, 1 k/ft = 14.6 kN/m

Figure 6.6 Comparison of ANSYS and Analytic Beam Deflection Prediction

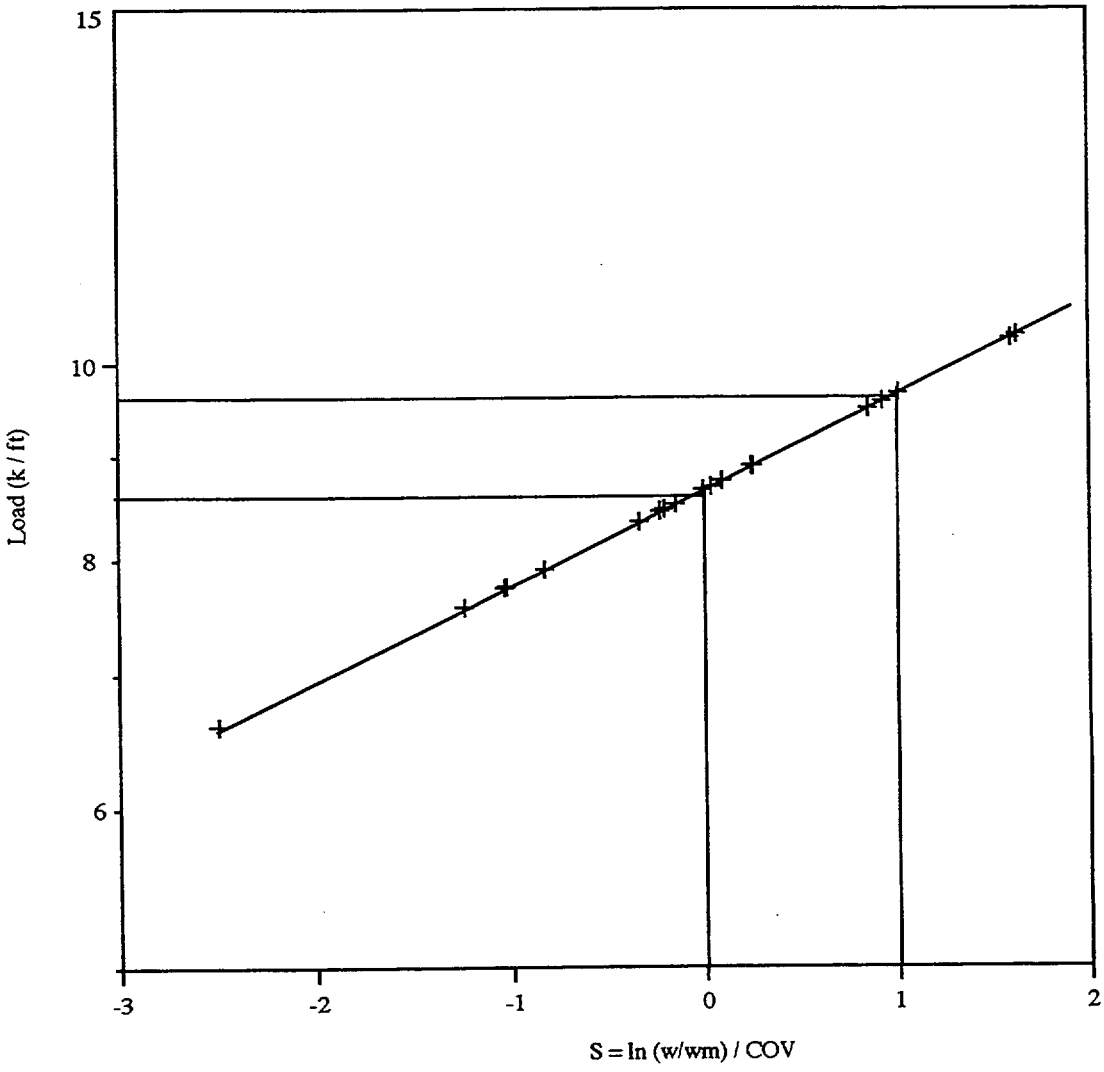

Note: 1 k/ft = 14.6 kN/m

Figure 6.7 Lognormal Distribution for Undegraded Beam

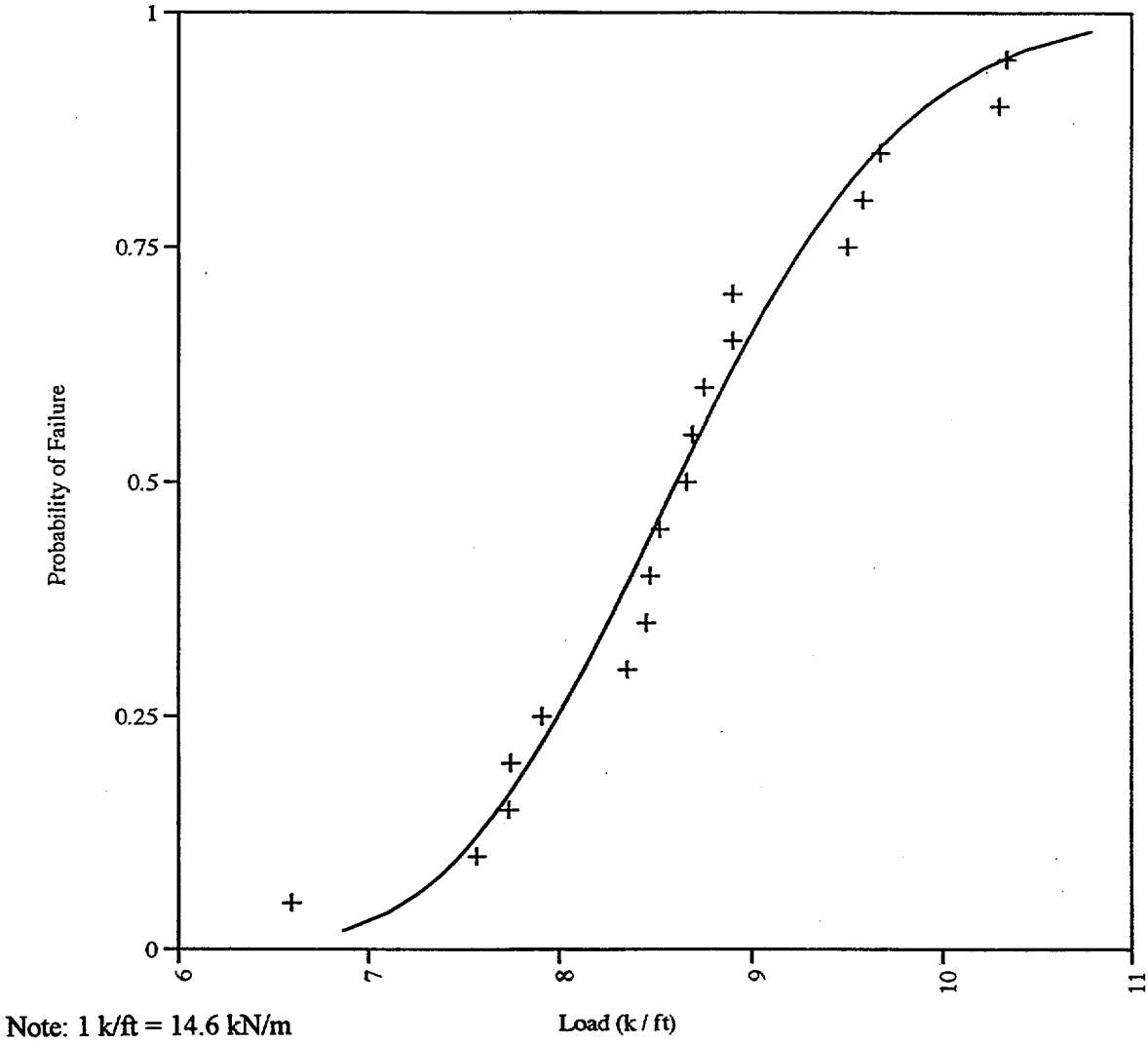

Note: 1 k/ft = 14.6 kN/m

Figure 6.8 Fragility Curve for Undegraded Beam

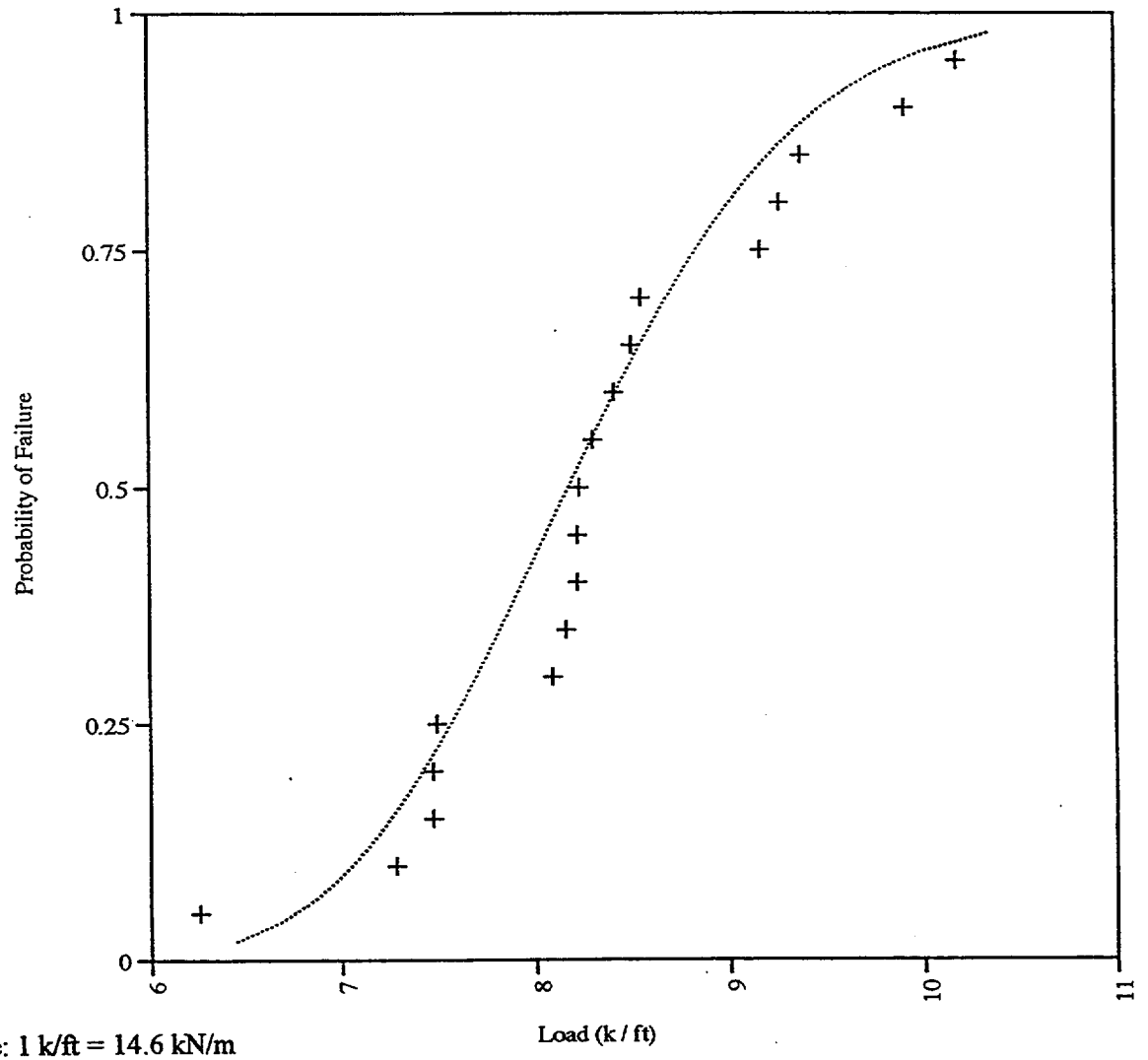

Note: 1 k/ft = 14.6 kN/m

Figure 6.9 Fragility Curve for Bottom Spall

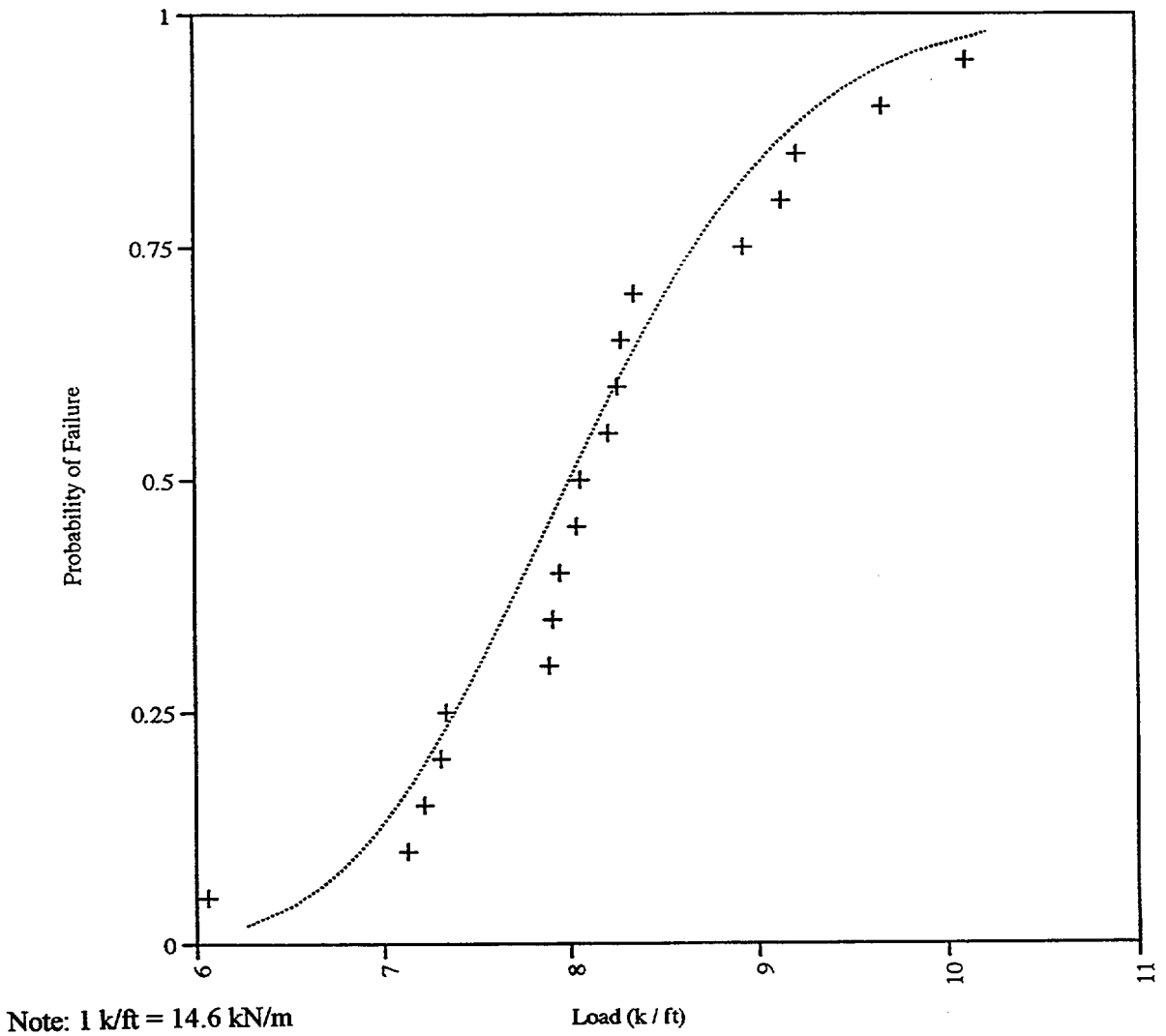

Note: 1 k/ft = 14.6 kN/m

Figure 6.10 Fragility Curve for Top Spall

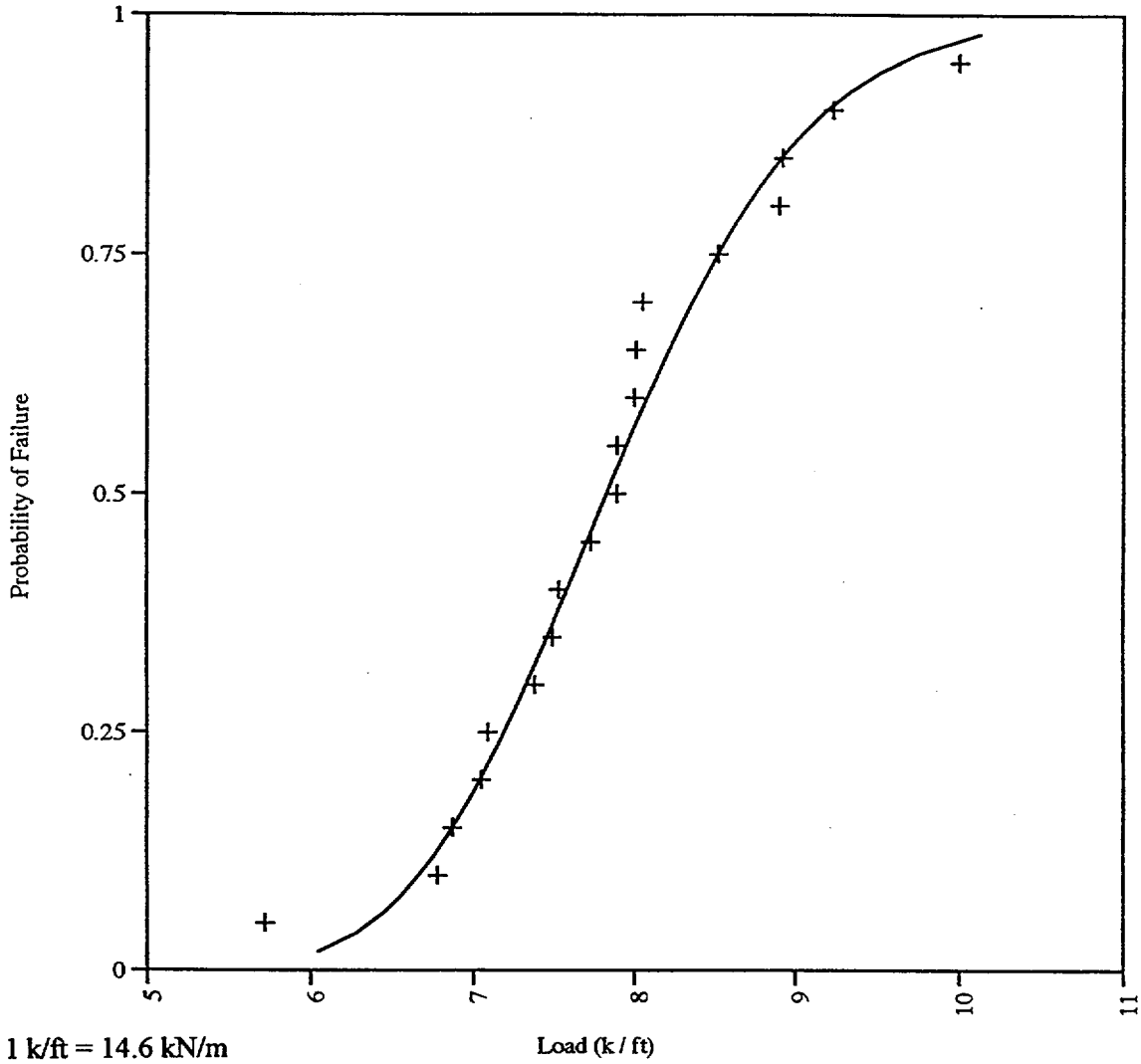

Note: 1 k/ft = 14.6 kN/m

Figure 6.11 Fragility Curve for Top and Bottom Spall

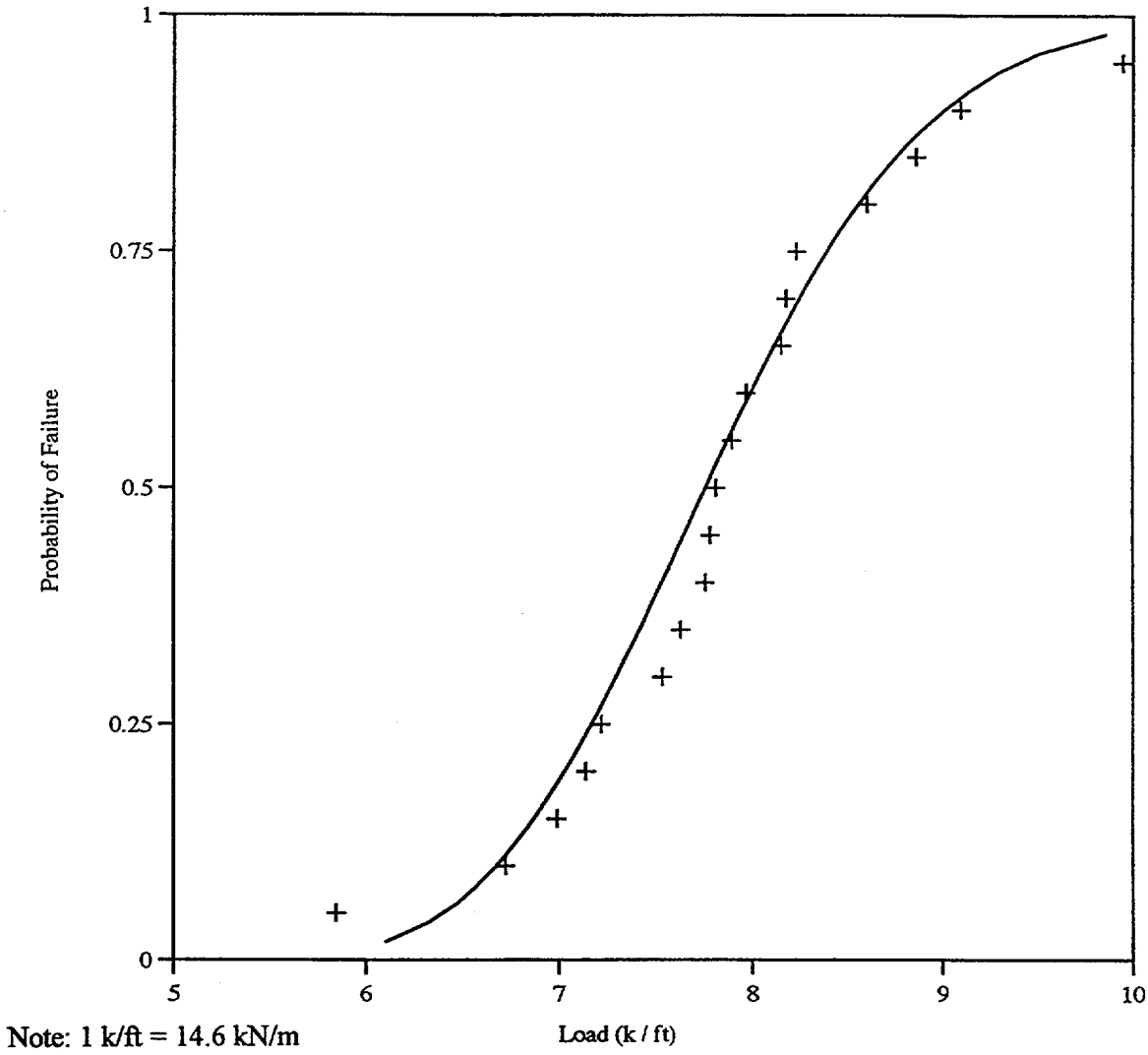

Figure 6.12 Fragility Curve for 10 % Steel Loss Top and Bottom

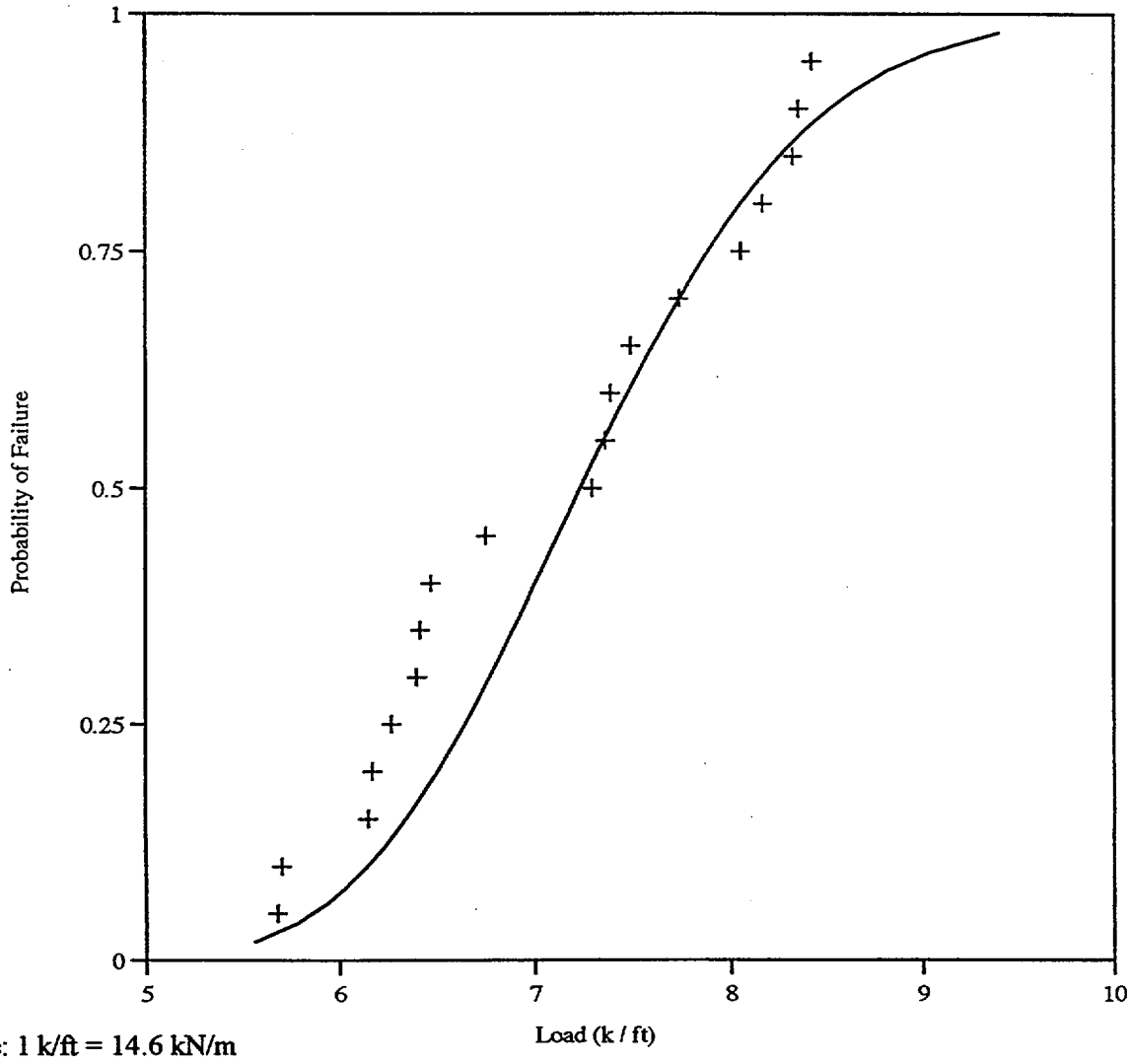

Note: 1 k/ft = 14.6 kN/m

Figure 6.13 Fragility Curve for 20 % Steel Loss Top and Bottom

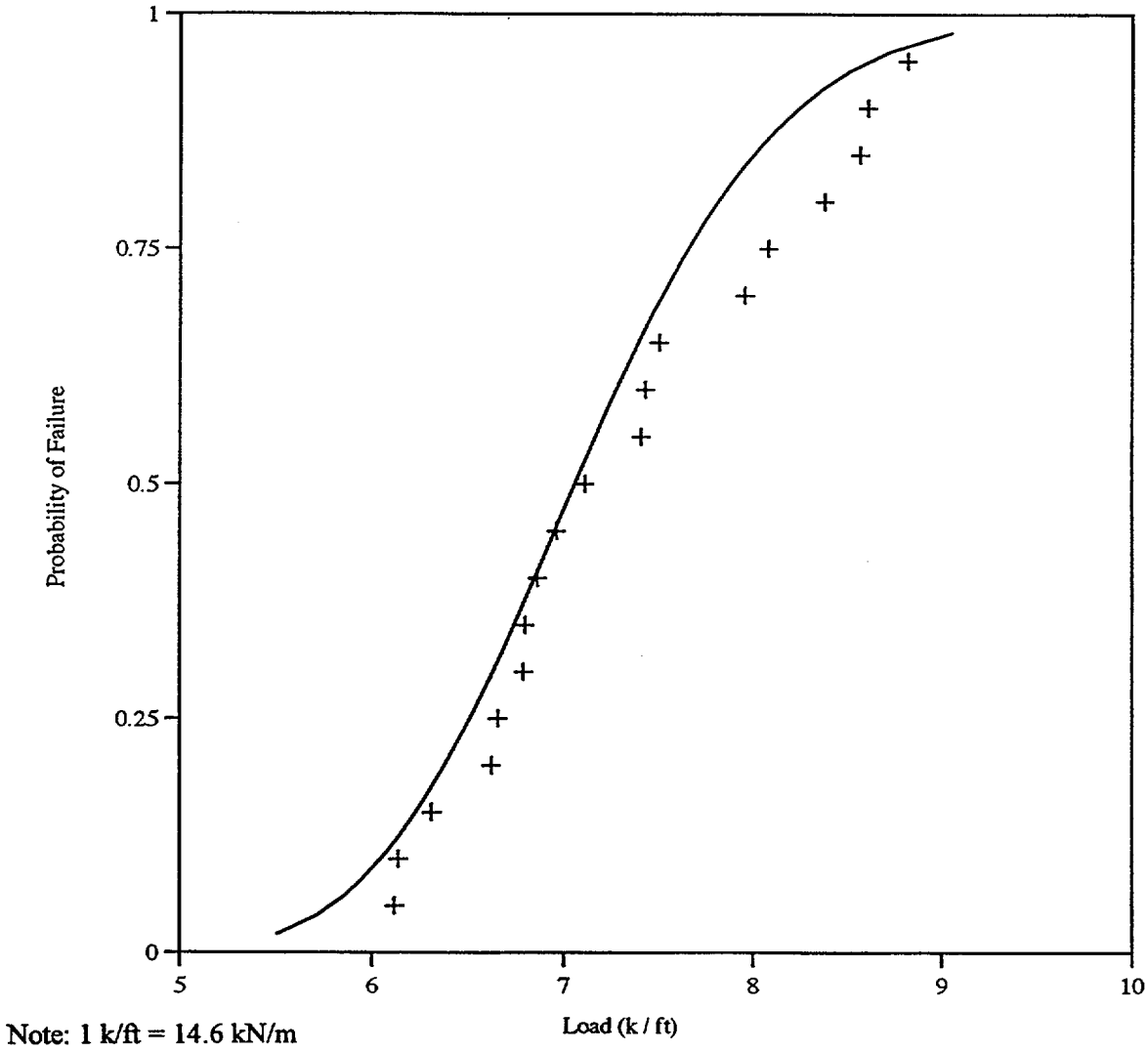

Figure 6.14 Fragility Curve for 20 % Bottom Steel Loss and Bottom Spall

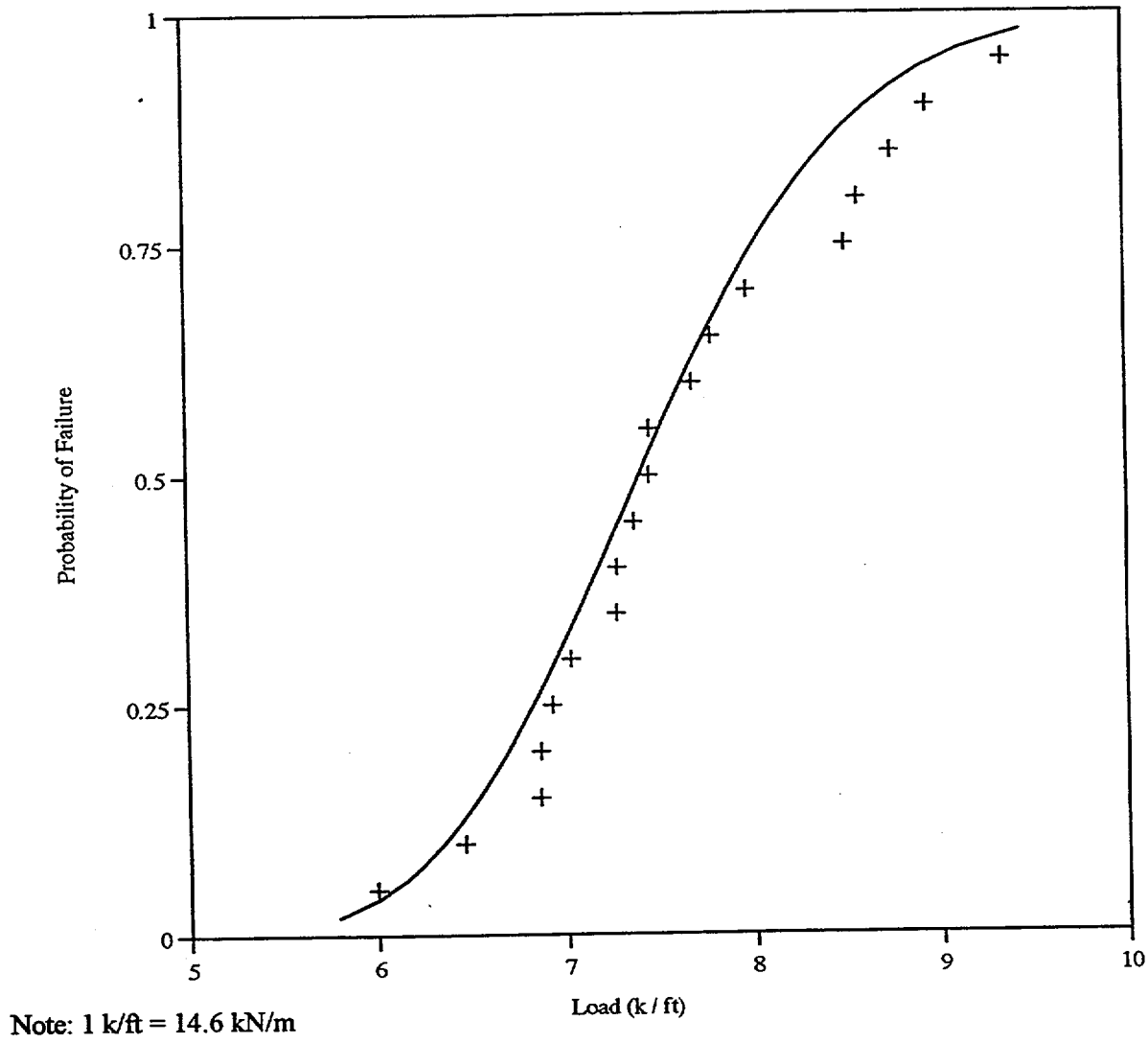

Note: 1 k/ft = 14.6 kN/m

Figure 6.15 Fragility Curve for 20 % Top Steel Loss and Top Spall

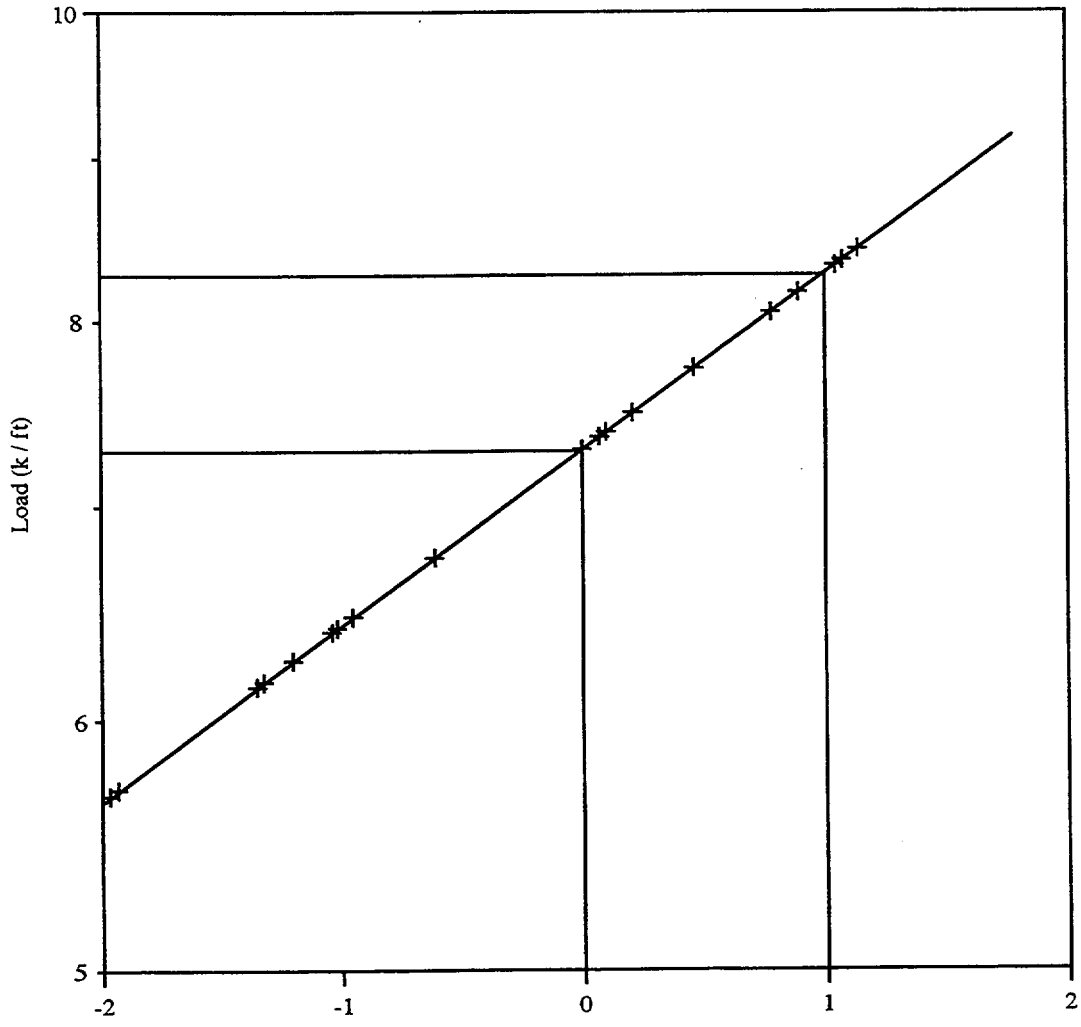

Note: 1 k/ft = 14.6 kN/m

Figure 6.16 Lognormal Distribution for 20 % Steel Loss

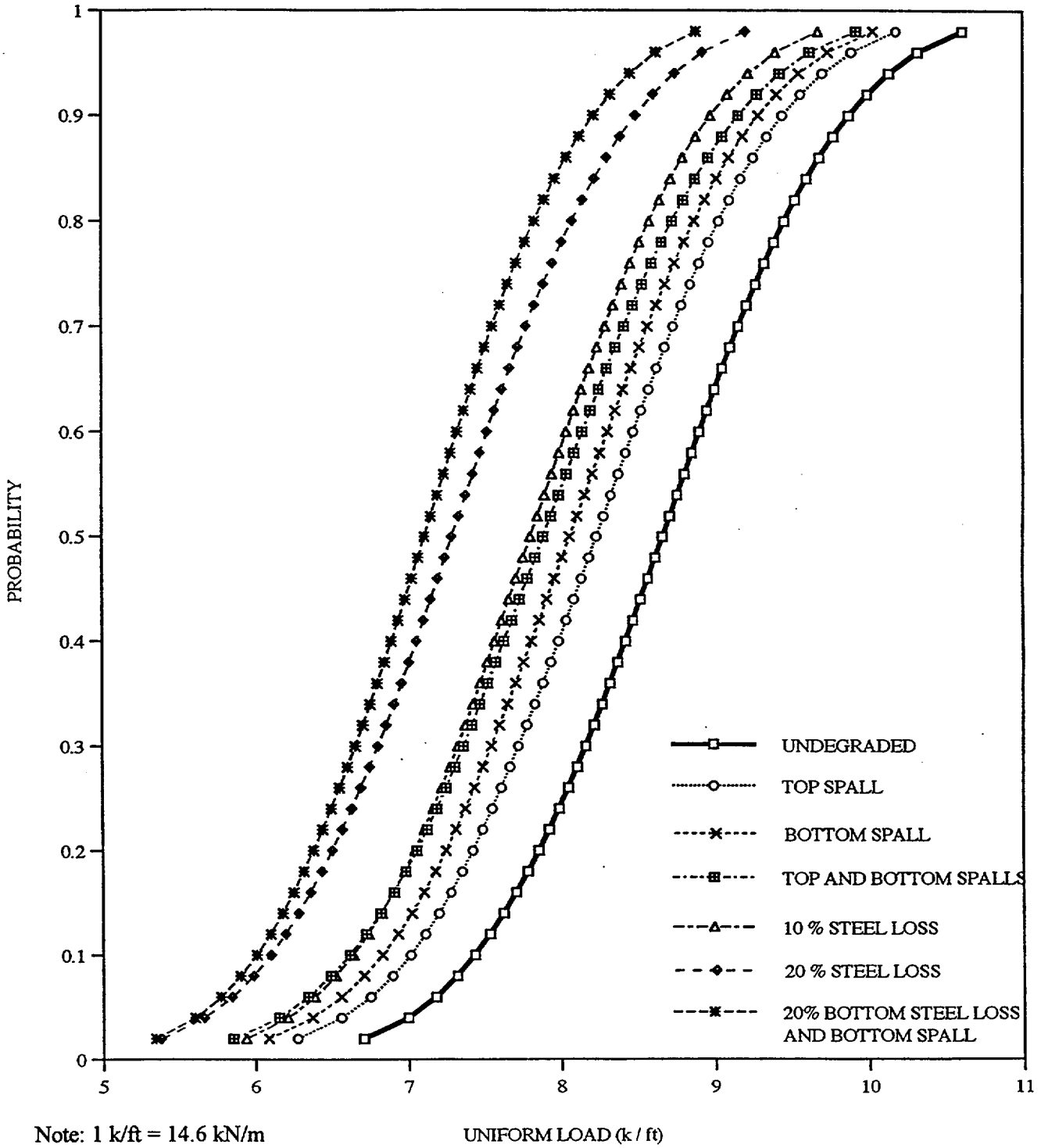

Figure 6.17 Comparison of Fragility Curves

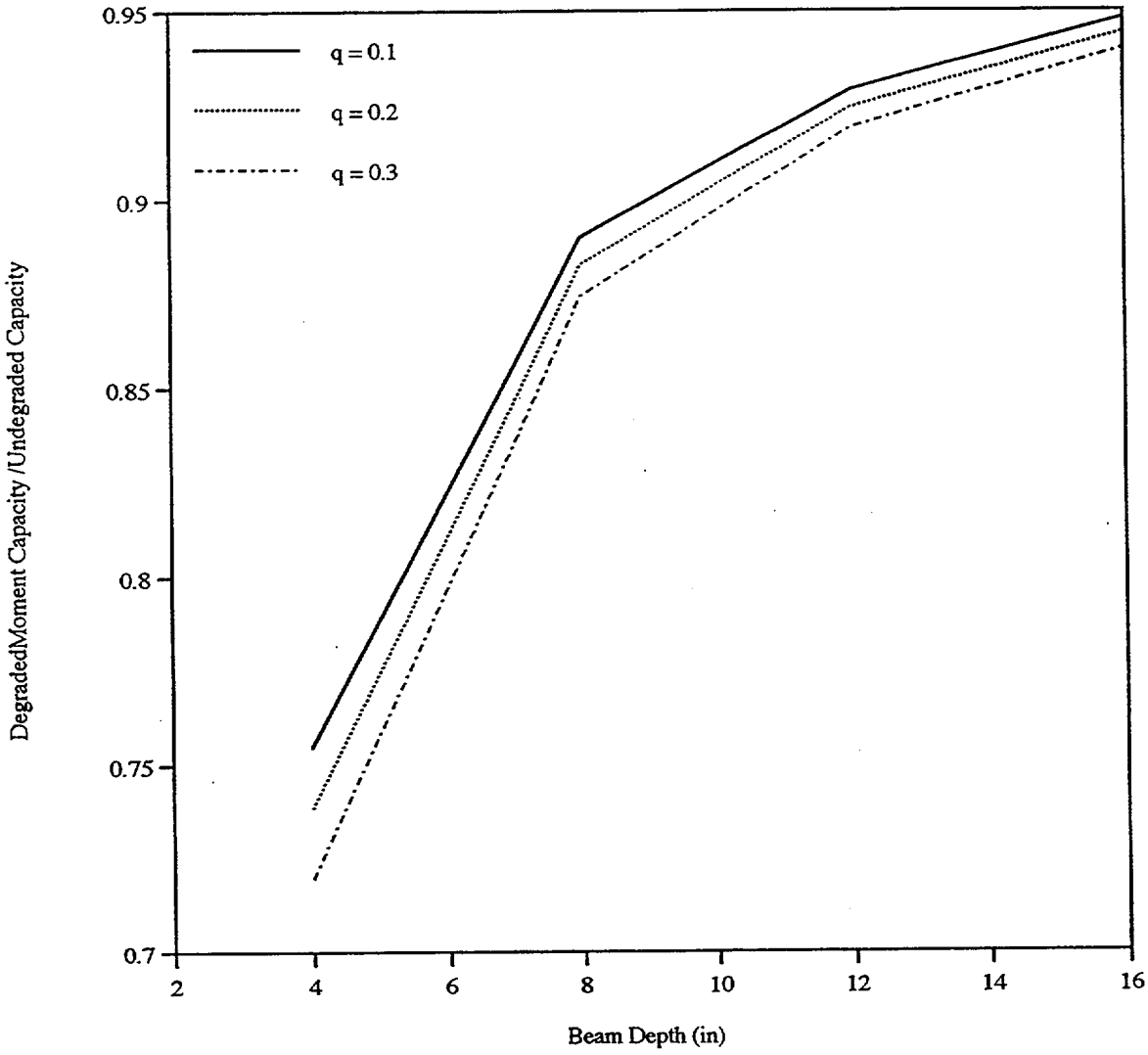

Note: 1 in. = 25.4 mm

Figure 6.18 Effect of Spall in Flexural Member with 3/4" Cover

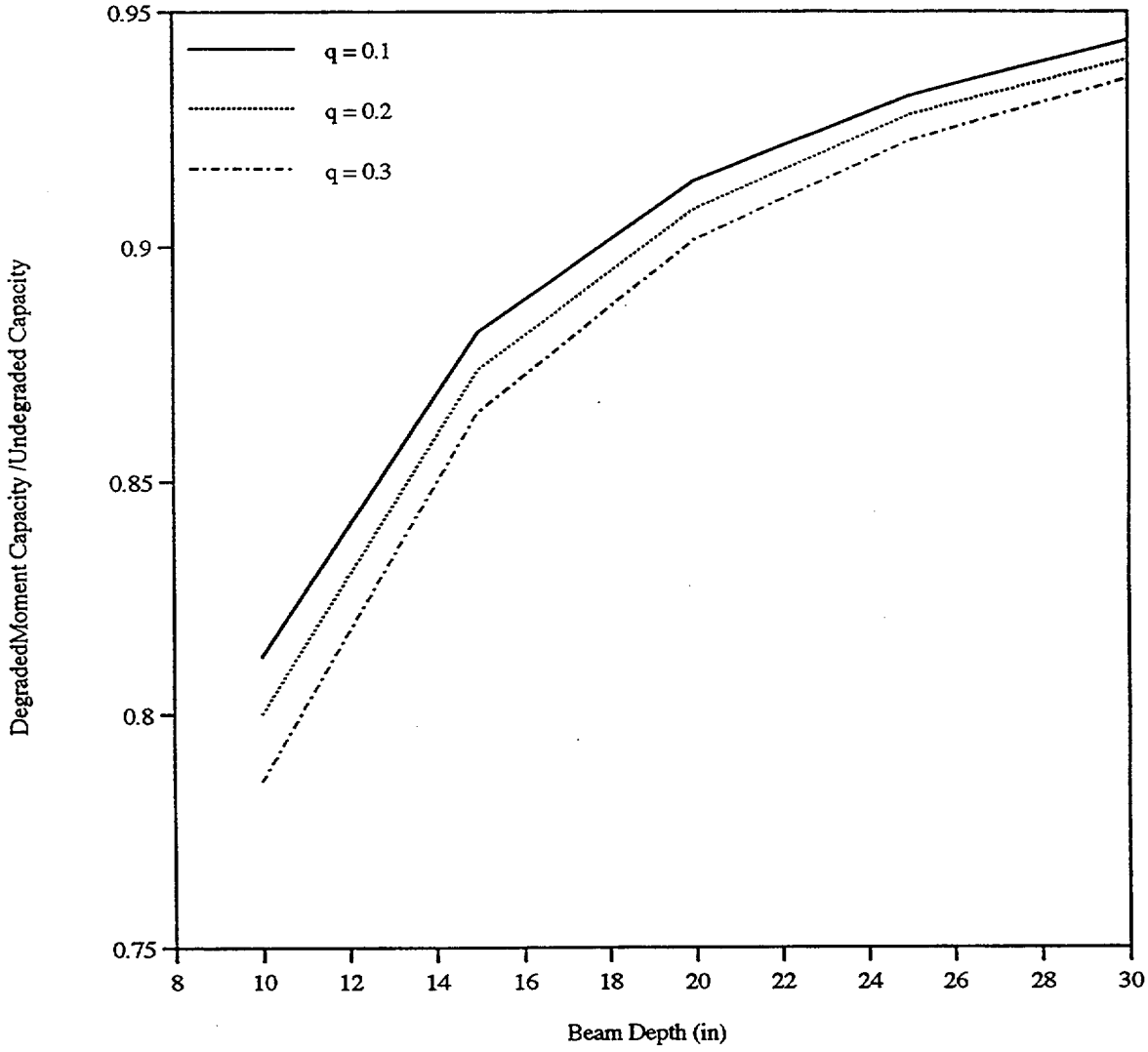

Note: 1 in. = 25.4 mm

Figure 6.19 Effect of Spall in Flexural Member with 1-1/2" Cover

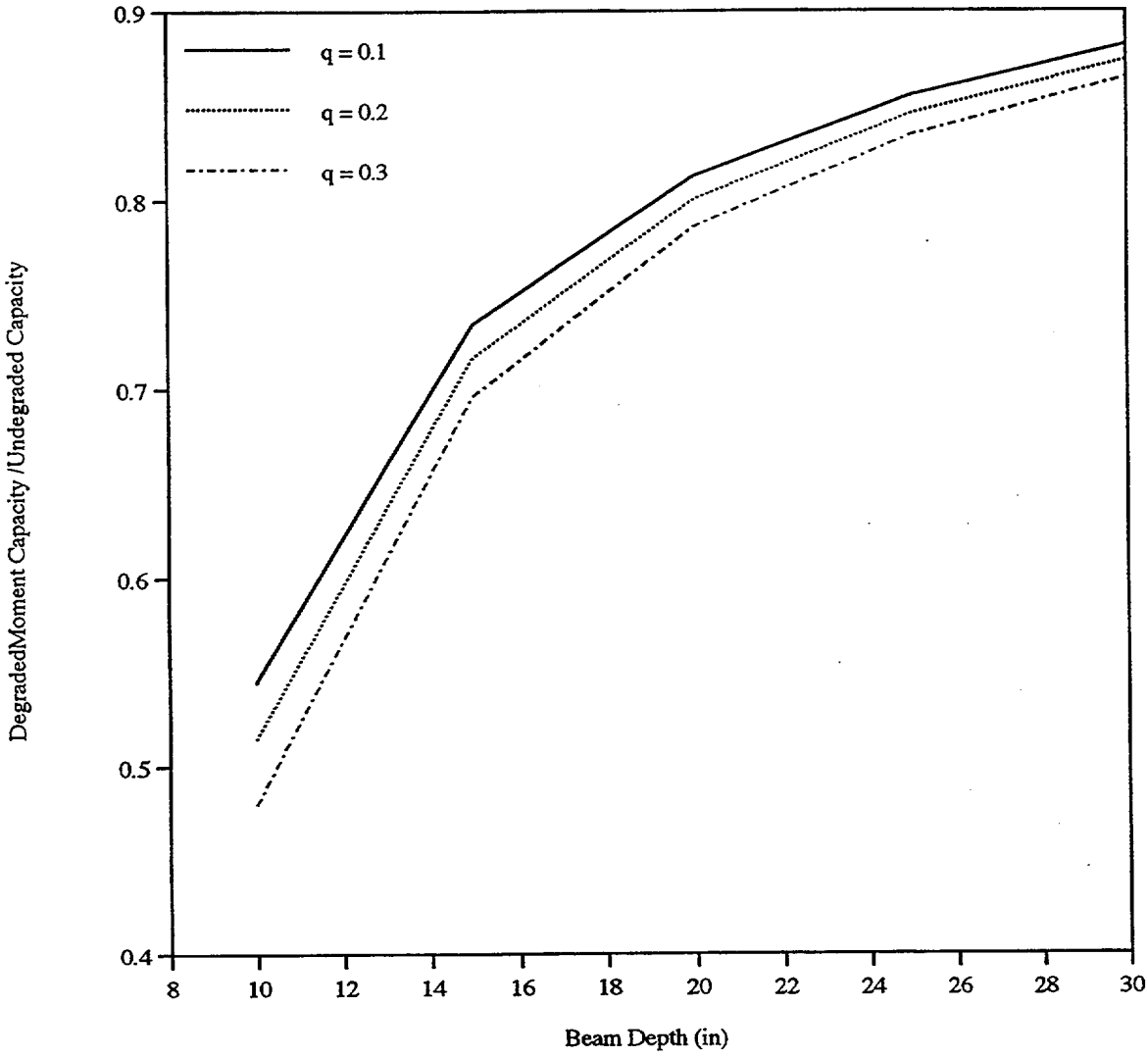

Note: 1 in. = 25.4 mm

Figure 6.20 Effect of Spall in Flexural Member with 3" Cover

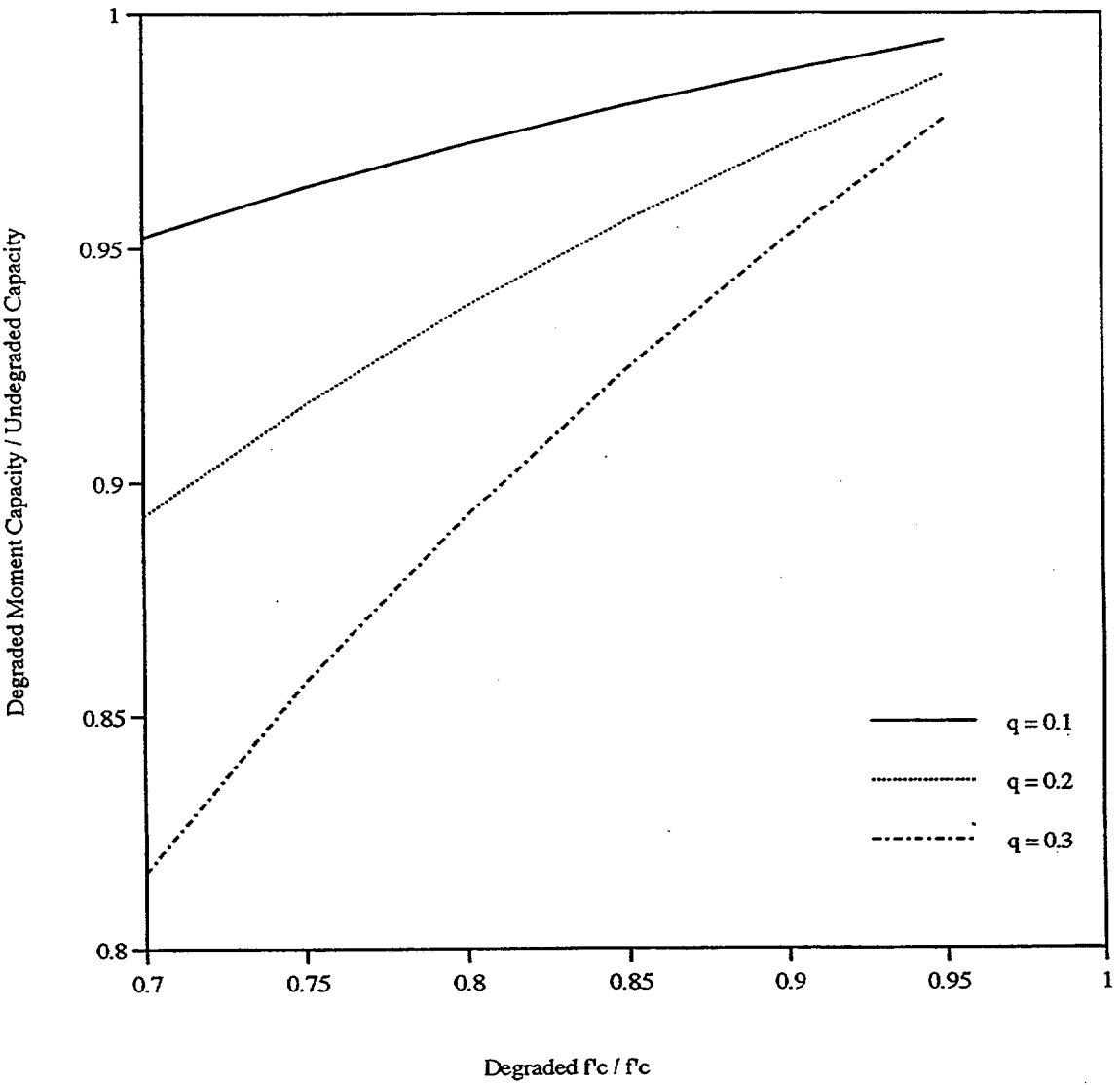

Figure 6.21 Effect of Degraded Concrete Strength on Beam Moment Capacity

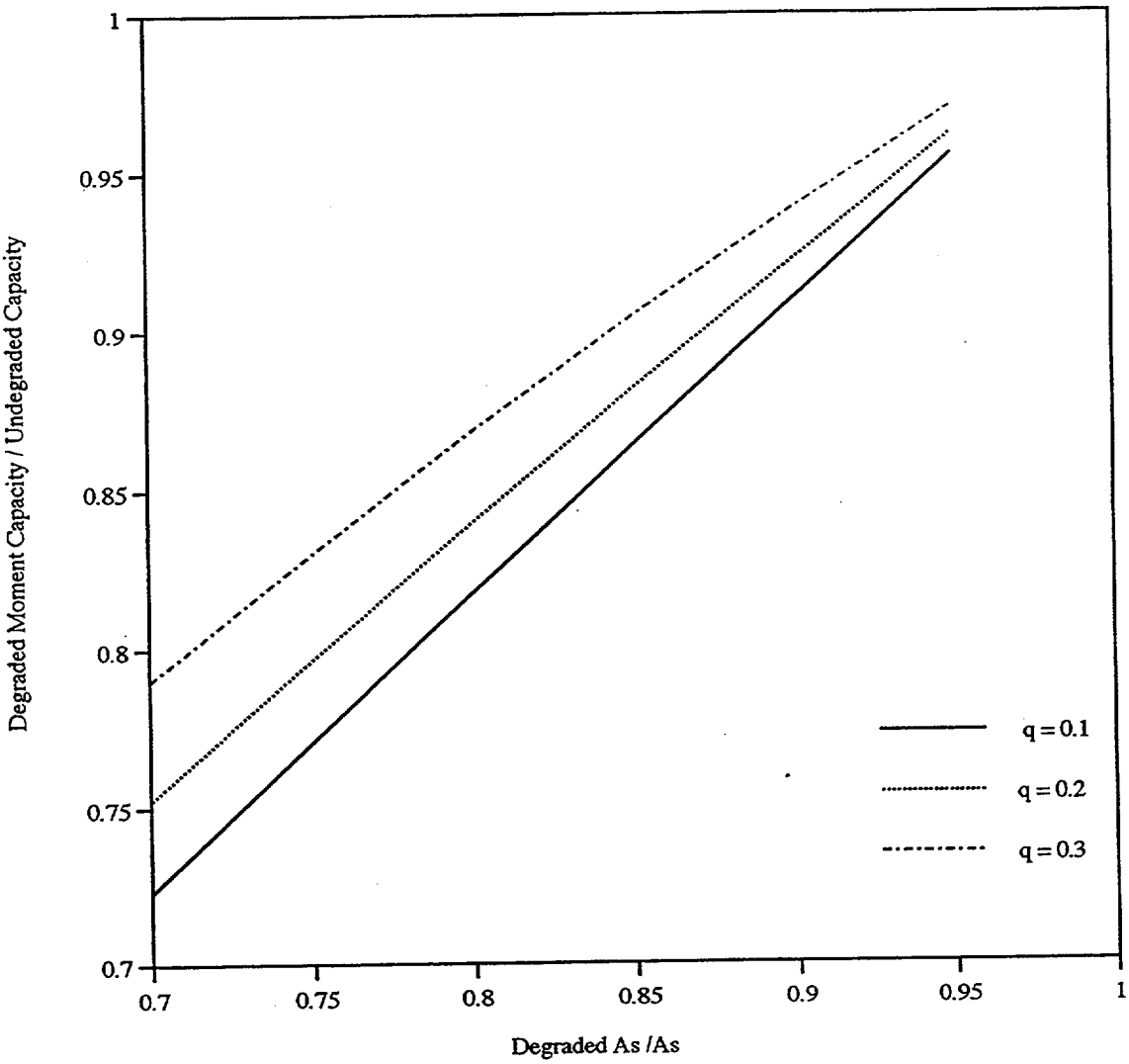

Figure 6.22 Effect of Degraded Steel Area on Beam Moment Capacity

Table 6.1

Statisical Analysis of Undegraded Propped Cantilever Beam

	fy (ksi)	f'c (ksi)	ft (ksi)	εu	d (in)	Bf	Bsh	b (in)	As+ (sq in)	As- (sq in)	β1	a+ (in)	M+ (k in)	a- (in)	M- (k in)	wf (k / ft)	As bal (sq in)
	66.9	3.321	0.332	0.0024	21.1	0.94	0.96	13	2.37	3.95	0.85	4.32	3003	7.20	4624	7.91	5.02
	54.4	4.653	0.483	0.0041	21.3	1.03	0.87	13	2.37	3.95	0.817	2.51	2585	4.18	4128	7.57	11.28
	62.4	3.783	0.384	0.0043	20.9	0.97	1	13	2.37	3.95	0.85	3.54	2829	5.90	4425	7.74	7.93
	80.1	2.915	0.286	0.0039	20.5	1.05	1.13	13	2.37	3.95	0.85	5.89	3332	9.82	4932	9.67	4.10
	70.9	3.959	0.404	0.0040	21.1	1.14	0.84	13	2.37	3.95	0.85	3.84	3223	6.40	5013	10.34	6.87
	59	4.354	0.449	0.0044	21.7	1.04	1.1	13	2.37	3.95	0.832	2.91	2831	4.84	4493	8.35	10.07
	63.4	3.552	0.358	0.0029	21	0.96	1.08	13	2.37	3.95	0.85	3.83	2868	6.38	4460	7.75	6.30
	73.8	4.063	0.416	0.0046	21.6	0.99	0.9	13	2.37	3.95	0.847	3.90	3437	6.49	5350	9.58	7.17
	66	3.4	0.341	0.0047	21.4	1.02	1.02	13	2.37	3.95	0.85	4.16	3022	6.94	4674	8.66	6.98
	67.8	3.477	0.349	0.0031	20.3	1.06	1.16	13	2.37	3.95	0.85	4.18	2926	6.97	4503	8.69	5.57
	64.3	2.75	0.267	0.0036	20.8	1.09	1.2	13	2.37	3.95	0.85	5.01	2788	8.36	4221	8.47	5.17
	69.8	4.189	0.43	0.0038	21.5	1.12	0.8	13	2.37	3.95	0.841	3.57	3261	5.96	5107	10.30	7.34
	76	2.451	0.233	0.0037	20.4	1.01	0.94	13	2.37	3.95	0.85	6.65	3076	11.08	4460	8.52	3.62
	72.2	3.627	0.367	0.0033	20.7	1	0.73	13	2.37	3.95	0.85	4.27	3177	7.12	4889	8.90	5.57
	60.3	3.145	0.312	0.0051	22	1.11	1.06	13	2.37	3.95	0.85	4.11	2850	6.85	4424	8.90	7.66
	68.7	3.704	0.375	0.0042	21.2	1.08	1.27	13	2.37	3.95	0.85	3.98	3128	6.63	4853	9.50	6.86
	61.4	3.237	0.322	0.0034	20	0.9	0.92	13	2.37	3.95	0.85	4.07	2614	6.78	4028	6.60	6.10
	57.3	3.867	0.394	0.0056	20.9	1.18	1.04	13	2.37	3.95	0.85	3.18	2622	5.30	4131	8.75	9.79
	65.1	3.041	0.3	0.0049	20.6	1.07	0.98	13	2.37	3.95	0.85	4.59	2824	7.65	4313	8.45	6.20
Mean	66	3.552	0.358	0.0040	21	1.04	1				0.85	4.07	2926	6.78	4493	8.66	6.86
Std Dev	6.59	0.56	0.06	0.0008	0.52	0.07	0.14				0.01	0.96	246.87	1.59	362.36	0.95	1.97
COV	0.100	0.159	0.179	0.1995	0.025	0.069	0.140				0.010	0.235	0.084	0.235	0.081	0.109	0.286

Note: 1 ksi = 6.89 MPa, 1 in. = 25.4 mm, 1 sq in = 6.45 cm^2, 1 k-in = 113 N-m, 1 k/ft = 14.6 kN/m

Table 6.2

Summary of Results for Degraded Beams

Degradation Mechanism	Mean wf (k / ft)	COV	2 % POF Load (k / ft)	Analysis Table	Fragility Curve
None	8.66	0.109	6.87	6.1	Fig. 6.8
Bottom Spall	8.23	0.116	6.45	6.3	Fig. 6.9
Top Spall	8.06	0.119	6.27	6.4	Fig. 6.10
Top & Bottom Spall	7.89	0.126	6.05	6.5	Fig. 6.11
10 % Loss of Top & Bottom Steel	7.81	0.117	6.11	6.6	Fig. 6.12
20 % Loss of Top and Bottom Steel	7.29	0.127	5.57	6.7	Fig. 6.13
20 % Loss of Bottom Steel & Bottom Spall	7.11	0.121	5.51	6.8	Fig. 6.14
20 % Loss of Top Steel and Top Spall	7.45	0.119	5.79	6.9	Fig. 6.15

Note: 1 k/ft = 14.6 kN/m

Table 6.3

Statisical Analysis of Degraded Propped Cantilever (Bottom Spall)

	fy (ksi)	f'c (ksi)	ft (ksi)	d (in)	Cover (in)	Bf	Bsh	b (in)	As+ (sq in)	As- (sq in)	β1	a+ (in)	M+ (k in)	a- (in)	M- (k in)	wf (k / ft)
	66.9	3.321	0.332	21.1	2.63	0.94	0.96	13	2.37	3.95	0.85	4.32	3003	7.20	3929	7.47
	54.4	4.653	0.483	21.3	1.75	1.03	0.87	13	2.37	3.95	0.817	2.61	2578	4.35	3734	7.28
	62.4	3.783	0.384	20.9	1.67	0.97	1	13	2.37	3.95	0.85	3.54	2829	5.90	4013	7.47
	80.1	2.915	0.286	20.5	1.3	1.05	1.13	13	2.37	3.95	0.85	5.89	3332	9.82	4521	9.38
	70.9	3.959	0.404	21.1	2	1.14	0.84	13	2.37	3.95	0.85	3.84	3223	6.40	4453	9.91
	59	4.354	0.449	21.7	1.05	1.04	1.1	13	2.37	3.95	0.832	2.97	2827	4.95	4236	8.16
	63.4	3.552	0.358	21	1.58	0.96	1.08	13	2.37	3.95	0.85	3.83	2868	6.38	4064	7.49
	73.8	4.063	0.416	21.6	2.1	0.99	0.9	13	2.37	3.95	0.847	3.91	3436	6.52	4735	9.17
	66	3.4	0.341	21.4	1.4	1.02	1.02	13	2.37	3.95	0.85	4.16	3022	6.94	4309	8.41
	67.8	3.477	0.349	20.3	2.45	1.06	1.16	13	2.37	3.95	0.85	4.18	2926	6.97	3847	8.23
	64.3	2.75	0.267	20.8	0.87	1.09	1.2	13	2.37	3.95	0.85	5.01	2788	8.36	4000	8.30
	69.8	4.189	0.43	21.5	0.54	1.12	0.8	13	2.37	3.95	0.841	3.61	3258	6.02	4949	10.18
	76	2.451	0.233	20.4	1.5	1.01	0.94	13	2.37	3.95	0.85	6.65	3076	11.08	4010	8.22
	72.2	3.627	0.367	20.7	1.83	1	0.73	13	2.37	3.95	0.85	4.27	3177	7.12	4367	8.55
	60.3	3.145	0.312	22	2.2	1.11	1.06	13	2.37	3.95	0.85	4.11	2850	6.85	3900	8.50
	68.7	3.714	0.375	21.2	1.19	1.08	1.27	13	2.37	3.95	0.85	3.97	3129	6.61	4533	9.27
	61.4	3.237	0.322	20	2.31	0.9	0.92	13	2.37	3.95	0.85	4.07	2614	6.78	3468	6.26
	57.3	3.867	0.394	20.9	2.96	1.18	1.04	13	2.37	3.95	0.85	3.18	2622	5.30	3461	8.22
	65.1	3.041	0.3	20.6	1.92	1.07	0.98	13	2.37	3.95	0.85	4.59	2824	7.65	3820	8.09
Mean	66	3.552	0.358	21	1.75	1.04	1				0.850	4.068	2926	6.78	4013	8.23
Std Dev	6.59	0.56	0.06	0.52	0.62	0.07	0.14				0.008	0.942	247.27	1.57	402.47	0.95
COV	0.100	0.159	0.179	0.025	0.355	0.069	0.140				0.010	0.231	0.085	0.231	0.100	0.116

Note: 1 ksi = 6.89 MPa, 1 in. = 25.4 mm, 1 sq in = 6.45 cm^2, 1 k-in = 113 N-m, 1 k/ft = 14.6 kN/m

Table 6.4

Statisical Analysis of Propped Cantilever (Top Spall)

	fy (ksi)	f'c (ksi)	ft (ksi)	d (in)	Cover (in)	Bf	Bsh	b (in)	As+ (sq in)	As- (sq in)	β1	a+ (in)	M+ (k in)	a- (in)	M- (k in)	wf (k / ft)
	66.9	3.321	0.332	21.1	2.63	0.94	0.96	13	2.37	3.95	0.85	4.32	2586	7.20	4624	7.22
	54.4	4.653	0.483	21.3	1.75	1.03	0.87	13	2.37	3.95	0.817	2.61	2352	4.35	4110	7.13
	62.4	3.783	0.384	20.9	1.67	0.97	1	13	2.37	3.95	0.85	3.54	2582	5.90	4425	7.31
	80.1	2.915	0.286	20.5	1.3	1.05	1.13	13	2.37	3.95	0.85	5.89	3085	9.82	4932	9.21
	70.9	3.959	0.404	21.1	2	1.14	0.84	13	2.37	3.95	0.85	3.84	2887	6.40	5013	9.66
	59	4.354	0.449	21.7	1.05	1.04	1.1	13	2.37	3.95	0.832	2.97	2680	4.95	4481	8.06
	63.4	3.552	0.358	21	1.58	0.96	1.08	13	2.37	3.95	0.85	3.83	2630	6.38	4460	7.34
	73.8	4.063	0.416	21.6	2.1	0.99	0.9	13	2.37	3.95	0.847	3.91	3069	6.52	5347	8.93
	66	3.4	0.341	21.4	1.4	1.02	1.02	13	2.37	3.95	0.85	4.16	2803	6.94	4674	8.26
	67.8	3.477	0.349	20.3	2.45	1.06	1.16	13	2.37	3.95	0.85	4.18	2532	6.97	4503	7.95
	64.3	2.75	0.267	20.8	0.87	1.09	1.2	13	2.37	3.95	0.85	5.01	2655	8.36	4221	8.21
	69.8	4.189	0.43	21.5	0.54	1.12	0.8	13	2.37	3.95	0.841	3.61	3169	6.02	5098	10.11
	76	2.451	0.233	20.4	1.5	1.01	0.94	13	2.37	3.95	0.85	6.65	2805	11.08	4460	8.04
	72.2	3.627	0.367	20.7	1.83	1	0.73	13	2.37	3.95	0.85	4.27	2864	7.12	4889	8.35
	60.3	3.145	0.312	22	2.2	1.11	1.06	13	2.37	3.95	0.85	4.11	2536	6.85	4424	8.28
	68.7	3.714	0.375	21.2	1.19	1.08	1.27	13	2.37	3.95	0.85	3.97	2935	6.61	4856	9.13
	61.4	3.237	0.322	20	2.31	0.9	0.92	13	2.37	3.95	0.85	4.07	2278	6.78	4028	6.06
	57.3	3.867	0.394	20.9	2.96	1.18	1.04	13	2.37	3.95	0.85	3.18	2220	5.30	4131	7.91
	65.1	3.041	0.3	20.6	1.92	1.07	0.98	13	2.37	3.95	0.85	4.59	2528	7.65	4313	7.89
Mean	66	3.552	0.358	21	1.75	1.04					0.850	4.068	2655	6.78	4481	8.06
Std Dev	6.59	0.56	0.06	0.52	0.62	0.07					0.008	0.942	268	1.57	362.82	0.96
COV	0.100	0.159	0.179	0.025	0.355	0.069					0.010	0.231	0.101	0.231	0.081	0.119

Note: 1 ksi = 6.89 MPa, 1 in. = 25.4 mm, 1 sq in = 6.45 cm^2, 1 k-in = 113 N-m, 1 k/ft = 14.6 kN/m

Table 6.5

Statisical Analysis of Propped Cantilever (Top and Bottom Spall)

	fy (ksi)	f'c (ksi)	ft (ksi)	d (in)	Cover (in)	Bf	Bsh	b (in)	As+ (sq in)	As- (sq in)	β1	a+ (in)	M+ (k in)	a- (in)	M- (k in)	wf (k / ft)
	66.9	3.321	0.332	21.1	2.63	0.94	0.96	13	2.37	3.95	0.85	4.32	2586	7.20	3929	6.78
	54.4	4.653	0.483	21.3	1.75	1.03	0.87	13	2.37	3.95	0.817	2.61	2352	4.35	3734	6.87
	62.4	3.783	0.384	20.9	1.67	0.97	1	13	2.37	3.95	0.85	3.54	2582	5.90	4013	7.05
	80.1	2.915	0.286	20.5	1.3	1.05	1.13	13	2.37	3.95	0.85	5.89	3085	9.82	4521	8.92
	70.9	3.959	0.404	21.1	.2	1.14	0.84	13	2.37	3.95	0.85	3.84	2887	6.40	4453	9.23
	59	4.354	0.449	21.7	1.05	1.04	1.1	13	2.37	3.95	0.832	2.97	2680	4.95	4236	7.89
	63.4	3.552	0.358	21	1.58	0.96	1.08	13	2.37	3.95	0.85	3.83	2630	6.38	4064	7.09
	73.8	4.063	0.416	21.6	2.1	0.99	0.9	13	2.37	3.95	0.847	3.91	3069	6.52	4735	8.52
	66	3.4	0.341	21.4	1.4	1.02	1.02	13	2.37	3.95	0.85	4.16	2803	6.94	4309	8.01
	67.8	3.477	0.349	20.3	2.45	1.06	1.16	13	2.37	3.95	0.85	4.18	2532	6.97	3847	7.49
	64.3	2.75	0.267	20.8	0.87	1.09	1.2	13	2.37	3.95	0.85	5.01	2655	8.36	4000	8.05
	69.8	4.189	0.43	21.5	0.54	1.12	0.8	13	2.37	3.95	0.841	3.61	3169	6.02	4949	10.00
	76	2.451	0.233	20.4	1.5	1.01	0.94	13	2.37	3.95	0.85	6.65	2805	11.08	4010	7.73
	72.2	3.627	0.367	20.7	1.83	1	0.73	13	2.37	3.95	0.85	4.27	2864	7.12	4367	8.00
	60.3	3.145	0.312	22	2.2	1.11	1.06	13	2.37	3.95	0.85	4.11	2536	6.85	3900	7.89
	68.7	3.714	0.375	21.2	1.19	1.08	1.27	13	2.37	3.95	0.85	3.97	2935	6.61	4533	8.90
	61.4	3.237	0.322	20	2.31	0.9	0.92	13	2.37	3.95	0.85	4.07	2278	6.78	3468	5.72
	57.3	3.867	0.394	20.9	2.96	1.18	1.04	13	2.37	3.95	0.85	3.18	2220	5.30	3461	7.38
	65.1	3.041	0.3	20.6	1.92	1.07	0.98	13	2.37	3.95	0.85	4.59	2528	7.65	3820	7.53
Mean	66	3.552	0.358	21	1.75	1.04					0.850	4.068	2655	6.78	4013	7.89
Std Dev	6.59	0.56	0.06	0.52	0.62	0.07					0.008	0.942	268	1.57	402.47	0.99
COV	0.100	0.159	0.179	0.025	0.355	0.069					0.010	0.231	0.101	0.231	0.100	0.126

Note: 1 ksi = 6.89 MPa, 1 in. = 25.4 mm, 1 sq in = 6.45 cm^2, 1 k-in = 113 N-m, 1 k/ft = 14.6 kN/m

Table 6.6

Statisical Analysis of Propped Cantilever (10 % Steel Loss)

	fy (ksi)	f'c (ksi)	ft (ksi)	d (in)	Cover (in)	Bf	Bsh	b (in)	As (10%) (sq in)	As (20%) (sq in)	As+ (sq in)	As- (sq in)	β1	a+ (in)	M+ (k in)	a- (in)	M- (k in)	wf (k / ft)
	66.9	3.321	0.332	21.1	2.63	0.94	0.96	13	0.710	0.726	2.13	3.55	0.85	3.883	2730	6.472	4243	7.219
	54.4	4.653	0.483	21.3	1.75	1.03	0.87	13	0.725	0.581	2.175	3.625	0.817	2.301	2384	3.835	3822	6.989
	62.4	3.783	0.384	20.9	1.67	0.97	1	13	0.675	0.646	2.025	3.375	0.85	3.023	2450	5.038	3871	6.726
	80.1	2.915	0.286	20.5	1.3	1.05	1.13	13	0.731	0.600	2.193	3.655	0.85	5.453	3122	9.089	4671	9.094
	70.9	3.959	0.404	21.1	2	1.14	0.84	13	0.756	0.619	2.268	3.78	0.85	3.676	3097	6.126	4834	9.948
	59	4.354	0.449	21.7	1.05	1.04	1.1	13	0.706	0.569	2.118	3.53	0.832	2.597	2549	4.329	4069	7.533
	63.4	3.552	0.358	21	1.58	0.96	1.08	13	0.720	0.636	2.16	3.6	0.85	3.489	2637	5.815	4129	7.141
	73.8	4.063	0.416	21.6	2.1	0.99	0.9	13	0.658	0.677	1.974	3.29	0.847	3.245	2910	5.408	4588	8.148
	66	3.4	0.341	21.4	1.4	1.02	1.02	13	0.745	0.537	2.235	3.725	0.85	3.926	2867	6.544	4457	8.227
	67.8	3.477	0.349	20.3	2.45	1.06	1.16	13	0.692	0.591	2.076	3.46	0.85	3.663	2599	6.106	4046	7.755
	64.3	2.75	0.267	20.8	0.87	1.09	1.2	13	0.697	0.555	2.091	3.485	0.85	4.425	2499	7.374	3835	7.627
	69.8	4.189	0.43	21.5	0.54	1.12	0.8	13	0.667	0.610	2.001	3.335	0.841	3.017	2792	5.029	4420	8.857
	76	2.451	0.233	20.4	1.5	1.01	0.94	13	0.701	0.656	2.103	3.505	0.85	5.901	2789	9.835	4124	7.781
	72.2	3.627	0.367	20.7	1.83	1	0.73	13	0.715	0.628	2.145	3.575	0.85	3.864	2907	6.440	4512	8.173
	60.3	3.145	0.312	22	2.2	1.11	1.06	13	0.681	0.705	2.043	3.405	0.85	3.545	2492	5.908	3911	7.809
	68.7	3.714	0.375	21.2	1.19	1.08	1.27	13	0.640	0.689	1.92	3.2	0.85	3.214	2584	5.357	4072	7.892
	61.4	3.237	0.322	20	2.31	0.9	0.92	13	0.687	0.764	2.061	3.435	0.85	3.538	2307	5.896	3596	5.847
	57.3	3.867	0.394	20.9	2.96	1.18	1.04	13	0.775	0.665	2.325	3.875	0.85	3.118	2577	5.196	4064	8.600
	65.1	3.041	0.3	20.6	1.92	1.07	0.98	13	0.737	0.504	2.211	3.685	0.85	4.283	2657	7.139	4086	7.965
Mean	66	3.552	0.358	21	1.75	1.04	1		0.706	0.628			0.850	3.545	2637	5.908	4086	7.809
Std Dev	6.59	0.56	0.06	0.52	0.62	0.07	0.14		0.03	0.07			0.008	0.878	227	1.46	325.68	0.91
COV	0.100	0.159	0.179	0.025	0.355	0.069	0.140		0.049	0.106			0.010	0.248	0.086	0.248	0.080	0.117

Note: 1 ksi = 6.89 MPa, 1 in. = 25.4 mm, 1 sq in = 6.45 cm^2, 1 k-in = 113 N-m, 1 k/ft = 14.6 kN/m

Table 6.7

Statisical Analysis of Propped Cantilever (20 % Steel Loss)

	fy (ksi)	f'c (ksi)	ft (ksi)	d (in)	Cover (in)	Bf	Bsh	b (in)	As (10%) (sq in)	As (20%) (sq in)	As+ (sq in)	As- (sq in)	β1	a+ (in)	M+ (k in)	a- (in)	M- (k in)	wf (k / ft)
	66.9	3.321	0.332	21.1	2.63	0.94	0.96	13	0.710	0.726	2.178	3.63	0.85	3.971	2785	6.618	4321	7.360
	54.4	4.653	0.483	21.3	1.75	1.03	0.87	13	0.725	0.581	1.743	2.905	0.817	1.844	1932	3.074	3123	5.682
	62.4	3.783	0.384	20.9	1.67	0.97	1	13	0.675	0.646	1.938	3.23	0.85	2.893	2353	4.822	3727	6.465
	80.1	2.915	0.286	20.5	1.3	1.05	1.13	13	0.731	0.600	1.8	3	0.85	4.476	2633	7.460	4030	7.733
	70.9	3.959	0.404	21.1	2	1.14	0.84	13	0.756	0.619	1.857	3.095	0.85	3.010	2580	5.016	4080	8.327
	59	4.354	0.449	21.7	1.05	1.04	1.1	13	0.706	0.569	1.707	2.845	0.832	2.093	2080	3.489	3350	6.167
	63.4	3.552	0.358	21	1.58	0.96	1.08	13	0.720	0.636	1.908	3.18	0.85	3.082	2354	5.137	3716	6.394
	73.8	4.063	0.416	21.6	2.1	0.99	0.9	13	0.658	0.677	2.031	3.385	0.847	3.339	2987	5.564	4701	8.358
	66	3.4	0.341	21.4	1.4	1.02	1.02	13	0.745	0.537	1.611	2.685	0.85	2.830	2125	4.717	3374	6.146
	67.8	3.477	0.349	20.3	2.45	1.06	1.16	13	0.692	0.591	1.773	2.955	0.85	3.129	2252	5.215	3545	6.747
	64.3	2.75	0.267	20.8	0.87	1.09	1.2	13	0.697	0.555	1.665	2.775	0.85	3.523	2038	5.872	3188	6.264
	69.8	4.189	0.43	21.5	0.54	1.12	0.8	13	0.667	0.610	1.83	3.05	0.841	2.760	2570	4.599	4088	8.167
	76	2.451	0.233	20.4	1.5	1.01	0.94	13	0.701	0.656	1.968	3.28	0.85	5.522	2638	9.204	3938	7.385
	72.2	3.627	0.367	20.7	1.83	1	0.73	13	0.715	0.628	1.884	3.14	0.85	3.394	2585	5.657	4052	7.294
	60.3	3.145	0.312	22	2.2	1.11	1.06	13	0.681	0.705	2.115	3.525	0.85	3.670	2572	6.116	4026	8.052
	68.7	3.714	0.375	21.2	1.19	1.08	1.27	13	0.640	0.689	2.067	3.445	0.85	3.460	2765	5.767	4335	8.427
	61.4	3.237	0.322	20	2.31	0.9	0.92	13	0.687	0.764	2.292	3.82	0.85	3.934	2538	6.557	3922	6.411
	57.3	3.867	0.394	20.9	2.96	1.18	1.04	13	0.775	0.665	1.995	3.325	0.85	2.675	2236	4.459	3557	7.488
	65.1	3.041	0.3	20.6	1.92	1.07	0.98	13	0.737	0.504	1.512	2.52	0.85	2.929	1884	4.882	2979	5.706
Mean	66	3.552	0.358	21	1.75	1.04	1		0.706	0.628			0.850	3.129	2538	5.215	3922	7.294
Std Dev	6.59	0.56	0.06	0.52	0.62	0.07	0.14		0.03	0.07			0.008	0.828	309	1.38	456.90	0.93
COV	0.100	0.159	0.179	0.025	0.355	0.069	0.140		0.049	0.106			0.010	0.265	0.122	0.265	0.116	0.127

Note: 1 ksi = 6.89 MPa, 1 in. = 25.4 mm, 1 sq in = 6.45 cm^2, 1 k-in = 113 N-m, 1 k/ft = 14.6 kN/m

Table 6.8

Statisical Analysis of Propped Cantilever (20 % Bottom Steel Loss and Bottom Spall)

	fy (ksi)	f'c (ksi)	ft (ksi)	d (in)	Cover (in)	Bf	Bsh	b (in)	As (20%) (sq in)	As+ (sq in)	As- (sq in)	β1	a+ (in)	M+ (k in)	a- (in)	M- (k in)	wf (k / ft)
	66.9	3.321	0.332	21.1	2.63	0.94	0.96	13	0.726	2.178	3.95	0.85	3.971	2785	7.201	3929	7.112
	54.4	4.653	0.483	21.3	1.75	1.03	0.87	13	0.581	1.743	3.95	0.817	1.844	1932	4.179	3752	6.117
	62.4	3.783	0.384	20.9	1.67	0.97	1	13	0.646	1.938	3.95	0.85	2.893	2353	5.896	4013	6.652
	80.1	2.915	0.286	20.5	1.3	1.05	1.13	13	0.600	1.8	3.95	0.85	4.476	2633	9.823	4521	8.080
	70.9	3.959	0.404	21.1	2	1.14	0.84	13	0.619	1.857	3.95	0.85	3.010	2580	6.402	4453	8.613
	59	4.354	0.449	21.7	1.05	1.04	1.1	13	0.569	1.707	3.95	0.832	2.093	2080	4.844	4248	6.795
	63.4	3.552	0.358	21	1.58	0.96	1.08	13	0.636	1.908	3.95	0.85	3.082	2354	6.380	4064	6.619
	73.8	4.063	0.416	21.6	2.1	0.99	0.9	13	0.677	2.031	3.95	0.847	3.339	2987	6.493	4738	8.383
	66	3.4	0.341	21.4	1.4	1.02	1.02	13	0.537	1.611	3.95	0.85	2.830	2125	6.939	4309	6.787
	67.8	3.477	0.349	20.3	2.45	1.06	1.16	13	0.591	1.773	3.95	0.85	3.129	2252	6.970	3847	6.963
	64.3	2.75	0.267	20.8	0.87	1.09	1.2	13	0.555	1.665	3.95	0.85	3.523	2038	8.358	4000	6.860
	69.8	4.189	0.43	21.5	0.54	1.12	0.8	13	0.610	1.83	3.95	0.841	2.760	2570	5.956	4958	8.822
	76	2.451	0.233	20.4	1.5	1.01	0.94	13	0.656	1.968	3.95	0.85	5.522	2638	11.084	4010	7.434
	72.2	3.627	0.367	20.7	1.83	1	0.73	13	0.628	1.884	3.95	0.85	3.394	2585	7.116	4367	7.506
	60.3	3.145	0.312	22	2.2	1.11	1.06	13	0.705	2.115	3.95	0.85	3.670	2572	6.854	3900	7.958
	68.7	3.714	0.375	21.2	1.19	1.08	1.27	13	0.689	2.067	3.95	0.85	3.460	2765	6.612	4533	8.571
	61.4	3.237	0.322	20	2.31	0.9	0.92	13	0.764	2.292	3.95	0.85	3.934	2538	6.780	3468	6.137
	57.3	3.867	0.394	20.9	2.96	1.18	1.04	13	0.665	1.995	3.95	0.85	2.675	2236	5.297	3461	7.411
	65.1	3.041	0.3	20.6	1.92	1.07	0.98	13	0.504	1.512	3.95	0.85	2.929	1884	7.652	3820	6.311
Mean	66	3.552	0.358	21	1.75	1.04	1		0.628			0.850	3.129	2538	6.780	4013	7.112
Std Dev	6.59	0.56	0.06	0.52	0.62	0.07	0.14		0.07			0.008	0.828	309	1.59	403.00	0.86
COV	0.100	0.159	0.179	0.025	0.355	0.069	0.140		0.106			0.010	0.265	0.122	0.235	0.100	0.121

Note: 1 ksi = 6.89 MPa, 1 in. = 25.4 mm, 1 sq in = 6.45 cm^2, 1 k-in = 113 N-m, 1 k/ft = 14.6 kN/m

Table 6.9

Statisical Analysis of Propped Cantilever (20 % Top Steel Loss and Top Spall)

	fy (ksi)	f'c (ksi)	ft (ksi)	d (in)	Cover (in)	Bf	Bsh	b (in)	As (20%) (sq in)	As+ (sq in)	As- (sq in)	β1	a+ (in)	M+ (k in)	a- (in)	M- (k in)	wf (k / ft)
	66.9	3.321	0.332	21.1	2.63	0.94	0.96	13	0.726	2.37	3.63	0.85	4.321	2586	6.618	4321	7.028
	54.4	4.653	0.483	21.3	1.75	1.03	0.87	13	0.581	2.37	2.905	0.817	2.508	2359	3.074	3123	6.459
	62.4	3.783	0.384	20.9	1.67	0.97	1	13	0.646	2.37	3.23	0.85	3.538	2582	4.822	3727	6.859
	80.1	2.915	0.286	20.5	1.3	1.05	1.13	13	0.600	2.37	3	0.85	5.894	3085	7.460	4030	8.573
	70.9	3.959	0.404	21.1	2	1.14	0.84	13	0.619	2.37	3.095	0.85	3.841	2887	5.016	4080	8.946
	59	4.354	0.449	21.7	1.05	1.04	1.1	13	0.569	2.37	2.845	0.832	2.906	2684	3.489	3350	7.278
	63.4	3.552	0.358	21	1.58	0.96	1.08	13	0.636	2.37	3.18	0.85	3.828	2630	5.137	3716	6.863
	73.8	4.063	0.416	21.6	2.1	0.99	0.9	13	0.677	2.37	3.385	0.847	3.896	3070	5.564	4701	8.503
	66	3.4	0.341	21.4	1.4	1.02	1.02	13	0.537	2.37	2.685	0.85	4.163	2803	4.717	3374	7.369
	67.8	3.477	0.349	20.3	2.45	1.06	1.16	13	0.591	2.37	2.955	0.85	4.182	2532	5.215	3545	7.272
	64.3	2.75	0.267	20.8	0.87	1.09	1.2	13	0.555	2.37	2.775	0.85	5.015	2655	5.872	3188	7.453
	69.8	4.189	0.43	21.5	0.54	1.12	0.8	13	0.610	2.37	3.05	0.841	3.574	3172	4.599	4088	9.359
	76	2.451	0.233	20.4	1.5	1.01	0.94	13	0.656	2.37	3.28	0.85	6.651	2805	9.204	3938	7.684
	72.2	3.627	0.367	20.7	1.83	1	0.73	13	0.628	2.37	3.14	0.85	4.269	2864	5.657	4052	7.787
	60.3	3.145	0.312	22	2.2	1.11	1.06	13	0.705	2.37	3.525	0.85	4.112	2536	6.116	4026	7.981
	68.7	3.714	0.375	21.2	1.19	1.08	1.27	13	0.689	2.37	3.445	0.85	3.967	2935	5.767	4335	8.752
	61.4	3.237	0.322	20	2.31	0.9	0.92	13	0.764	2.37	3.82	0.85	4.068	2278	6.557	3922	5.998
	57.3	3.867	0.394	20.9	2.96	1.18	1.04	13	0.665	2.37	3.325	0.85	3.178	2220	4.459	3557	7.455
	65.1	3.041	0.3	20.6	1.92	1.07	0.98	13	0.504	2.37	2.52	0.85	4.591	2528	4.882	2979	6.926
Mean	66	3.552	0.358	21	1.75	1.04	1		0.628			0.850	4.068	2655	5.215	3922	7.453
Std Dev	6.59	0.56	0.06	0.52	0.62	0.07	0.14		0.07			0.008	0.957	268	1.38	456.90	0.89
COV	0.100	0.159	0.179	0.025	0.355	0.069	0.140		0.106			0.010	0.235	0.101	0.265	0.116	0.119

Note: 1 ksi = 6.89 MPa, 1 in. = 25.4 mm, 1 sq in = 6.45 cm^2, 1 k-in = 113 N-m, 1 k/ft = 14.6 kN/m

7 EVALUATION OF REINFORCED CONCRETE SHEAR WALLS

The effects of degradation on the behavior of reinforced concrete shear walls are discussed in this section. Characteristics of the shear walls studied are selected to be representative of those found in nuclear power plants (NPPs). These characteristics are discussed in some detail in the ASCE Publication, "Stiffness of Low Rise Reinforced Concrete Shear Walls," (ASCE, 1994). A specific shear wall, selected as being representative, has a height/width ratio equal to one, a thickness equal to 2 ft (61.0 cm), and a reinforcement ratio equal to 0.003 in each direction. Fragility data are developed for this wall considering the concrete compressive strength, the concrete tensile strength, the steel yield strength, the concrete initial tangent modulus (initial modulus of elasticity), the concrete compressive failure strain, and shear wall modeling as random variables (see Tables 5.1 and 5.2). The load-deflection characteristics of the wall are evaluated with the ANSYS computer code. Lognormal fragility curves are then developed for degraded and undegraded conditions of the wall. Comparisons of the degraded and undegraded fragility curves are used to evaluate the effect of degradation on the wall.

As noted in Section 5, the limit state defined for the wall is based on the wall drift exceeding four times the drift at the yield load. This limit state is selected to represent the potential for damaging equipment and piping systems that may be mounted on or penetrate the wall. An equivalent static lateral force method of analysis is used making the evaluation similar to a nonlinear pushover analysis of the type often used in modern earthquake-resistant design and evaluation (e.g., Krawinkler, 1998). The objective of the study is to develop data describing the relative fragilities of degraded to undegraded walls. It is likely that dynamic effects play similar roles in modifying the fragilities for both conditions, and therefore the ratio of the degraded to undegraded fragility would be about the same in either case. Loads acting on the wall are assumed to include an axial gravity load followed by a monotonically increasing in-plane load applied at the top of the wall.

The ANSYS code is first validated by comparing predicted results with experimental data obtained for shear walls similar to those of interest here. The design of the example shear wall is then discussed together with deterministic predictions of the wall's behavior. Both ANSYS and standard design tools are used to make these predictions. The fragility of this wall in both the undegraded and degraded states is then developed. Finally, the results for the example wall are generalized to include a broader range of shear walls that would be found in NPPs.

It should be noted that this section utilizes some equations and coefficients in accordance with the ACI 318 Code which are only valid in English units (i.e., not SI units). Therefore, for these situations, only English units are provided. Where appropriate, SI units are provided in parenthesis following the English units.

7.1 Validation of ANSYS for Shear Walls

The ANSYS computer code (Version 5.4) is used to evaluate shear wall responses. The predictions made with this code are compared with the results of a test program (Yamakawa, 1995) on shear walls to validate this application of the code. Six structural walls were tested, two in an undegraded state and four artificially degraded by subjecting the walls to electrolytic corrosion. One of the undegraded walls is selected for comparison with the results obtained from the ANSYS code.

A sketch of the test wall is shown in Figure 7.1. It can be seen that the height to width ratio of the wall is 1.19 and the reinforcement ratio is 0.008 in both the horizontal and vertical directions. The yield strength of the steel was 62.2 ksi (429 MPa) and the compressive strength of the concrete was 3.57 ksi (24.6 MPa). A uniform compressive stress equal to 0.284 ksi (1.96 MPa) was applied and maintained on the wall followed by an in-plane horizontal load applied at the center of the stiff member at the top of the wall.

The horizontal load was cycled with increasing drifts applied to the wall. Load-deflection measurements were taken and crack patterns were noted as they developed.

The model used for the ANSYS comparison is shown in Figure 7.2. Due to symmetry along a vertical plane at the center of the shear wall, only one-half of the wall is modeled. Although the model represents one-half of the shear wall, all results presented in this report are for the full wall. The concrete is modeled with element type "SOLID65" of ANSYS. The uniaxial stress strain law, based on Hognestad's formulation (Park and Paulay, 1975), is prescribed for the concrete as follows:

$$f_c = f'_c \left[2 \varepsilon_c / \varepsilon_o - (\varepsilon_c / \varepsilon_o)^2\right] \qquad \text{for } \varepsilon_c \le \varepsilon_o \tag{7.1}$$

$$f_c = f'_c \qquad \text{for } \varepsilon_c > \varepsilon_o$$

where, $\varepsilon_o = 2 f'_c / E_{it}$ and E_{it} = initial tangent modulus

A tensile strength and compressive failure strain is also prescribed for the concrete. Cracking (at the tensile strength - f_t) and crushing (at the failure compressive strain - ε_{cu}) behavior of the concrete is considered in the solutions. The ANSYS model prescribes shear stiffness along cracks to be one half of the stiffness in the uncracked material and equal to the uncracked material after the cracks closes. No tensile stress can be transmitted across cracks, but compressive stresses can be transmitted after cracks close. The following concrete parameters are used for this problem:

f'_c = 3.57 ksi (24.6 MPa); f_t = 0.448 ksi (3.09 MPa); E_{it} = 3,670 ksi (25.3 GPa)

The steel reinforcement is modeled discretely with spar elements having elastic perfectly plastic material properties with a yield stress equal to 62.2 ksi (429 MPa).

The boundary conditions restrain all vertical and horizontal translation at all base nodes and horizontal out-of-plane translation at all the nodes on the vertical plane of symmetry.

The ANSYS code solves static nonlinear problems with the user usually specifying the initial load step size (also corresponds to the minimum load step size for the bisection method when convergence becomes a problem), the maximum number of iterations permitted per load step size, and the convergence criteria. The convergence criteria selected for this analysis is a force convergence criterion. Convergence is obtained when the size of the residual (summation of all unbalanced forces at every degree-of-freedom) is less than the user-specified value.

These parameters were varied in sensitivity studies to establish appropriate values which lead to good solutions with consideration given to the computer time required to obtain the solutions. For the ANSYS wall analysis validation, the loading increment in the elastic range (prior to concrete cracking), required very few solutions. When cracking was initiated, the load increments were reduced to a minimum of 0.2% of the maximum load applied to the wall. This corresponds to 80 lbs (356 N) per load step increment. The adequacy of this load step size increment was confirmed by reducing the load step size in half, which resulted in a minimal variation in the response of the shear wall. Similar sensitivity studies were performed for the convergence criteria to ensure that accurate results are achieved within a reasonable execution time.

The lateral load-deflection curve from the ANSYS solution is compared to the measured test data in Figure 7.3. The measured load-deflection experimental data is taken as the envelope of the data obtained during the cyclic loading. The predicted results are reasonably close to the measured data. Comparisons of crack patterns in the wall are shown in Figure 7.4. Note that the crack patterns in the experimental wall occurred as a result of cyclic loading. The cracks on the lower left corner of the wall result from left to

right loading while the cracks on the lower right corner of the wall result from the right to left portion of the cyclic load. The ANSYS results were obtained for monotonic loading from left to right so that the cracks grow in the lower left corner of the wall. The predicted and measured crack patterns are very similar. It is concluded that the ANSYS program is capable of predicting the behavior of low-rise shear walls.

7.2 Deterministic Analysis of a Representative Shear Wall

7.2.1 Shear Wall Design

As discussed earlier, a shear wall typical of those found in NPPs is used as a sample problem. A sketch of the shear wall is shown in Figure 7.5. The wall is 20 ft (6.1 m) high by 20 ft (6.1 m) wide and is 2 ft (61 cm) thick. The reinforcement consists of #5 bars spaced at 8.5 in. (21.6 cm) at each face in each direction resulting in a horizontal and vertical reinforcing ratio equal to 0.003. The shear wall is assumed to be part of an enclosure of a square room having similar shear walls on all sides and a ceiling with similar dimensions. The walls normal to the shear wall under consideration act as flanges and provide moment resistance. The ceiling slab acts as a stiff member to distribute the shear load uniformly across the wall. An axial load resulting from gravity loads in the building is included and selected to produce a uniform compressive stress in the wall equal to 300 psi (2.07 MPa). The concrete strength is taken as 4 ksi (27.6 MPa) and grade 60 reinforcement is used.

7.2.2 Evaluation of Shear Wall Using Analytical Solutions

The characteristics of this wall are evaluated with simple design models and with the ANSYS code. This section utilizes several analytical methods to calculate the ultimate capacities for comparison with the ANSYS solution, which is described in Section 7.2.3.

ACI Design Code Methodology

Using ACI 318-99 the shear capacity of the wall can be calculated using the expression:

$$\phi V_n = \phi \left[3.3 (f'_c)^{1/2} h d + N_u d / 4 L_w + A_v f_y d / s_2\right] \quad (7.2)$$

where, ϕ = capacity reduction factor, taken =1.0 here since true estimate of capacity is desired for use in fragility calculations

h = wall thickness = 24 in.

d = 0.8 * wall width = 0.8 * 240 = 192 in.

A_v = area of horizontal steel within distance s_2 = 2* 0.31 = 0.62 in.^{2}

s_2 = spacing of horizontal reinforcement = 8.5 in.

N_u = axial load = 0.3 * h * L_w = 0.3*24*240 = 1,728 kips

L_w = wall width = 240 in.

The resulting design capacity of the wall in shear is calculated to be 2,150 kips (9.56MN).

Barda et al. Methodology

There is experimental data indicating that the ACI code is conservative for low-rise walls. Barda et al. (1977) used empirical data (based on tests of low-rise shear walls) to develop the following equation for the concrete contribution to the wall shear strength:

$$V_c = \left[8.3 (f'_c)^{1/2} - 3.4 (f'_c)^{1/2} (H / L_w - 0.5) + N_u /(4 h L_w)\right] h d \quad (7.3)$$

where, H = wall height

For fragility analyses the term $f_t / 6$, in which f_t = splitting strength, should be substituted for $(f'_c)^{½}$. This is necessary because the variability in the shear strength is incorrectly reduced when $(f'_c)^{½}$ is used in Eq. 7.3.

To account for the contribution of vertical and horizontal reinforcement to wall strength, Wesley and Hashimoto (1981) developed the following equation for the shear strength developed from the horizontal and vertical reinforcement ratios (ρ_h and ρ_v):

$$V_s = [a\,\rho_h + b\,\rho_v]\, f_y\, h\, d \qquad (7.4)$$

where, $a = 1 - b$

$b = 1$; $H / L_w < 0.5$

$= 2\,(1 - h / L_w)$; $0.5 < H / L_w < 1$

$= 0$; $H / Lw > 1$

The total shear wall capacity is calculated as the sum of equations 7.3 and 7.4. This results in a shear capacity of 3,170 kips (14.1 MN), which is about 50% higher than the ACI code predicted capacity.

Potential Restriction on Shear Capacity Due to Flexure

The flexural capacity of the wall must also be considered. A sketch of the wall is shown in Figure 7.6. The wall is subjected to a shear load (V) and an axial load (N_u). The wall is reinforced and the flange of the wall contains an area of steel (A_b). The flange depth is t_f and the width of the flange is b. For simplicity the steel in the flange is assumed to be located at the center of the flange. The vertical reinforcement is distributed as a uniform thickness of steel (t_s) rather than treated as discrete areas. Plane sections are assumed to remain plane so that there is a linear strain distribution as shown. Flexural failure is assumed to occur when the peak concrete strain reaches ($\varepsilon_{cu} = 0.003$). The neutral axis is located at a distance (c) from the point of maximum compressive strain. The distance from the neutral axis to the point where the wall steel reaches yield is designated (c_y) and may be related to c and ε_{cu} as shown. The forces in the steel and concrete are then as shown in the figure. It is assumed that the concrete cannot carry any tensile stress. The steel forces in the compression flange and the wall steel on the compression side of the point where the steel strain reaches ε_y are neglected. It is further assumed that the depth (a) of the compressive stress block is less that the flange depth. If this is not the case the following results must be modified:

Equilibrium of the vertical forces requires that,

$$N_u = F_c - T_{pl} - T_b$$

or substituting for the forces and solving for the neutral axis location,

$$c = [N_u + t_s\, f_y\, (L_w + t_f) + A_b\, f_y] / [0.85\, f'_c\, \beta_1\, b + e_y\, f_y\, t_s / e_u + t_s\, f_y] \qquad (7.5)$$

Moment equilibrium about the compressive force F_c can then be used to evaluate the load V that may be placed on the wall as

$$V = [N_u\,(2\,t_f + L_w - a) / 2 + T_{pl}\,(L_w + t_f + c + c_y - a) / 2 + T_b\,(3\,t_f/2 + L_w - a / 2)] / H \qquad (7.6)$$

Application of this analysis to the example shear wall requires that the effective width of the flange be determined. The requirements in the ACI code would restrict the flange width to L/4 or 5 ft (1.52 m) for the 20 ft (6.1 m) rise of the wall. Data in Wang and Salmon (1979), however, indicate that this restriction is very conservative. The ACI code results generally apply to supports at both ends of the beam so that one could interpret the span of the cantilever as equivalent to a 40 ft (12.2 m) span for a beam supported at both ends. This would result in an effective flange width equal to 10 ft (3.05 m) which compares well with the data presented in Wang and Salmon. For this flange width the effective flange steel is $A_b = 0.003 * 120 * 24 = 8.64$ in.^{2} (55.7 cm^2). The depth of the neutral axis c = 9.27 in. (23.5 cm) is found from Eq. 7.5. Since the neutral axis lies in the flange, the analysis is applicable. For this value of c:

$$a = 7.88 \text{ in.}, \quad c_y = 6.40 \text{ in.}, \quad F_c = 3215 \text{ kips}, \quad T_{pl} = 969 \text{ kips}, \quad T_b = 518 \text{ kips}$$

The shear capacity as restricted by flexural consideration is:

$$V = (221{,}288 + 116{,}498 + 140{,}927) / 240 = 1{,}995 \text{ kips (8.87 MN)}$$

The three terms in the numerator represent the contributions from the axial load, the wall reinforcement, and the flange reinforcement respectively. It is found that the moment capacity limits the applied shear to 1,995 kips (8.87 MN). This is close to the shear load of 2,150 kips (9.56 MN) limited by the ACI code but significantly less than the shear capacity of 3,170 kips (14.1 MN) limited by the Barda et al. analysis.

7.2.3 Evaluation of Shear Wall Using Finite Element Method

Design Case

The ANSYS model used to evaluate the load-deflection characteristics of the example wall is shown in Figure 7.7. The same model characteristics are used as discussed above for the ANSYS validation except that the material properties reflect the design properties. The material properties used for this "design case" are $f'_c = 4$ ksi (27.6 MPa), $f_t = 448$ psi (3.09 MPa), $E_{it} = 3{,}834$ ksi (26.4 GPa), and $f_y = 60$ ksi (414 MPa).

The nonlinear analysis was performed using solution parameters (load step size, number of iterations, and convergence criteria) similar to those described for the ASNSYS validation study in Section 7.1. The major differences are: a constant load step increment was used once concrete cracking was initiated and a larger force convergence criterion was utilized. The constant load increment was selected in order to be able to compare solutions at the same load steps for the various samples and cases performed. The convergence criterion was increased because the representative shear wall problems studied were much larger than the validation model. Sensitivity studies were made for all of these parameters to confirm the accuracy of the selected values while minimizing the computer execution time.

A load-deflection plot derived from the ANSYS solution is shown in Figure 7.8. Straight lines are fit to the elastic and inelastic portion of the design curve so that various characteristics of the curve may be established. This shows that the yield load is about 2,550 kips (11.3 MN) and the corresponding yield deflection is 0.075 in. (1.91 mm) (drift ratio = 0.03%). The limit state is defined in the following section as occurring when the drift ratio reaches four times the yield drift ratio [a deflection of 0.3 in. (7.62 mm)] based on the "design case" in Figure 7.8.

Recall that the ACI Code and Barda et al. methodology predicted wall strengths are 2,150 kips (9.56 MN) and 3,170 kips (14.1 MN), respectively. These are shown in Figure 7.8. It can be seen that the ACI Code predicted strength is about 83% of the yield load while the Barda et al. methodology predicted strength results in a deflection equal to approximately 0.18 in. (4.57 mm) (2.3 times yield deflection).

Crack patterns predicted in ANSYS for the design case are shown in Figure 7.9 for increasing load acting on the wall. Inclined cracks begin at the lower left portion of the flange/wall interface and then proceed around this interface. This is likely caused by the stiffness discontinuity between the flange and wall. Diagonal tension cracks then proceed up from the lower left corner of the wall. The deformation of the wall at the ultimate load capacity is shown in Figure 7.10.

Sensitivity Analyses

Several sensitivity studies were made to determine the importance of certain design and analysis parameters used in this study. The first sensitivity evaluation was made to determine the effect of varying the concrete tensile strength. Three different analyses were performed for the design case utilizing concrete tensile strength equal to + 20% of design value, design value, and - 20% of design value. The results of these analyses are shown in Figure 7.11. As expected, the tensile strength of the concrete has little effect until cracking occurs and then there is about a 7% change in wall strength resulting from a ± 20% change in concrete tensile strength.

A second evaluation was performed to investigate the sensitivity of the shear wall response to variation in the shear transfer coefficient used as input for the ANSYS "SOLID65" element. Three different analyses were performed for the design case using shear transfer coefficients for an open crack equal to - 25% of the design value (.75 X .5 = 0.375), design value (0.5), and + 25% of design value (1.25 X .5 = .625). The results of these analyses are shown in Figure 7.12. The load-deflection curves demonstrate that there is no effect of varying the shear transfer coefficient up to a drift ratio approximately three times the yield deflection drift. Beyond this point, there is a maximum change of approximately 6% in wall strength from a ± 25% change in shear transfer coefficient. Based on these results and past experience, it was judged that using a shear transfer coefficient of 0.5 for an open crack is reasonable for this study.

7.3 Fragility Analysis of Shear Wall

The fragility curve for the shear wall is developed by considering the parameters in Tables 5.1 and 5.2 as random variables. Solutions are obtained for 19 sets of data representing a Latin Hypercube model of the statistical variations in material properties as discussed in Section 5. For each of these 19 samples, an ANSYS analysis is performed and a load–deflection curve is developed. The limit state (capacity) for each of these sample runs is obtained as the load corresponding to a drift ratio equal to four times the "design" yield drift ratio [a deflection of 0.3 in. (7.62 mm)].

Undegraded Shear Wall

The results of the 19 ANSYS solutions for the undegraded wall are summarized in Table 7.1 and indicate a mean capacity of 3,655 kips (16.3 MN) with a coefficient of variation equal to 0.15. These data are plotted on lognormal probability paper in Figure 7.13. This data plot is close to linear, indicating that the assumed lognormal distribution is appropriate for this data. Some indication of the variation in load deflection data for the 19 cases can be seen by the four sample cases (6, 13, 14, and 15) plotted in Figure 7.14. Case 6 represents a high concrete strength and a low steel strength while case 13 represents a low concrete strength and a high steel strength. It can be seen that the concrete strength has a major effect on the wall capacity. This conclusion may be different for walls with reinforcement ratios larger than the 0.003 for this wall.

Degraded Shear Wall - Loss of Steel Cross-Sectional Area

The steel area in the wall (but not in the flanges) is degraded by 20%, with the steel area treated as a random variable. The mean steel area is 80% of the undegraded area and the coefficient of variation in A_s is equal to 0.105. With this reduction in steel area, the mean wall capacity is found to be 3,634 kips (16.2 MN) with a coefficient of variation equal to 0.16. This degradation resulted in only a 1/2% reduction in the mean and a slight increase in the coefficient of variation (from 0.149 to 0.158). This effect is small because of the small effect that the steel has on the wall capacity for this wall configuration.

Degraded Shear Wall - Loss of Steel Cross-Sectional Area and Concrete Spalling

As the steel is corroded, the concrete outside of the reinforcement cage on both sides of the wall may spall. It is assumed that the spall depth equals the cover, with the depth of cover treated as a random variable [mean = 1.25 in. (31.8 mm) and coefficient of variation equal to 0.496 - Table 5.1]. The loss of concrete cover was assumed to occur over the entire width and height of the wall. The mean wall capacity was calculated to be 3,446 kips (15.3 MN) with a coefficient of variation equal to 0.15. This combined degradation of 20% wall steel loss and spall of the concrete outside the reinforcement results in a 6% reduction in the mean wall capacity.

Table 7.2 provides a summary of the ANSYS shear wall fragility analyses. Figure 7.15 shows the fragility curves for an undegraded wall, a wall with 20% loss of reinforcement area, and a wall with 20% loss of reinforcement in combination with spalling of the concrete outside of the reinforcement. These levels of degradation have relatively small effects on the wall fragility. It can also be noted that the three fragility curves are parallel so that the relative effects of degradation are approximately the same at any probability of failure.

Results Considering Degradation in the Flanges

The fragility analyses described above do not consider any degradation in the flange walls. Additional analyses were made to evaluate the effects of the loss of steel area in both the shear wall and flange walls. Table 7.3 presents the results for the wall. Each case was performed using one computer run, with the mean values for the random variables.

Comparing the results from Table 7.3 against the results from Table 7.2 demonstrates that the capacity of the wall for the undegraded case using mean values for the random variables [3,860 kips (17.2 MN)] is about 5.6% higher than the mean capacity using the 19 samples [3,655 kips (16.3 MN)]. Using the mean values for the random variables shows that the 20% loss of steel area results in a slight reduction in wall capacity from 3,860 kips (17.2 MN) to 3,840 kips (17.1 MN), a 1/2% reduction. This is the same magnitude of reduction in wall capacity shown in Table 7.2 for loss of steel area only in the shear wall. This occurs because the steel is a relatively small contributor to the wall total capacity for the steel ratio of 0.003 being investigated.

Table 7.3 also indicates that the combination of 20% loss of steel area (for both the shear wall and flange walls) with spalling of concrete (shear wall only) reduces the shear capacity from 3,860 kips (17.2 MN) to 3,700 kips (16.5 MN), a 4.1% reduction.

7.4 Generalization of Results

The above results apply to lightly reinforced walls (reinforcement ratio equals 0.003) with an aspect ratio of 1:1. Walls of different aspect ratios and larger reinforcement ratios are considered in this section.

Solutions are obtained based on the limit state defined by Eqs. 7.3 and 7.4. This limit state is shown by comparison with ANSYS solutions to result in loads well into the plastic range with deflections equal to 2 to 3 times the yield deflections. Solutions are obtained with EXCEL spreadsheets so that a wider variation of parameters can be studied than would be possible if ANSYS solutions were used. The width of the wall is fixed at 20 ft (6.1 m) while the height of the wall is varied to obtain the desired aspect ratio (0.5, 1, and 2 height to width aspect ratios are considered). In addition, two reinforcement ratios are considered: 0.003 and 0.012. This range of parameters covers most of the shear walls found in NPPs as described in the ASCE (1994) Publication.

Spread sheets showing the results for each of the six cases are shown in Tables 7.4 through 7.9. The fragility curves corresponding to the six cases are presented in Figures 7.16 through 7.21. A summary of the results is shown in Table 7.10. The spread sheet table and figure numbers on which the evaluations are made are also indicated in Table 7.10.

7.4.1 Results for Reinforcement Ratio = 0.003

It is interesting to compare these results with those obtained using the ANSYS code. The ANSYS code predicted a mean capacity equal to 3,655 kips (16.3 MN) with a coefficient of variation equal to 0.15 for the undegraded case of the shear wall considered (H/L = 1 and reinforcement ratio = 0.003). The Barda analysis used here predicts a mean capacity equal to 3,751 kips (16.7 MN) with a coefficient of variation equal to 0.18 (Table 7.10) for the same case. The ANSYS prediction for the case of 20% steel loss plus spalling of the concrete is 3,446 kips (15.3 MN) with a coefficient of variation equal to 0.153. The Barda prediction for this case is 3,244 kips (14.4 MN) with a coefficient of variation equal to 0.17. The predicted mean capacity is reduced by 5.7% based on the ANSYS results and 13.5% based on the Barda results. Different limit states are used for the two analyses so that exact comparisons are not to be expected. The Barda model also does not consider bending moment failures while they are inherently part of the ANSYS calculation. The results from the two analyses are similar, however, and the more extensive results obtained with the Barda models are useful to anticipate what would be expected if solutions for similar cases were found with ANSYS.

The effect of degradation for different aspect ratios is also presented in Table 7.10. Based on the Barda methodology, the reductions in mean capacity when there is a 20% loss of steel area plus concrete spalling is 13.1%, 13.5%, and 14.9% for H/L ratios equal to 0.5, 1, and 2 respectively. For comparison of these results with ASNYS, additional computer runs were made using the mean values for the random variables (concrete compressive strength, concrete tensile strength, steel yield strength, concrete initial tangent modulus, area of steel, and loss of concrete cover). The results which are presented in Table 7.11 show that the reductions in mean capacity when there is a 20% loss of steel area plus concrete spalling are 3.9%, 4.2%, and 18.2% for the H/L ratios equal to 0.5, 1, and 1.5 respectively. The significantly larger reduction in mean capacity at H/L equal to 1.5 is most likely because moment governs the capacity.

The reduction in mean capacity due to a 20% loss of steel area alone (no concrete spalling), is 16.9% for an H/L ratio equal to 1.5 as compared to a reduction of 18.2% for degradation of steel area and concrete. This indicates that the reduction in capacity is primarily due to steel degradation. Since the reduction in mean capacity is substantially higher for H/L equal to 1.5 as compared to 0.5 or 1.0 suggests that degradation due to loss of steel area is important for H/L ratios greater than 1.0, where moment seems to govern the capacity rather than shear.

7.4.2 Results for Reinforcement Ratio = 0.012

As expected the Barda solutions for the higher reinforcement ratio of 0.012 (Tables 7.7 to 7.9) predict larger effects of degradation when the reinforcement ratio is increased. As summarized in Table 7.10, there is a 13.5% reduction in mean capacity from the undegraded wall (H/L=1) when the 20% steel loss plus concrete spall is considered for the low reinforcement ratio, and a 16.8% reduction in mean capacity for the wall with the larger reinforcement ratio. It can be noted that the reductions in mean capacity, when there is a 20% loss of steel area plus concrete spalling, are 16.3%, 16.8%, and 18.2% for the H/L ratios equal to 0.5, 1, and 2 respectively. The reduction in mean capacities due to the loss of steel area alone (no concrete spalling) is 11%, 12%, and 15% for H/L ratios equal to 0.5, 1, and 2 respectively.

These results indicate that (1) most of the reductions are due to the effect of loss of steel area rather than concrete spalling, (2) the reductions in mean capacity increase as the aspect ratio of the wall increases, and (3) reductions in mean capacity increases as the steel reinforcement ratio increases.

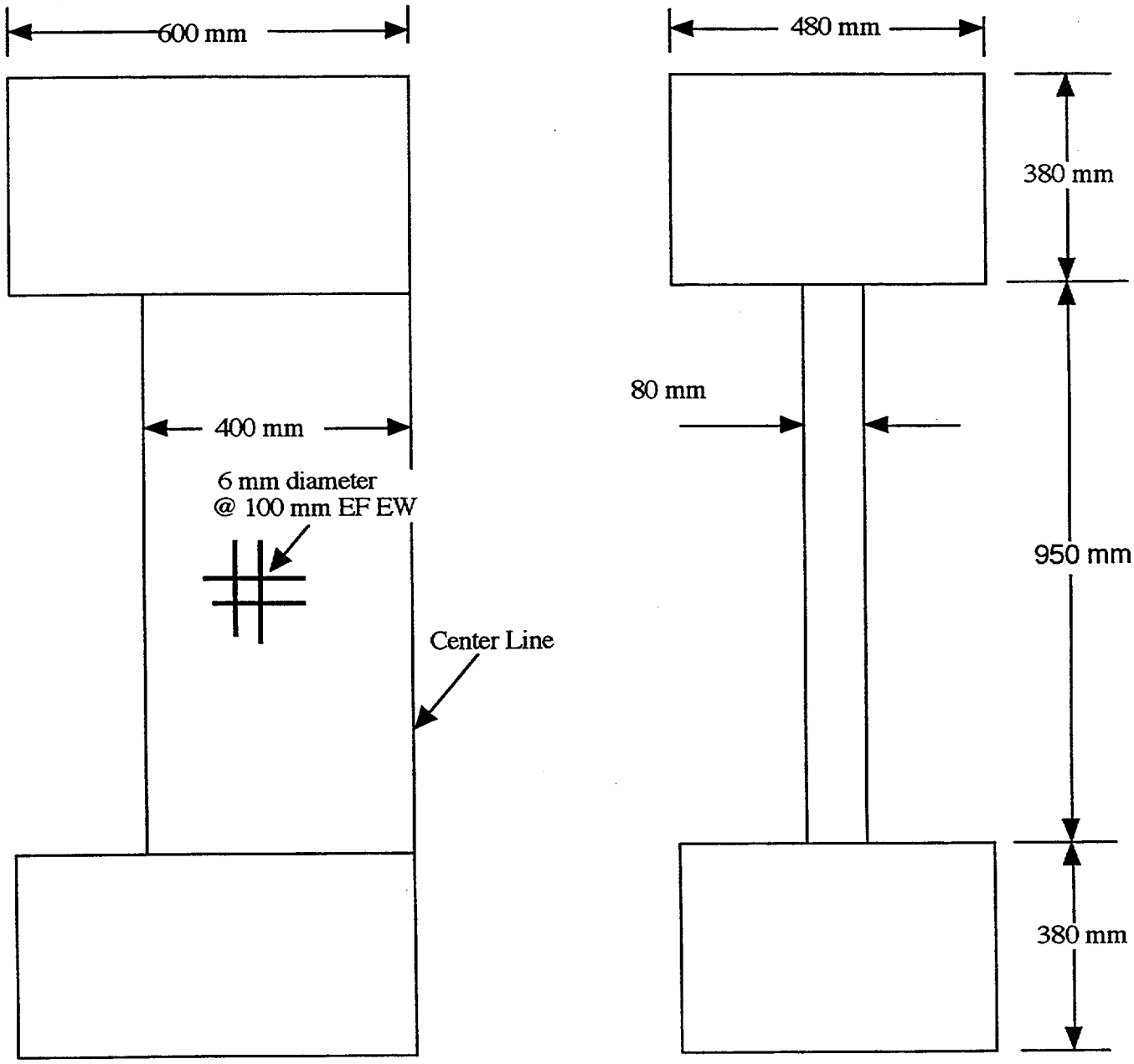

Note: 1mm = .0394 in.

Figure 7.1 Configuration of Experimental Shear Walls (Yamakawa, 1995)

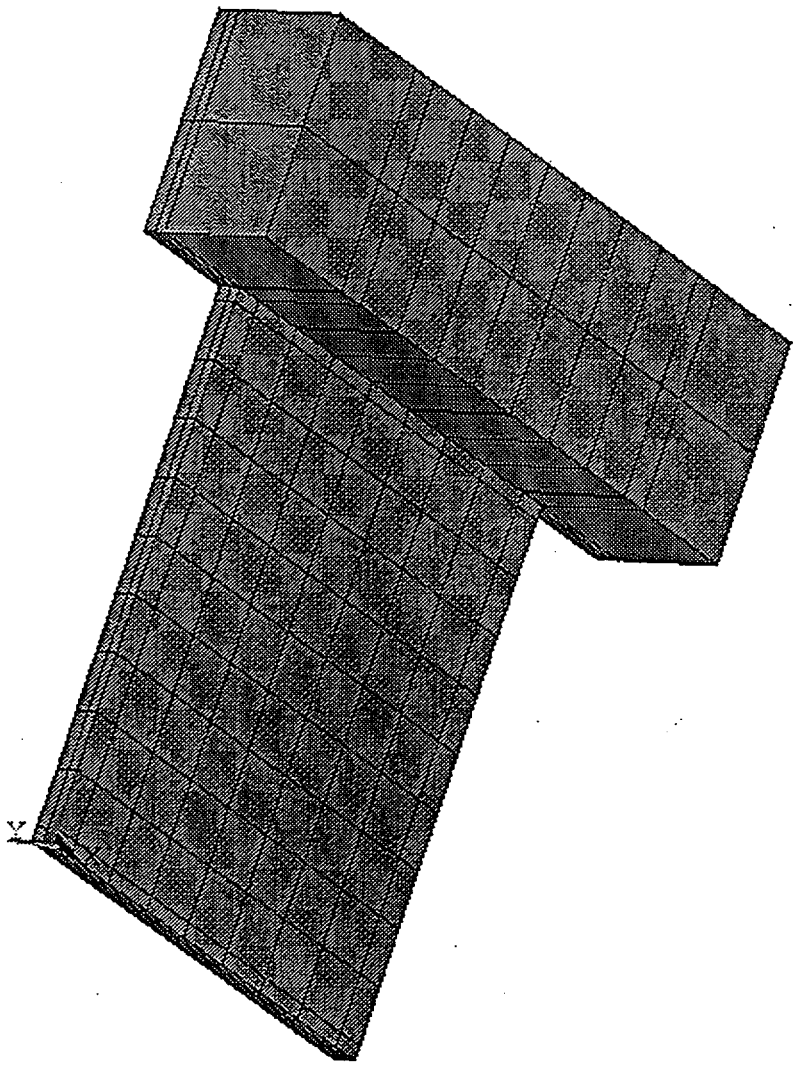

Figure 7.2 ANSYS Model of Experimental Wall

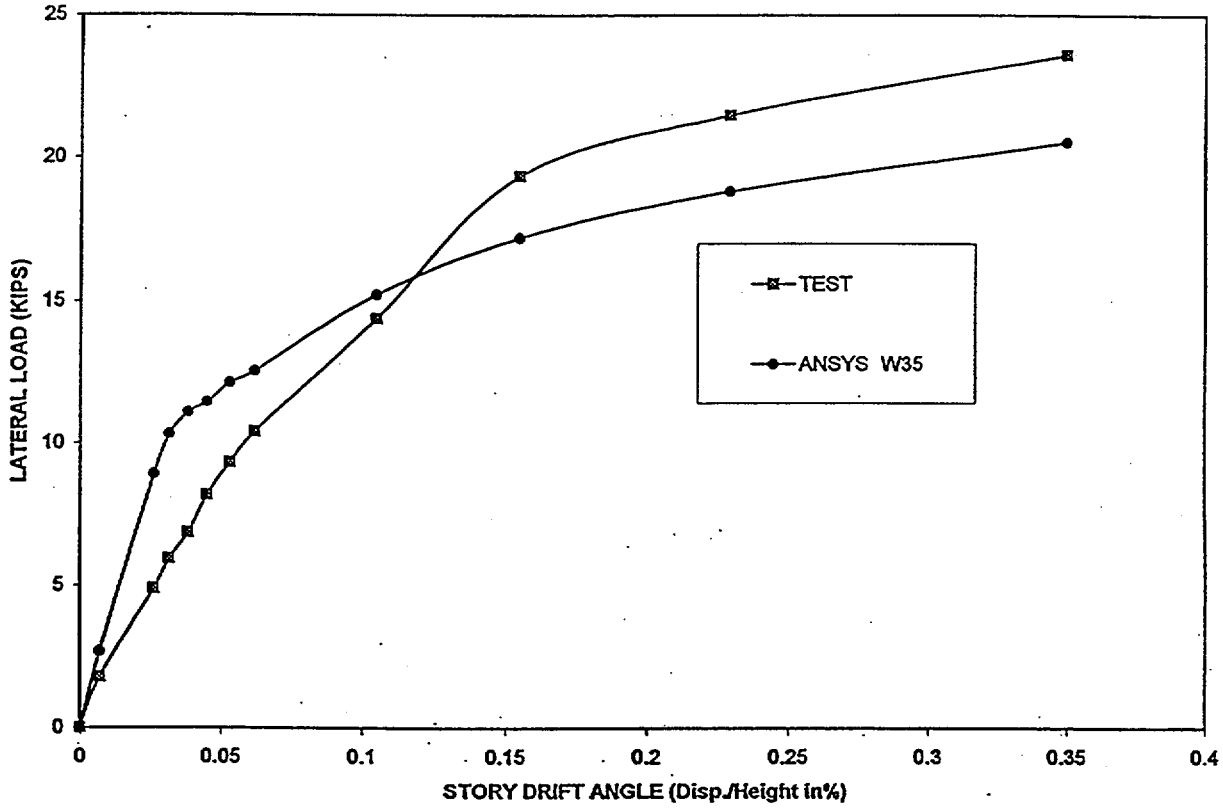

Note: 1 kip = 4.45 kN

Figure 7.3 Comparison of Measured and Predicted Load – Deflection Behavior

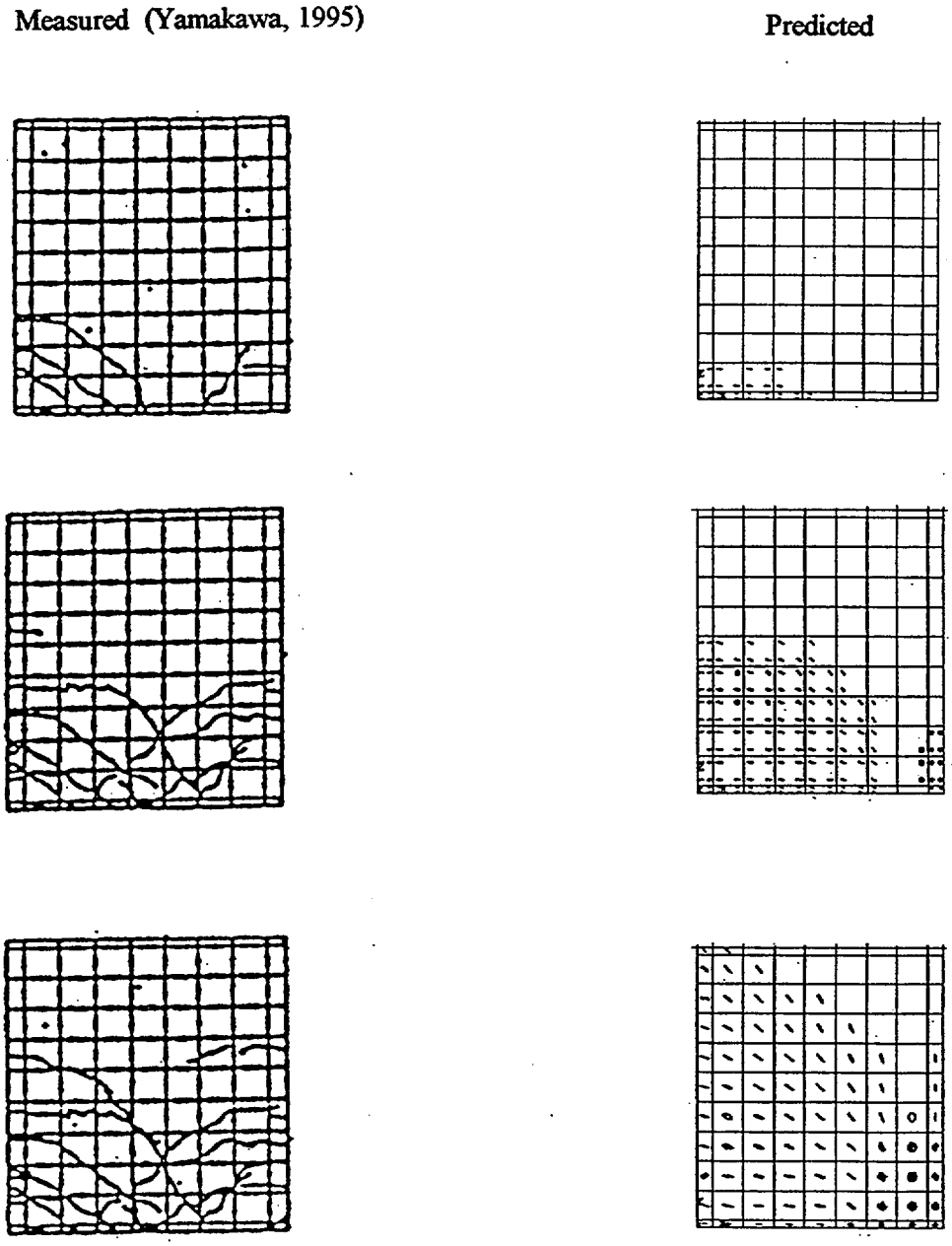

Figure 7.4 Comparison of Measured and Predicted Crack Patterns

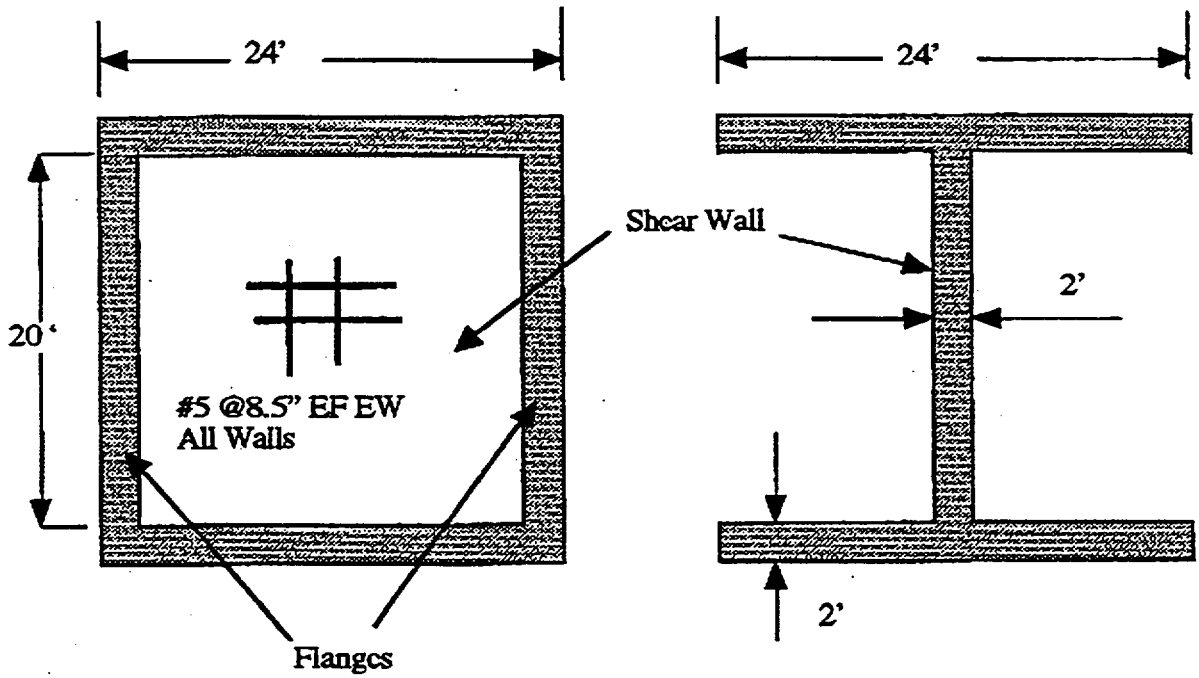

Note: 1 ft = 30.5 cm, 1 in. = 25.4 mm

Figure 7.5 Example Problem Shear Wall Design

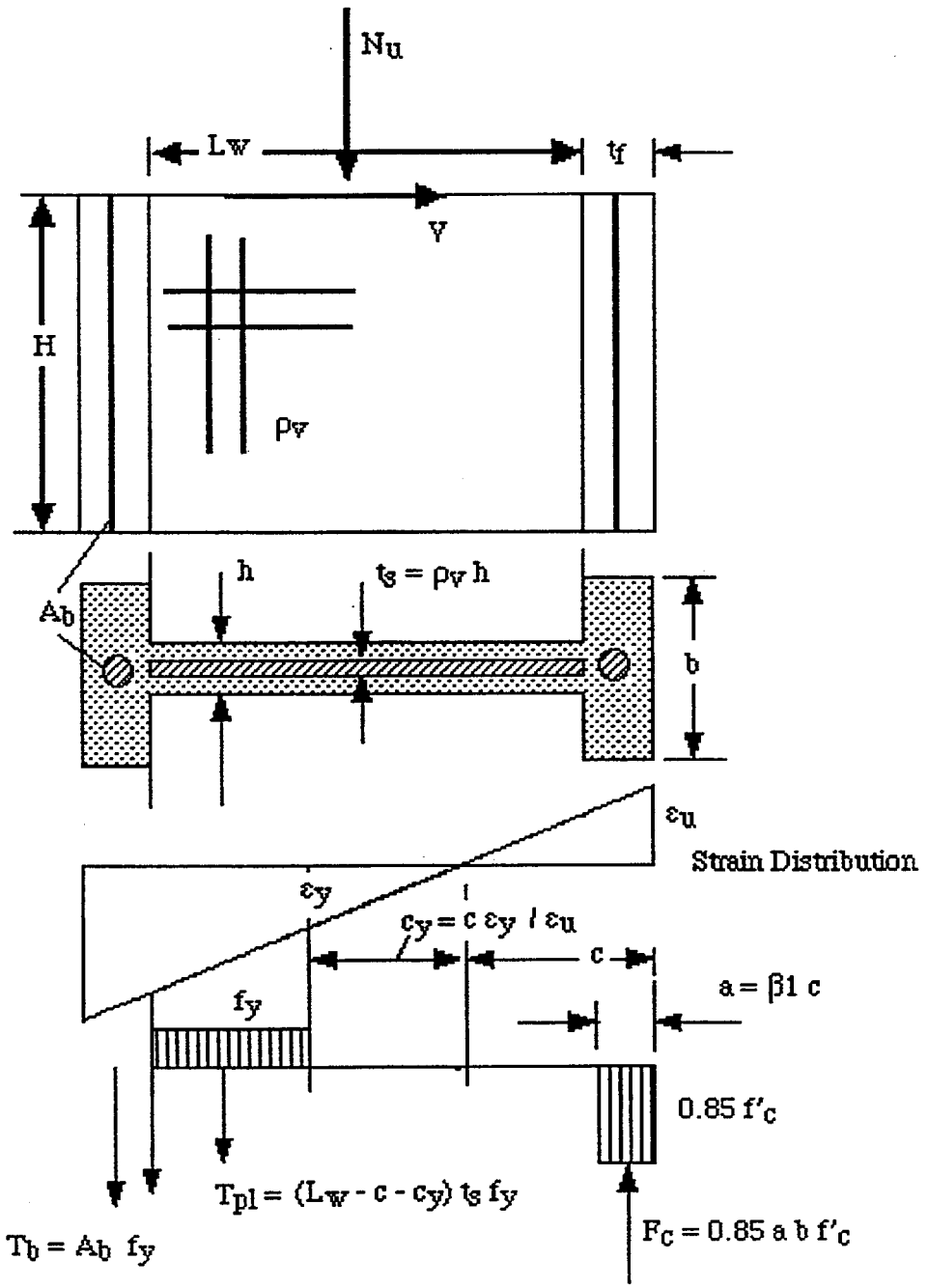

Figure 7.6 Moment Capacity of Wall

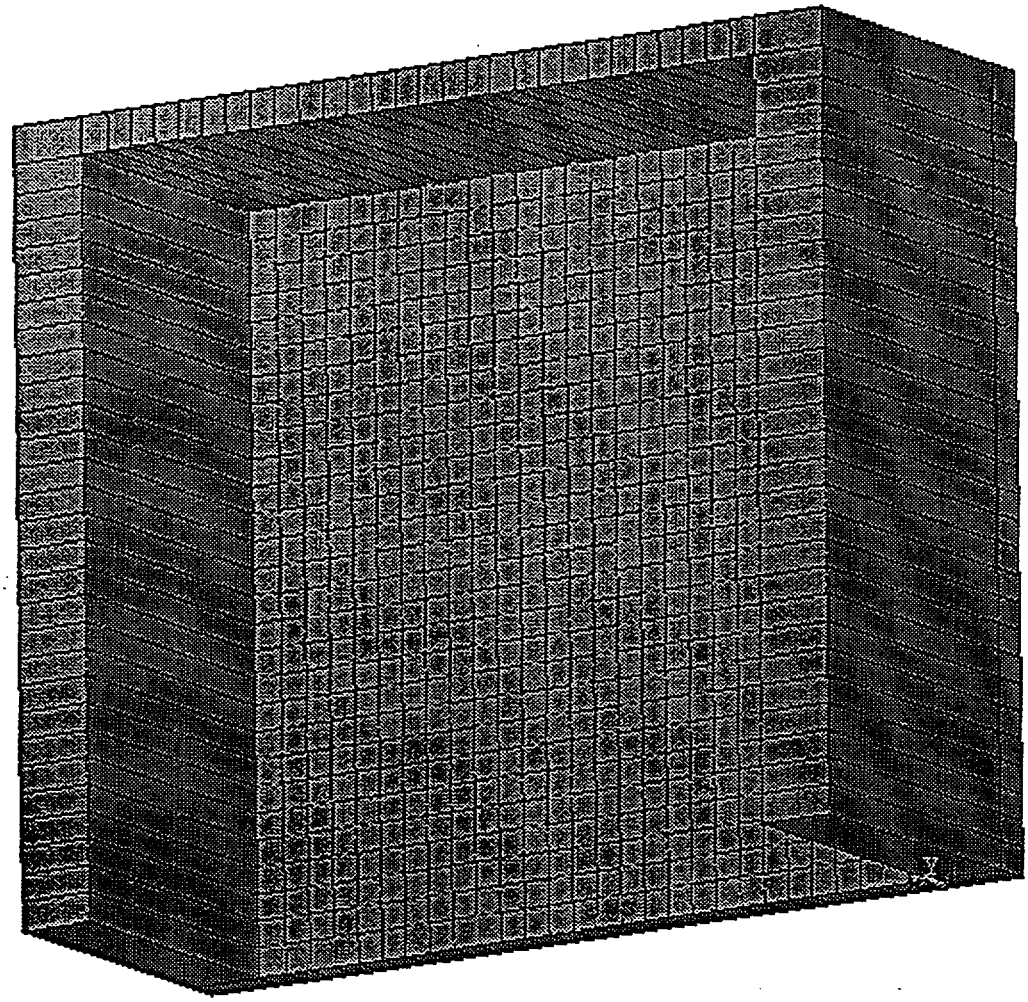

Figure 7.7 Sample Shear Wall

Figure 7.8 Shear Wall Design Case – Undegraded Load-Deflection Curve (Fwall 35)

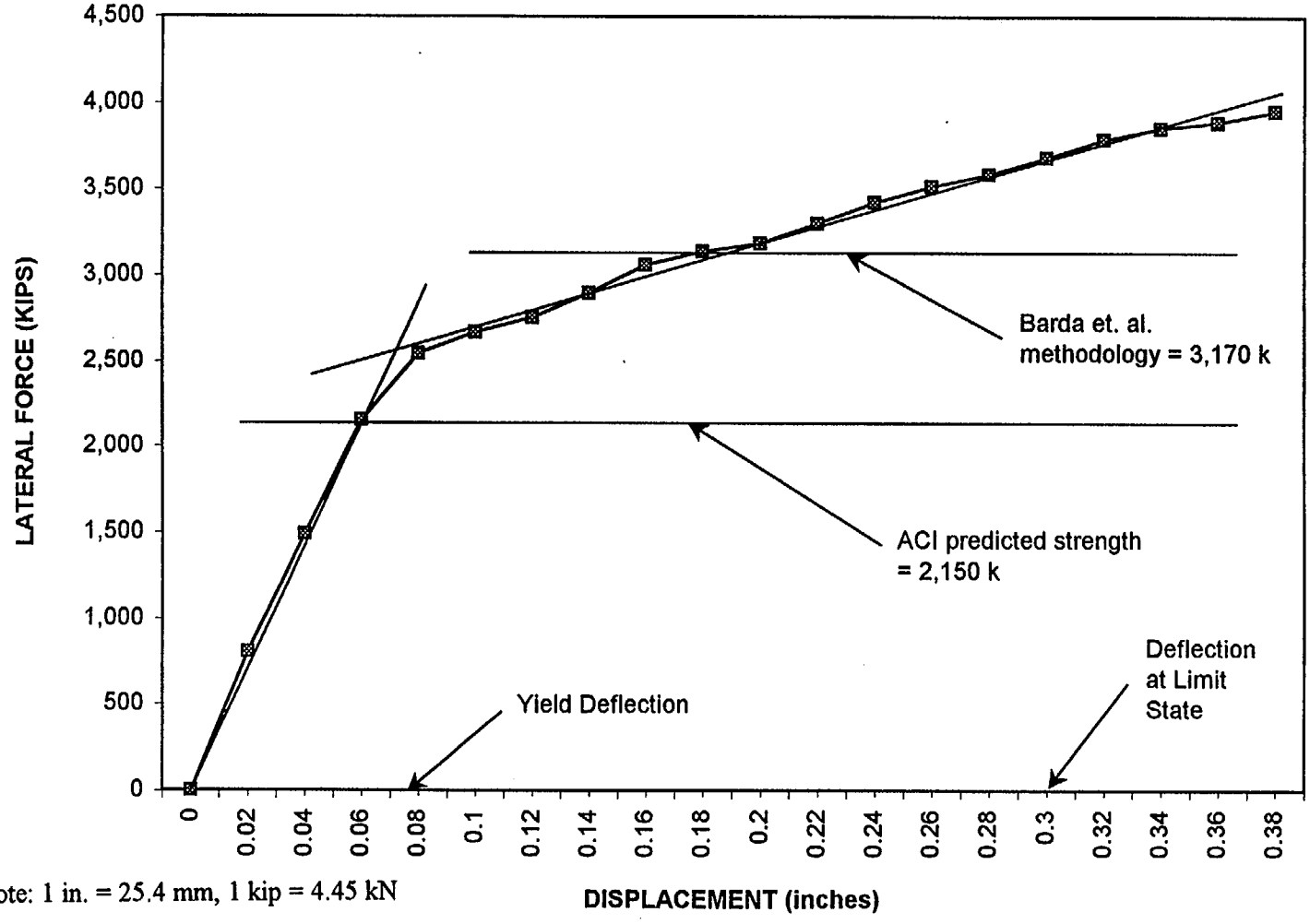

Note: 1 in. = 25.4 mm, 1 kip = 4.45 kN

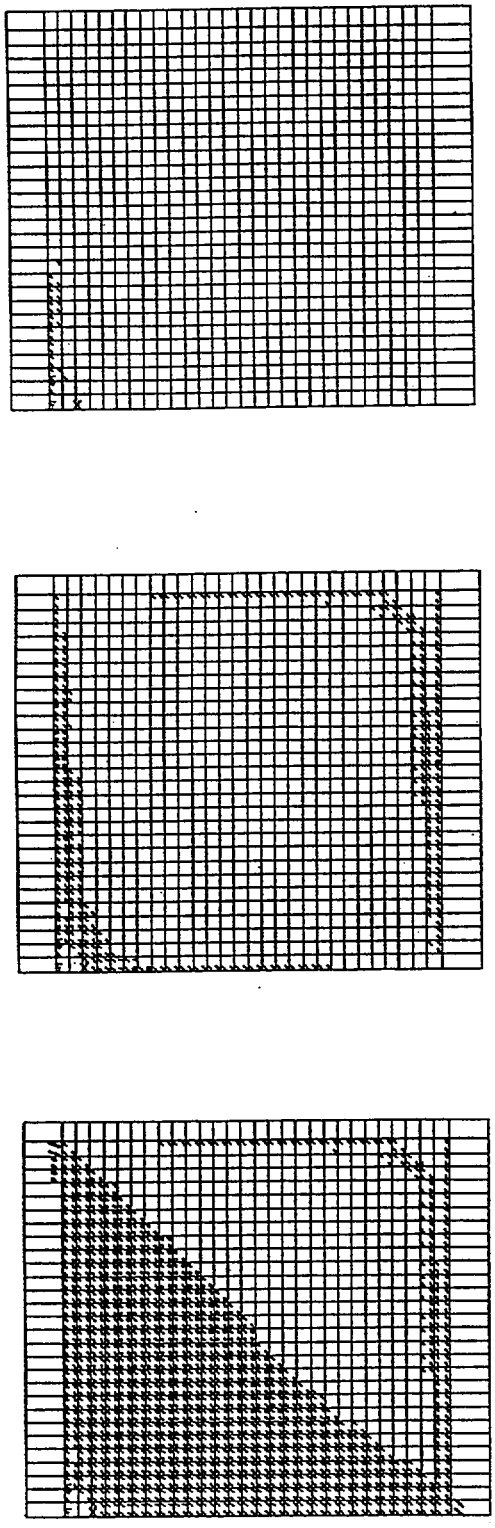

Fig. 7.9 Sample Shear Wall – Design Case
Crack Patterns

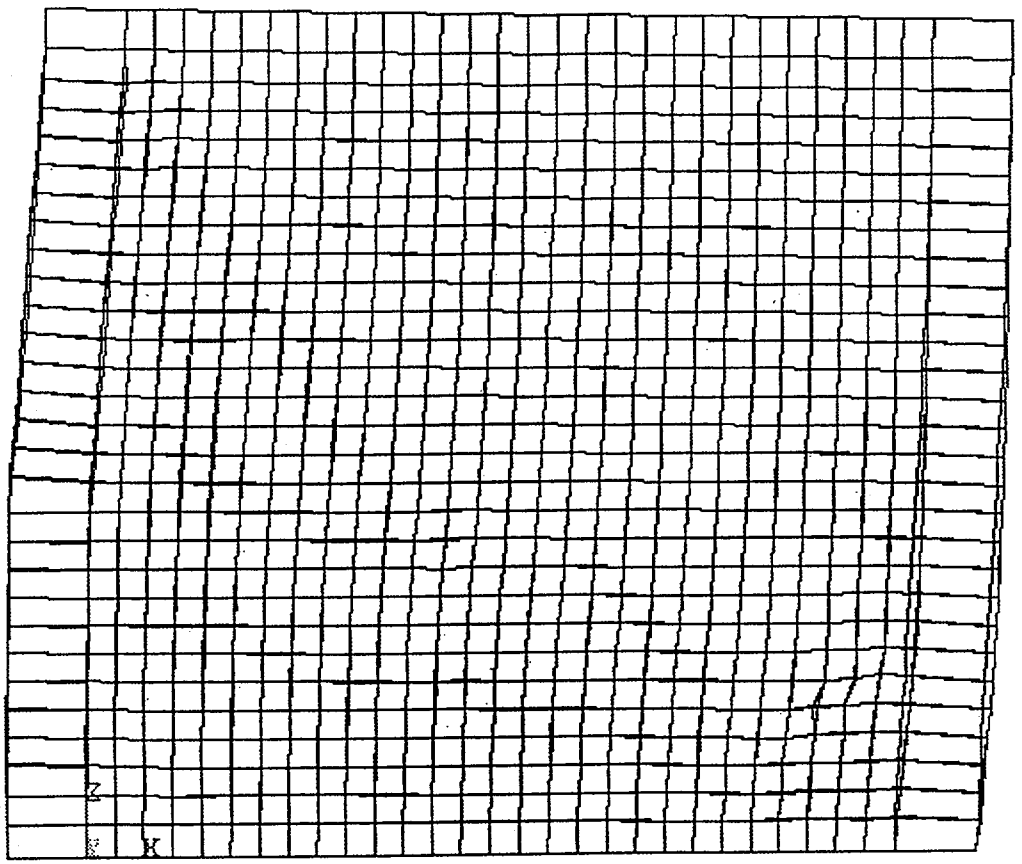

Fig. 7.10 Sample Shear Wall – Design Case
Deformation

Figure 7.11 Shear Wall – Design Case – Undegraded
Variation on Ft – Tensile Strength; + & - 20%

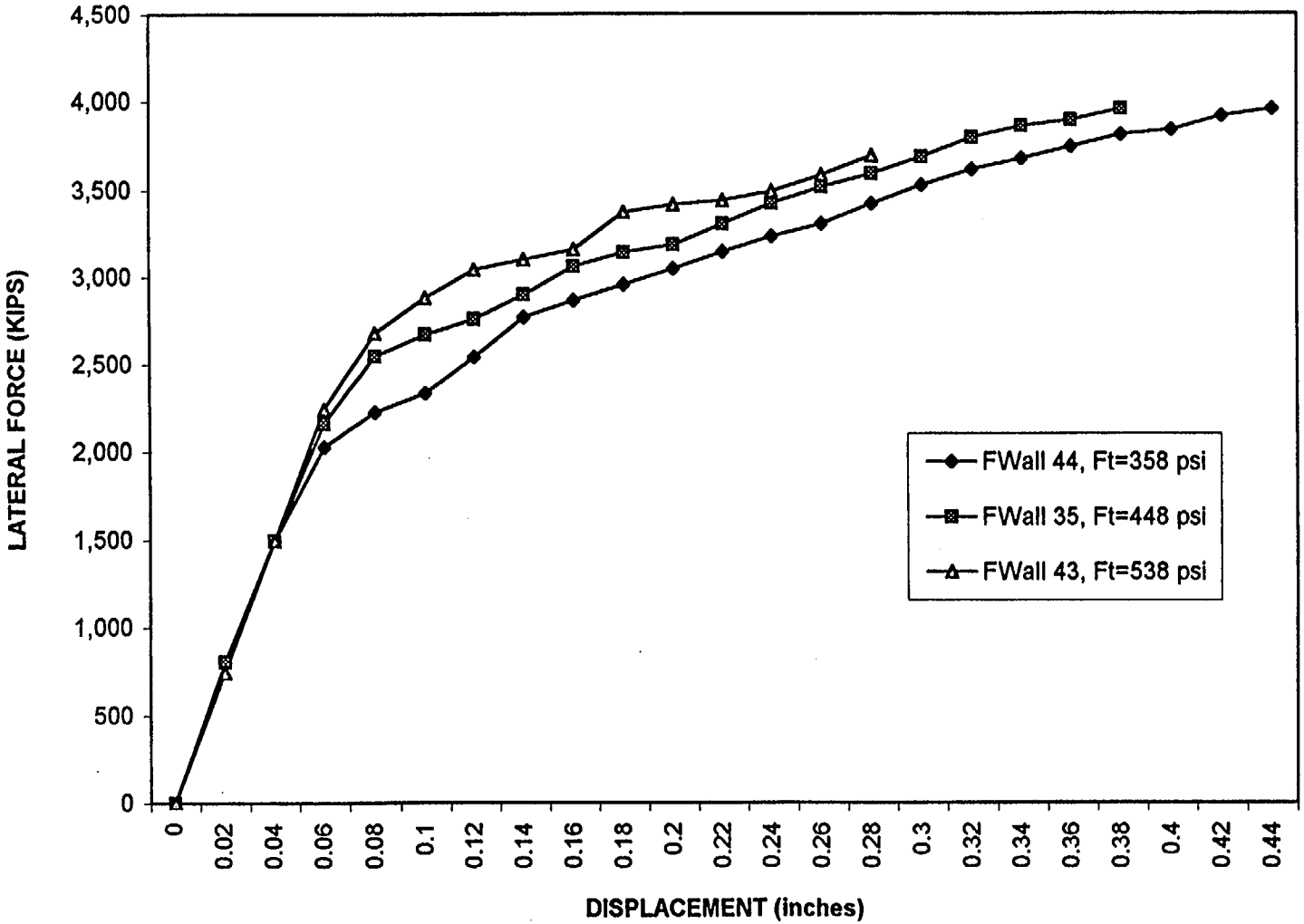

Note: 1 in. = 25.4 mm, 1 kip = 4.45 kN, 1 psi = 6.89 kPa

Figure 7.12 Shear Wall – Design Case – Undegraded
Variation on Bt – Coeff. Of Friction; + & - 25%

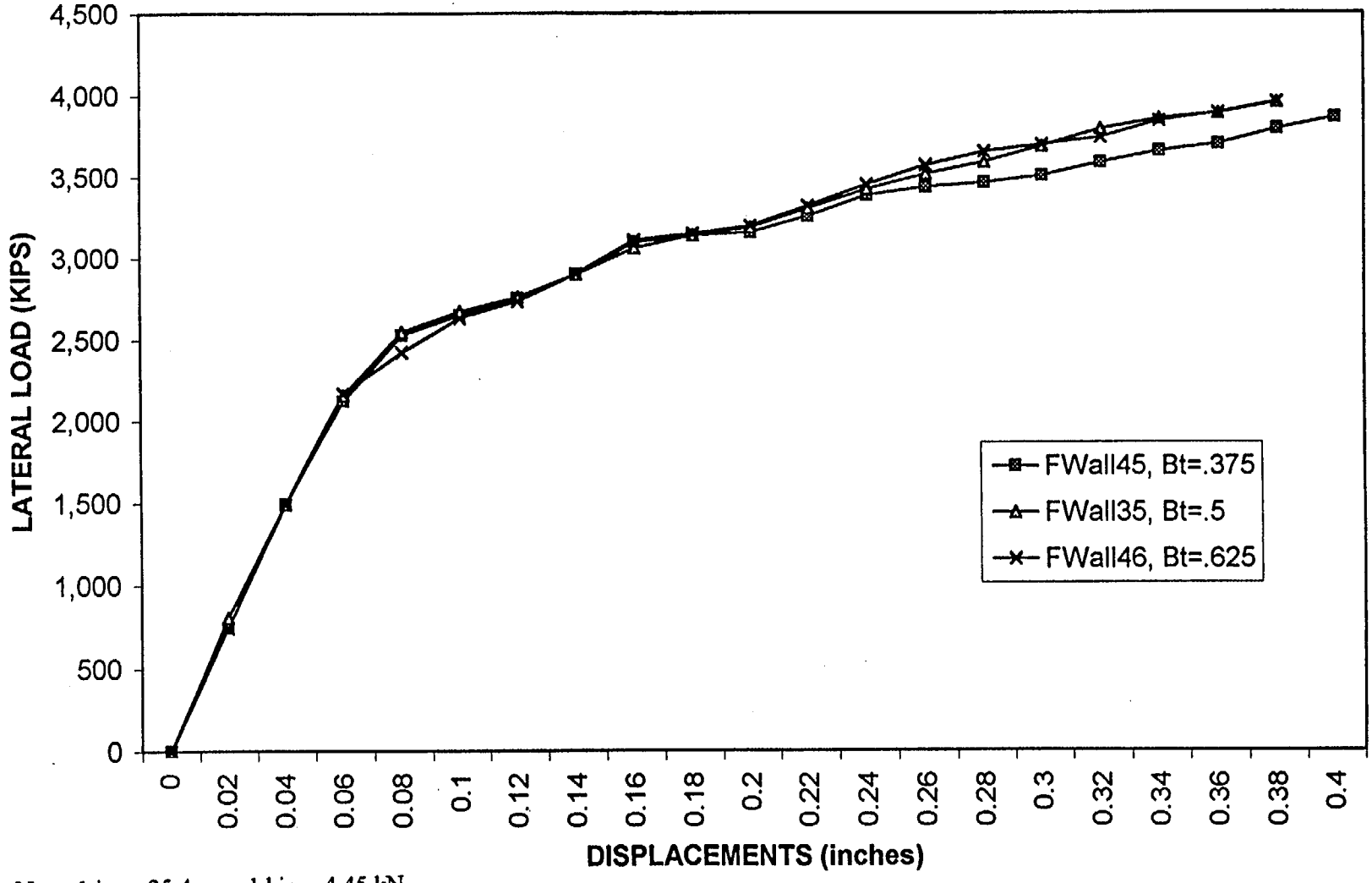

Note: 1 in. = 25.4 mm, 1 kip = 4.45 kN

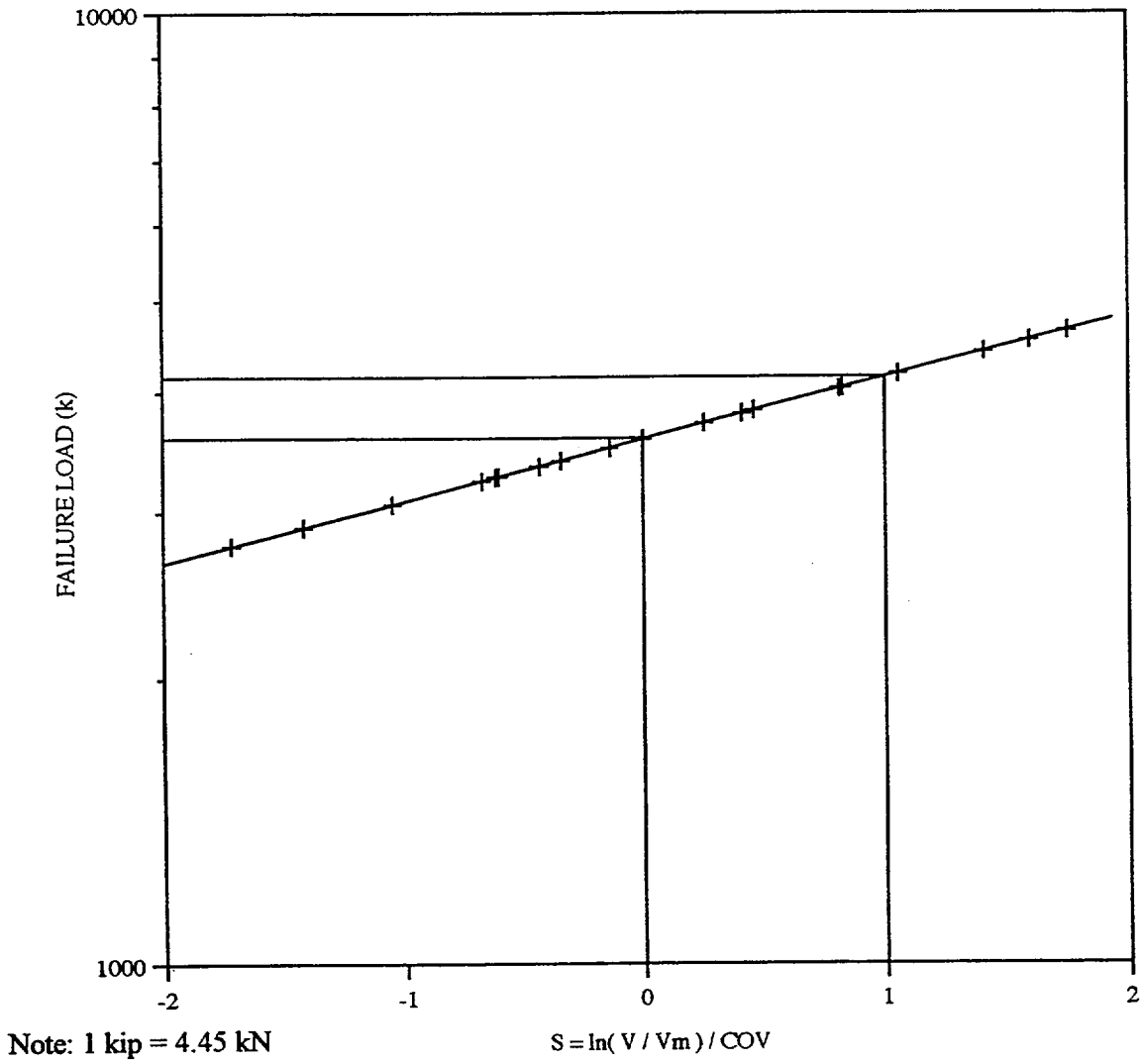

Figure 7.13 Lognormal Distribution for Undegraded Shear Wall

Figure 7.14 Shear Wall – Sample Results – Undegraded Variation on Sample Data

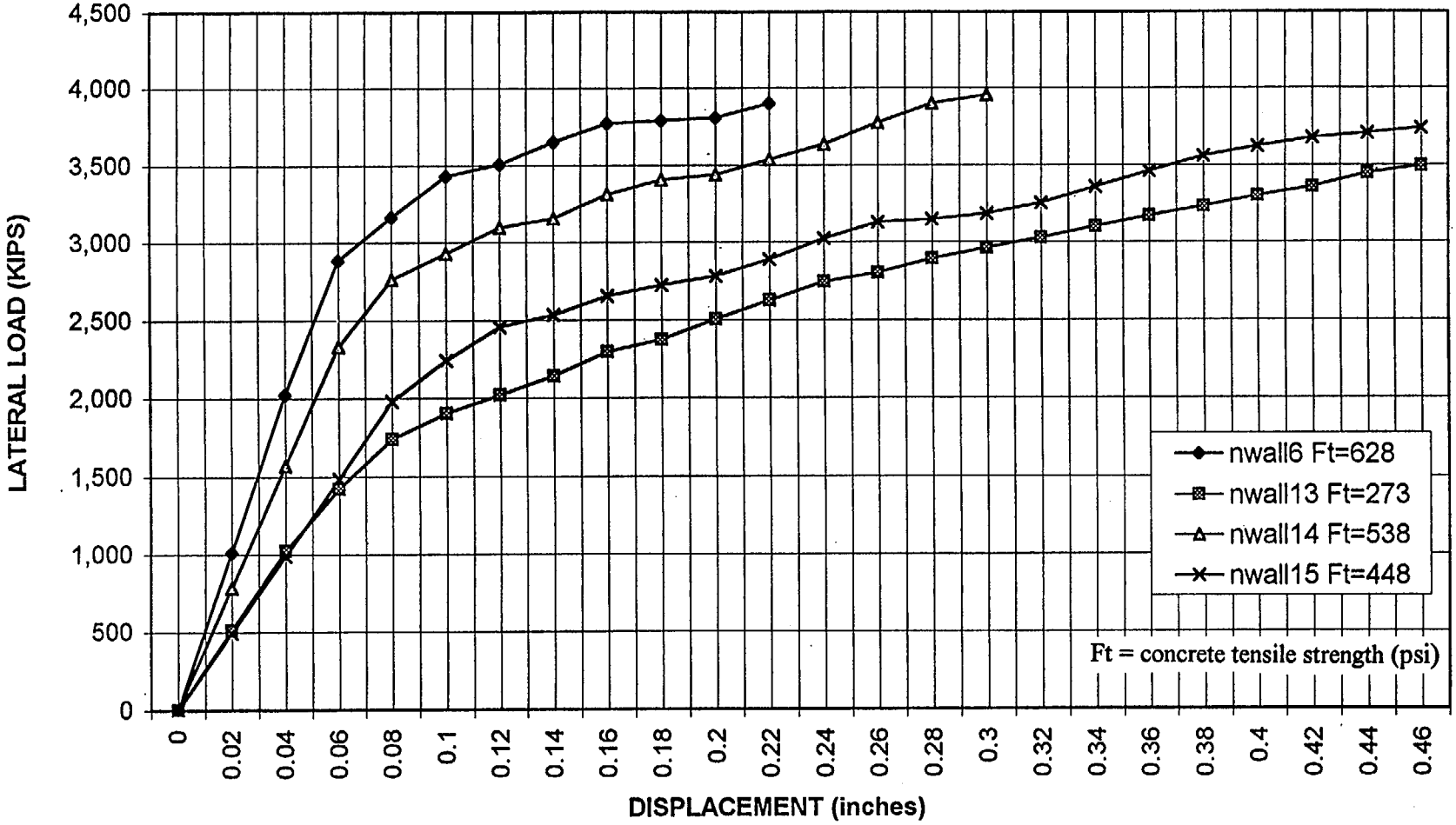

Note: 1 in. = 25.4 mm, 1 kip = 4.45 kN, 1 psi = 6.89 kPa

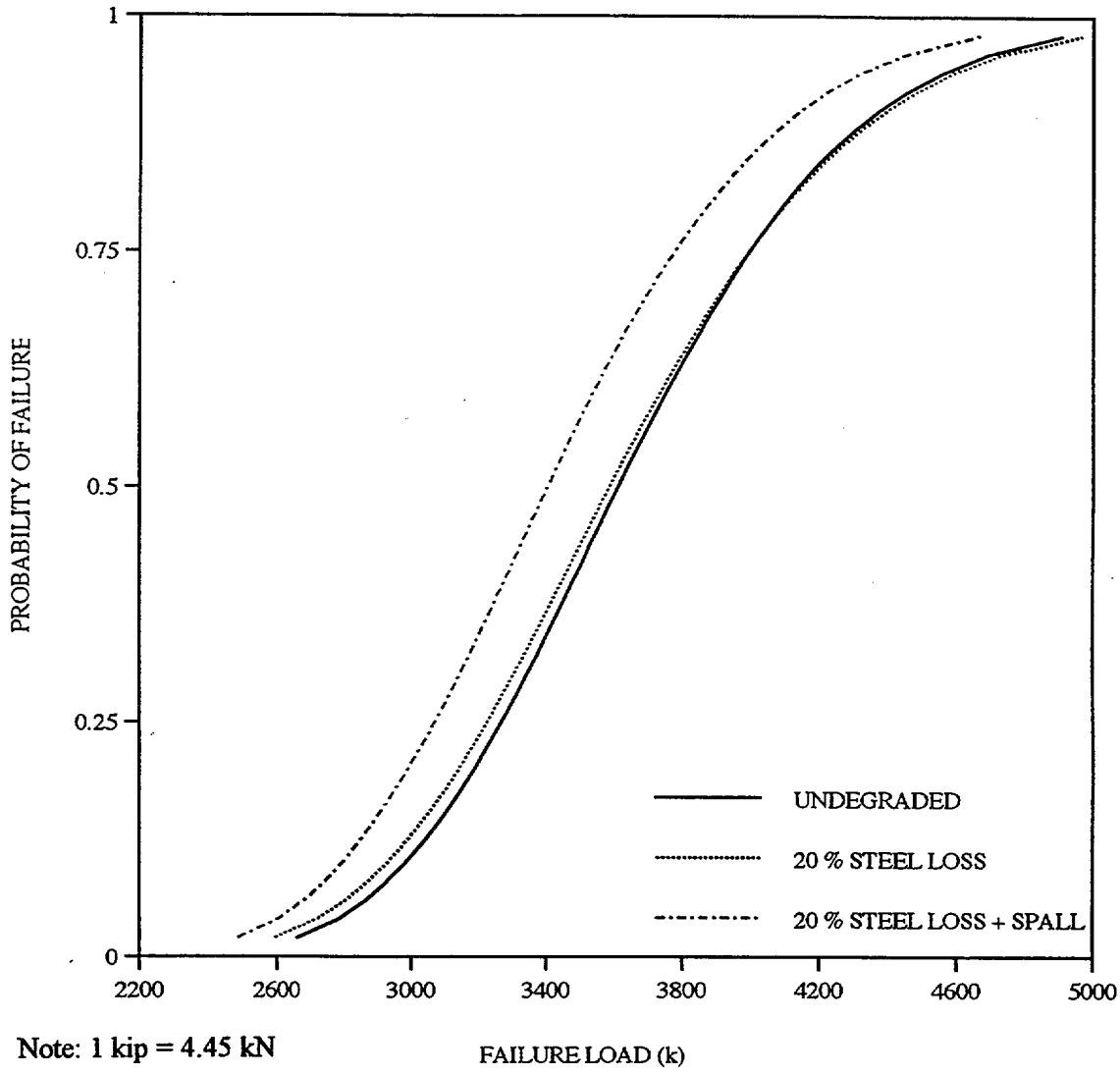

Figure 7.15 Fragility Curve for Example Shear Wall

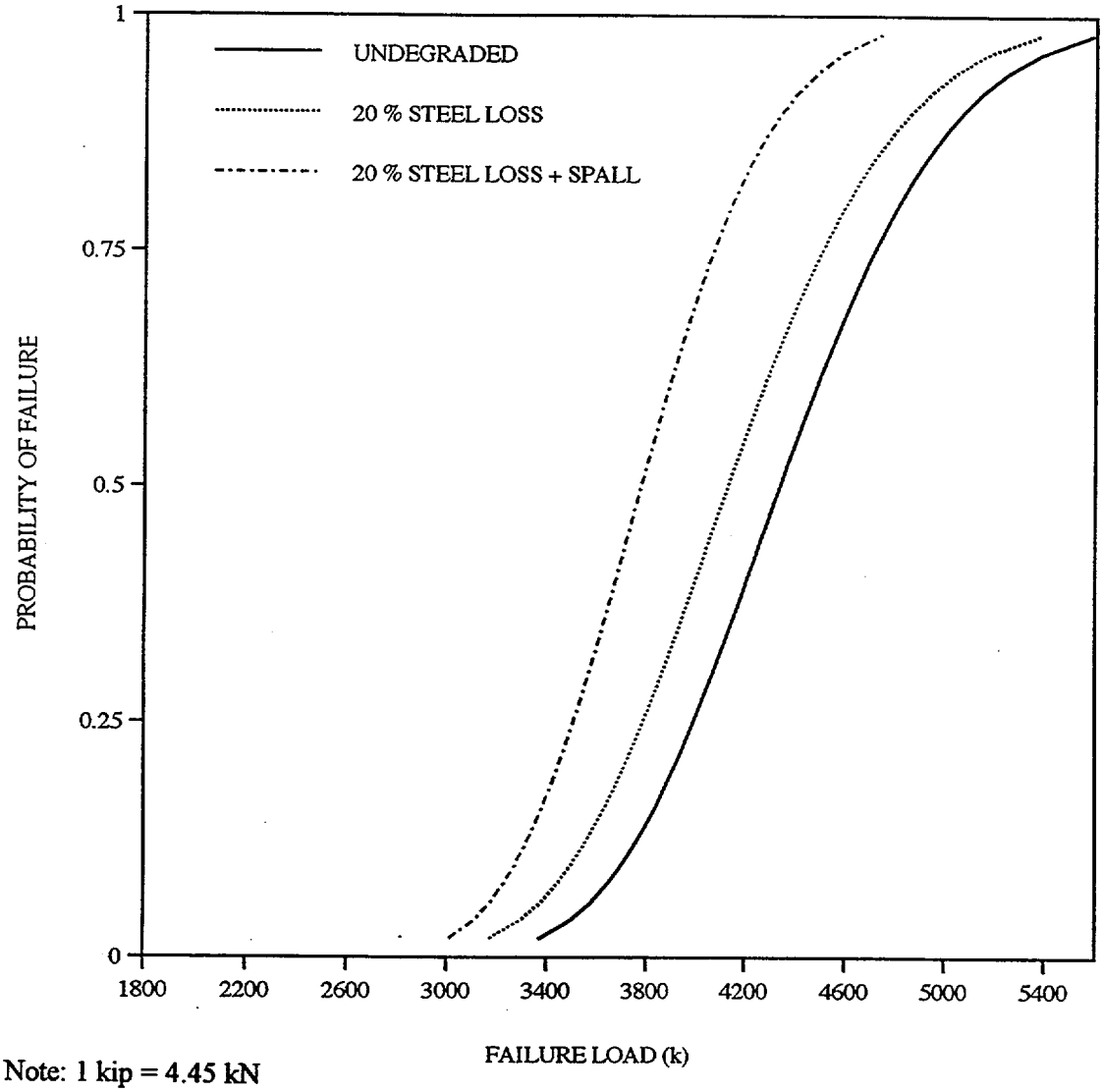

Note: 1 kip = 4.45 kN

Figure. 7.16 Fragility Curve for H/L = 0.5 ; ρ = 0.003

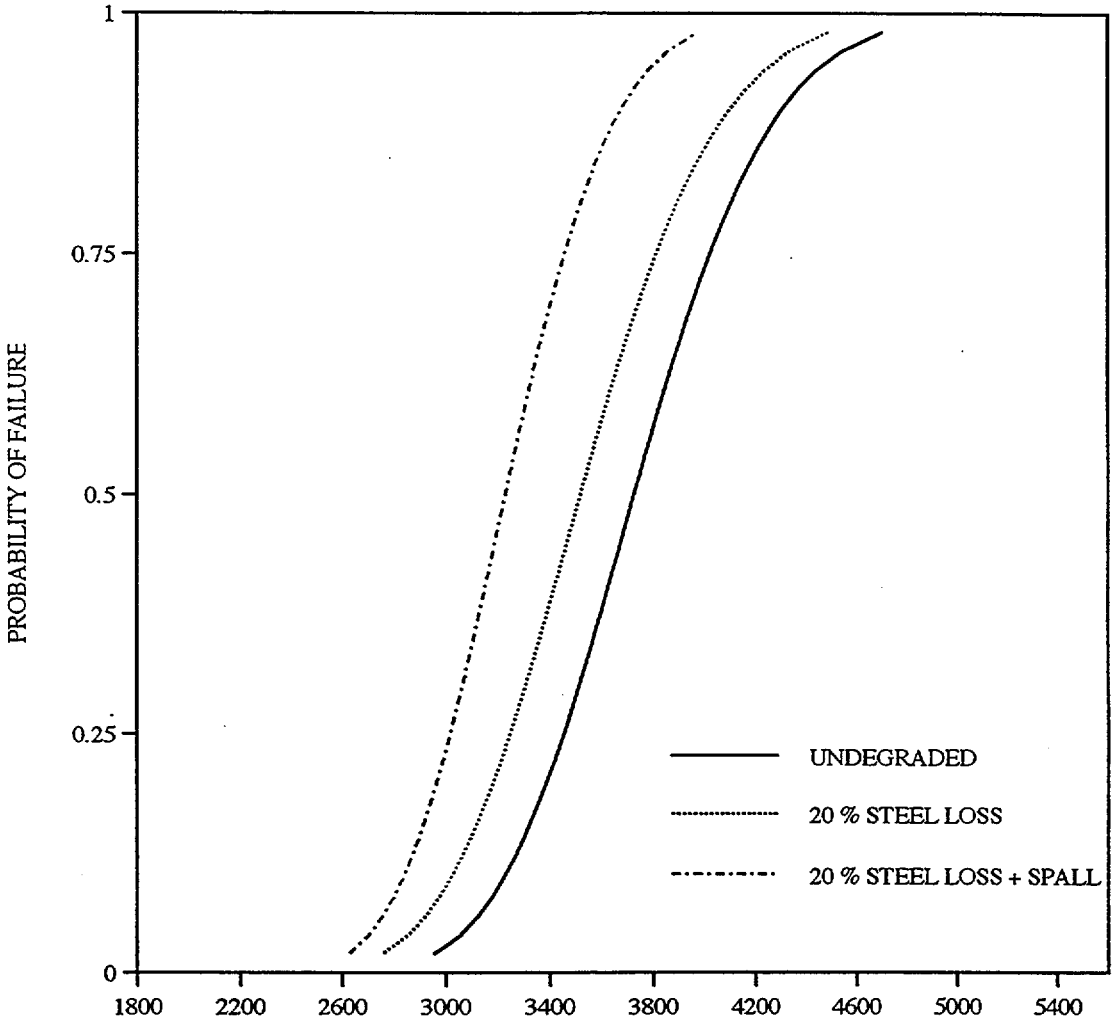

Note: 1 kip = 4.45 kN

Figure 7.17 Fragility Curve for H/L = 1 ;ρ = 0.003

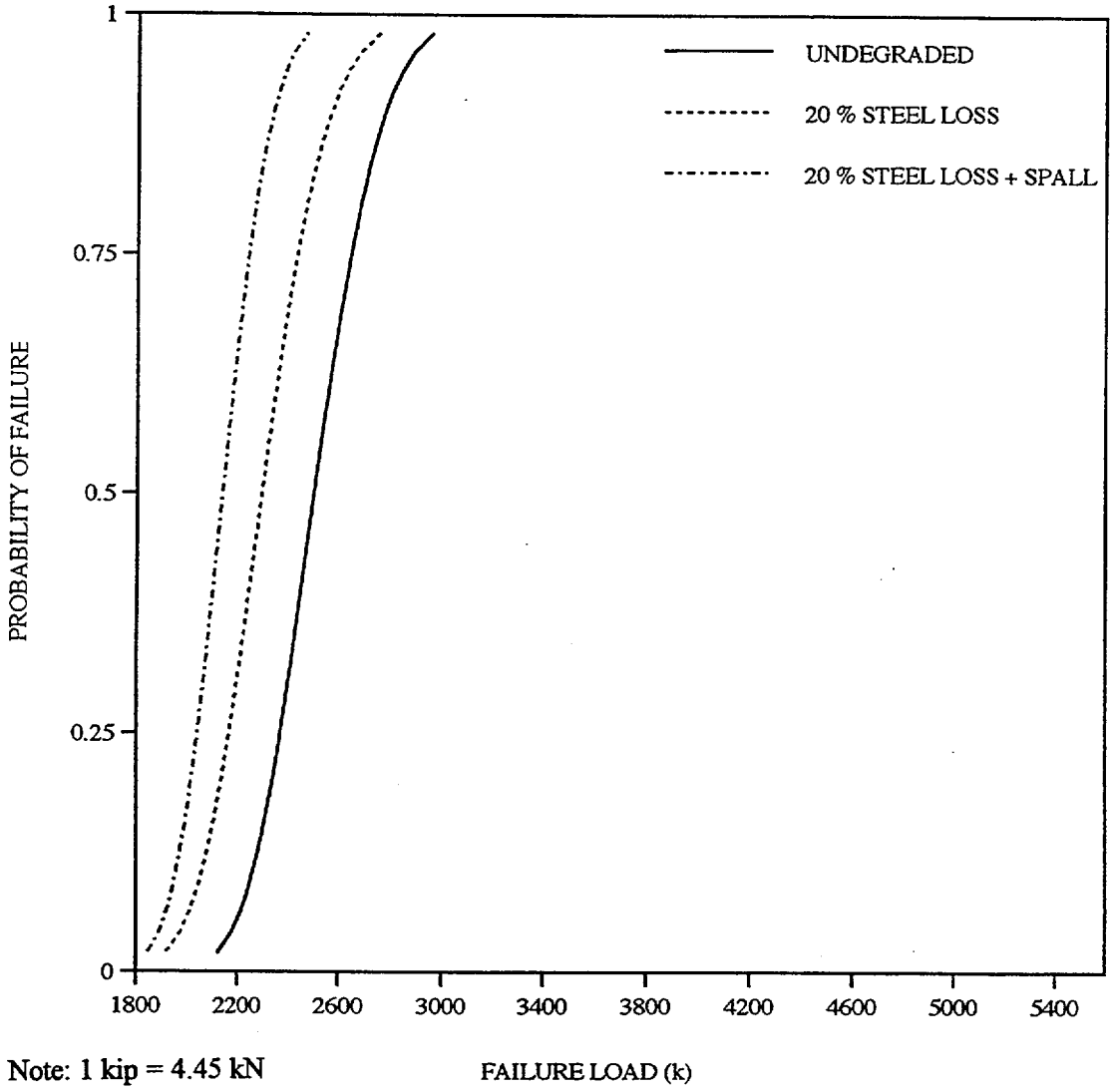

Note: 1 kip = 4.45 kN

Figure 7.18 Fragility Curve for H/L = 2 ;ρ = 0.003

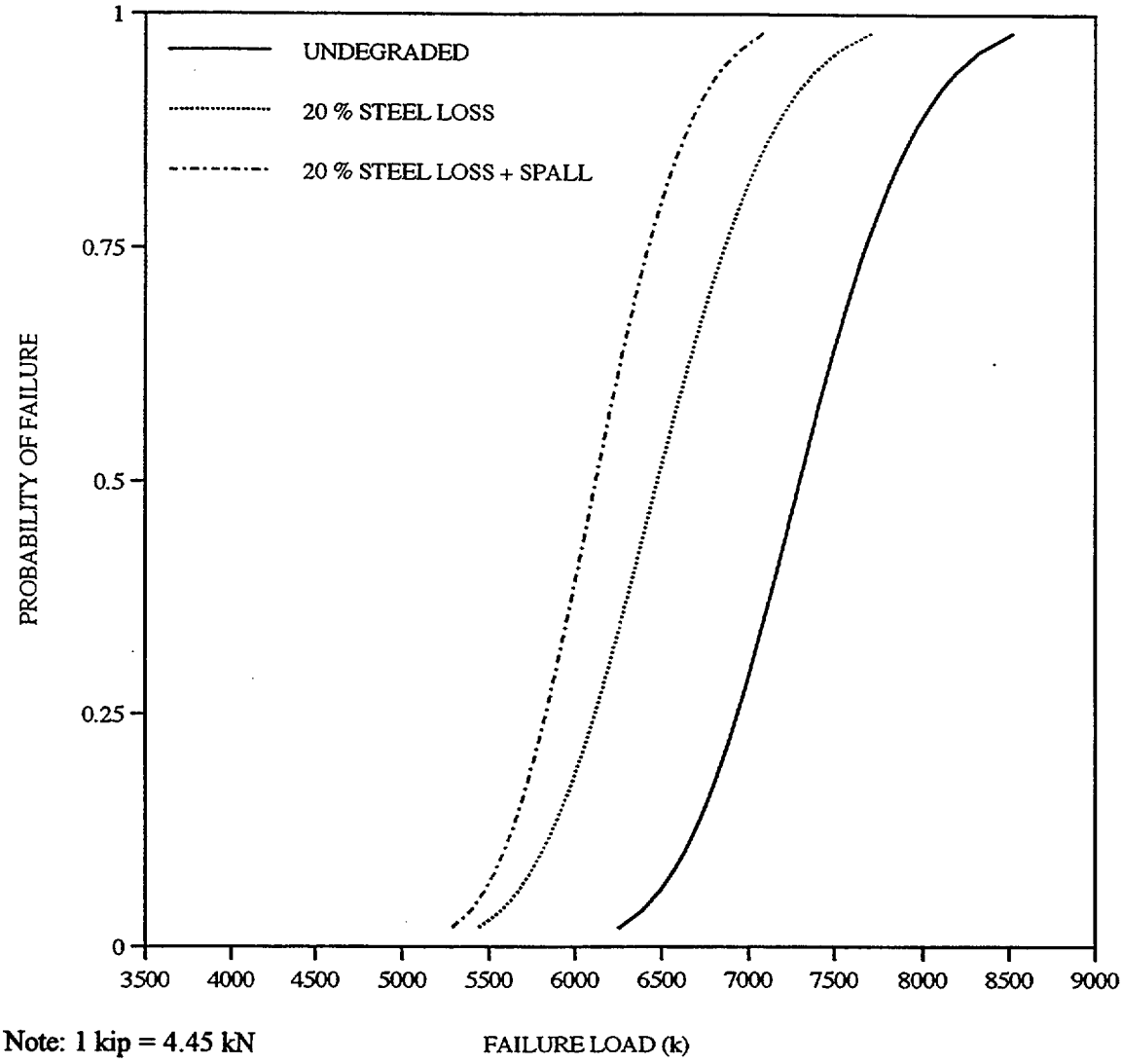

Note: 1 kip = 4.45 kN

Figure 7.19 Fragility Curve for H/L = 0.5 ;ρ = 0.012

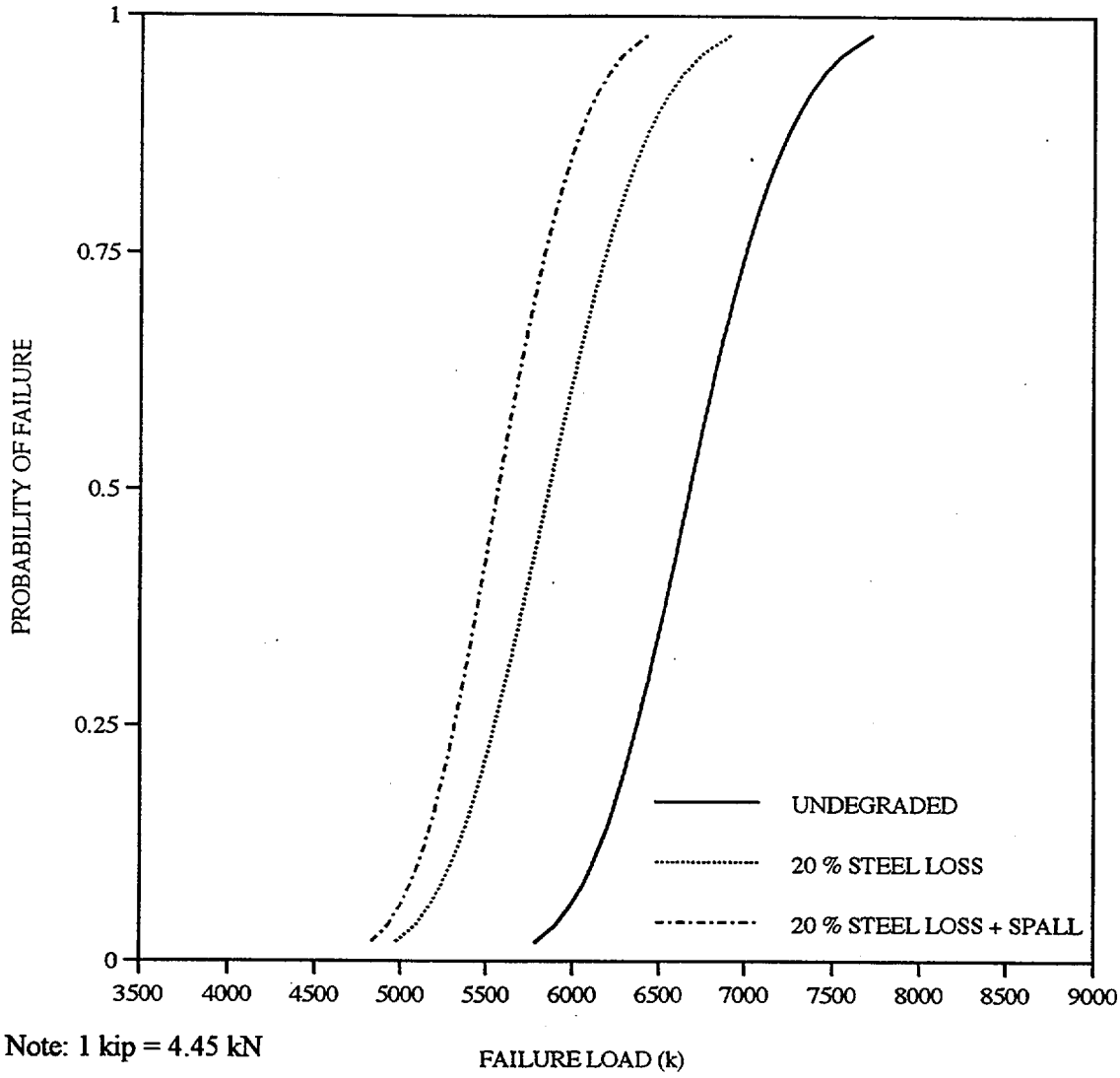

Figure 7.20 Fragility Curve for H/L = 1 ;ρ = 0.012

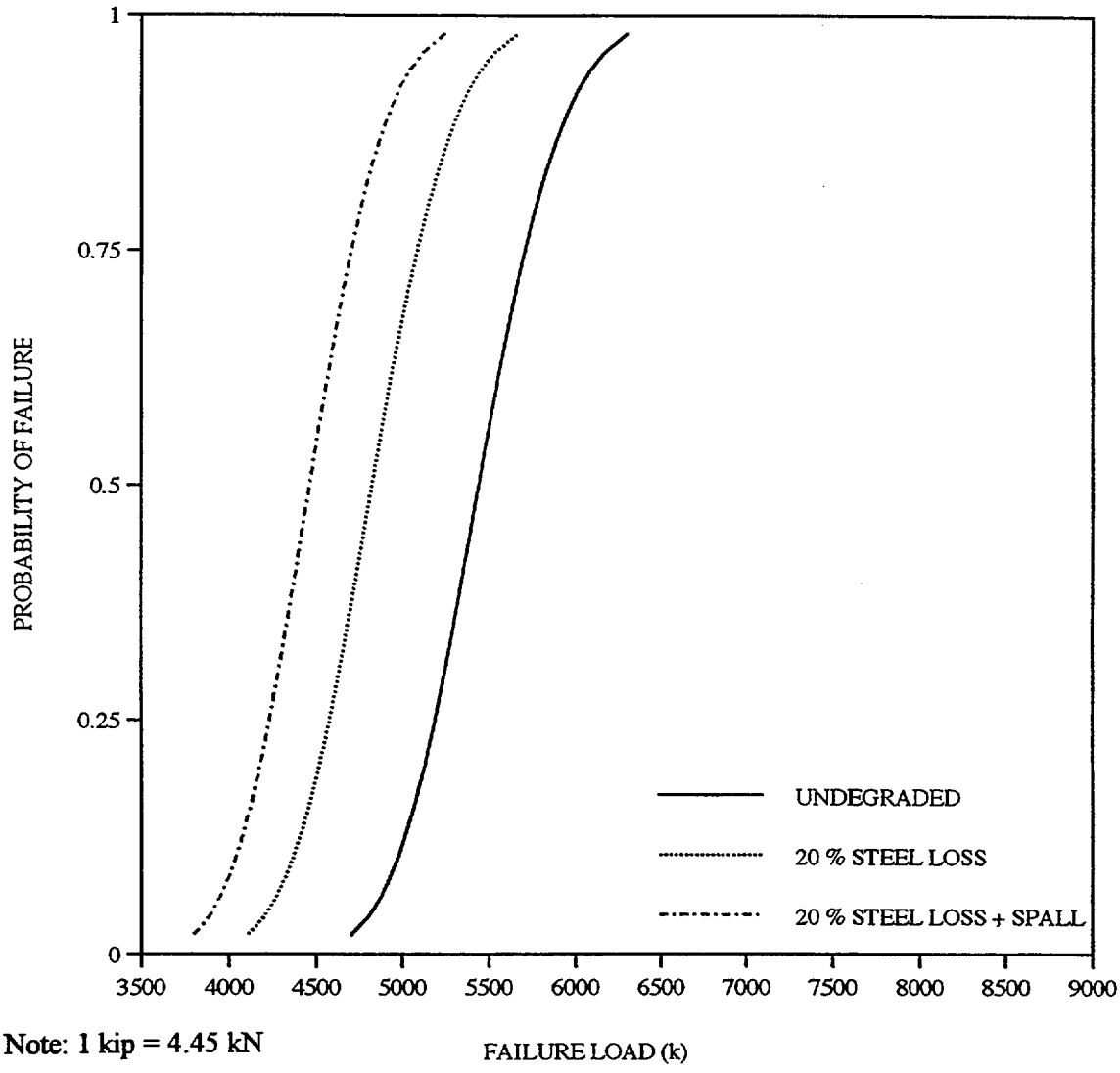

Note: 1 kip = 4.45 kN

Figure 7.21 Fragility Curve for H/L = 2 ;ρ = 0.012

Table 7.1

Statisical Analysis of Undegraded Wall

	fy (ksi)	f'c (ksi)	ft (ksi)	Ec (ksi)	Bsh	Capacity (k)
	72	4.113	0.459	4190	0.96	3572
	58.5	5.764	0.677	5123	0.87	3498
	67.1	4.686	0.533	3830	1	3800
	86.2	3.611	0.526	3736	1.13	4182
	76.3	4.904	0.493	4180	0.84	3260
	63.5	5.393	0.628	5212	1.1	4532
	68.2	4.4	0.42	4789	1.08	4040
	79.4	5.033	0.46	3825	0.9	3348
	71	4.212	0.443	3906	1.02	3712
	72.9	4.307	0.511	3835	1.16	4408
	69.2	3.407	0.415	3087	1.2	4032
	75.1	5.189	0.424	4649	0.8	3232
	81.8	3.036	0.273	2624	0.94	2764
	77.7	4.493	0.538	4029	0.73	2890
	64.9	3.896	0.448	2533	1.06	3392
	73.9	4.588	0.483	3610	1.27	4638
	66.1	4.01	0.398	3014	0.92	3054
	61.7	4.79	0.508	3406	1.04	3828
	70	3.767	0.387	3268	0.98	3266
Mean	71.34	4.40	0.47	3834	1.00	3655
Std Dev	7.10	0.70	0.089	759	0.14	545
COV	0.099	0.159	0.188	0.198	0.140	0.149

Note: 1 ksi = 6.89 MPa, 1 kip = 4.45 kN

Table 7.2

Summary of ANSYS Shear Wall Fragility Analyses
(Using 19 Latin Hypercube Samples)

Case	Wall Capacity[1] kips / MN	COV
Undegraded	3,655 / 16.3	0.149
20% Loss of Steel Area	3,634 / 16.2	0.158
20% Loss of Steel Area & Concrete Spalling	3,446 / 15.3	0.153

Note:

1. Based on limit state defined as 4 X "Design Case" yield deflection.

Table 7.3

Summary of ANSYS Shear Wall Fragility Analyses
(Using Mean Values for Random Variables)

Case	Wall Capacity[1] kips / MN	COV
Undegraded	3,860 / 17.2	Note 3
20% Loss of Steel Area[2]	3,840 / 17.1	Note 3
20% Loss of Steel Area[2] & Concrete Spalling[4]	3,700 / 16.5	Note 3

Notes:

1. Based on limit state defined as 4 X "Design Case" yield deflection.
2. Based on loss of steel area for shear wall and flanges
3. Since only one computer run is made using mean values for random variables, the COV is not directly available. However, based on Table 7.2 results and other runs made, the COV is expected to be very similar to those in Table 7.2
4. Concrete spalling in shear wall but not in flanges

Table 7.4

Statistical Analysis of Shear Wall Using the Barda et. al. Methodology
Aspect Ratio = 0.5 Steel Ratio = .00304

CASE #	Statistical Data					Undegraded Case			20% Loss of Steel			20% Loss of Steel & Cover		
	ft	fy	20% loss of Steel	Loss of Cover	Bsh	Concrete Vc	Steel Vs	Total V=(Vc+Vs)Bsh	Concrete Vc	Steel Vs	Total V=(Vc+Vs)Bsh	Concrete Vc	Steel Vs	Total V=(Vc+Vs)Bsh
	psi	ksi	sq in	in		lbs	lbs	lbs	lbs	lbs	lbs	lbs	lbs	lbs
1	459	72	0.238	1.42	0.96	3,271,450	1,008,599	4,108,847	3,271,450	774,144	3,883,770	2,884,328	774,144	3,512,133
2	677	58.5	0.249	1.81	0.87	4,661,069	819,487	4,768,083	4,661,069	658,063	4,627,645	3,958,024	658,063	4,015,996
3	533	67.1	0.284	2.46	1.00	3,743,155	939,958	4,683,113	3,743,155	860,901	4,604,056	2,975,808	860,901	3,836,709
4	526	86.2	0.217	1.33	1.13	3,698,534	1,207,517	5,543,838	3,698,534	845,044	5,134,244	3,288,614	845,044	4,671,033
5	493	76.3	0.270	1.25	0.84	3,488,179	1,068,835	3,827,892	3,488,179	930,680	3,711,842	3,124,827	930,680	3,406,626
6	628	63.5	0.210	1.08	1.10	4,348,723	889,528	5,762,077	4,348,723	602,428	5,446,267	3,957,338	602,428	5,015,743
7	420	68.2	0.275	0.55	1.08	3,022,848	955,367	4,296,473	3,022,848	847,285	4,179,743	2,884,301	847,285	4,030,112
8	460	79.4	0.223	0.37	0.90	3,277,824	1,112,261	3,951,076	3,277,824	799,904	3,669,955	3,176,758	799,904	3,578,995
9	443	71	0.264	1.70	1.02	3,169,459	994,591	4,247,331	3,169,459	846,788	4,096,572	2,720,452	846,788	3,638,585
10	511	72.9	0.231	0.80	1.16	3,602,918	1,021,207	5,363,985	3,602,918	760,767	5,061,875	3,362,724	760,767	4,783,250
11	415	69.2	0.235	1.17	1.20	2,990,976	969,376	4,752,422	2,990,976	734,660	4,470,763	2,699,356	734,660	4,120,819
12	424	75.1	0.253	0.69	0.80	3,048,346	1,052,025	3,280,296	3,048,346	858,366	3,125,370	2,873,066	858,366	2,985,146
13	273	81.8	0.227	0.04	0.94	2,085,811	1,145,881	3,037,790	2,085,811	838,864	2,749,195	2,078,858	838,864	2,742,659
14	538	77.7	0.256	1.95	0.73	3,775,027	1,088,446	3,550,336	3,775,027	898,614	3,411,758	3,161,585	898,614	2,963,946
15	448	64.9	0.198	0.90	1.06	3,201,331	909,140	4,357,099	3,201,331	580,527	4,008,769	2,961,231	580,527	3,754,264
16	483	73.9	0.242	2.13	1.27	3,424,435	1,035,215	5,663,756	3,424,435	807,927	5,375,100	2,816,598	807,927	4,603,147
17	398	66.1	0.260	1.60	0.92	2,882,611	925,950	3,503,876	2,882,611	776,403	3,366,293	2,498,263	776,403	3,012,693
18	508	61.7	0.245	1.00	1.04	3,583,795	864,313	4,626,033	3,583,795	682,910	4,437,374	3,285,146	682,910	4,126,778
19	387	70	0.299	1.50	0.98	2,812,493	980,582	3,717,214	2,812,493	945,544	3,682,876	2,460,931	945,544	3,338,345
Mean	474.9	71.34	0.246	1.250	1.000	3,373,105	999,383	4,370,607	3,373,105	792,096	4,160,182	3,008,853	792,096	3,796,683
Std. Dev.	89.09	7.096	0.026	0.620	0.140	567,876	99,401	810,160	567,876	102,749	763,972	461,874	102,749	657,754
COV	0.188	0.099	0.105	0.496	0.140	0.168	0.099	0.185	0.168	0.130	0.184	0.154	0.130	0.173

Note: 1 psi = 6.89 kPa, 1 ksi = 6.89 MPa, 1 sq in = 6.45 cm^2, 1 in. = 25.4 mm, 1 lb = 4.45 kN

Table 7.5

Statistical Analysis of Shear Wall Using the Barda et. al. Methodology
Aspect Ratio = 1.0 Steel Ratio = .00304

CASE #	Statistical Data					Undegraded Case			20% Loss of Steel			20% Loss of Steel & Cover		
	ft	fy	20% loss of Steel	Loss of Cover	Bsh	Concrete Vc	Steel Vs	Total V=(Vc+Vs)Bsh	Concrete Vc	Steel Vs	Total V=(Vc+Vs)Bsh	Concrete Vc	Steel Vs	Total V=(Vc+Vs)Bsh
	psi	ksi	sq in	in		lbs	lbs	lbs	lbs	lbs	lbs	lbs	lbs	lbs
1	459	72	0.238	1.42	0.96	2,672,179	1,008,599	3,533,547	2,672,179	774,144	3,308,470	2,355,971	774,144	3,004,911
2	677	58.5	0.249	1.81	0.87	3,777,178	819,487	3,999,098	3,777,178	658,063	3,858,659	3,207,453	658,063	3,362,999
3	533	67.1	0.284	2.46	1.00	3,047,270	939,958	3,987,229	3,047,270	860,901	3,908,171	2,422,580	860,901	3,283,481
4	526	86.2	0.217	1.33	1.13	3,011,789	1,207,517	4,767,816	3,011,789	845,044	4,358,221	2,677,982	845,044	3,981,020
5	493	76.3	0.270	1.25	0.84	2,844,518	1,068,835	3,287,217	2,844,518	930,680	3,171,167	2,548,214	930,680	2,922,272
6	628	63.5	0.210	1.08	1.10	3,528,806	889,528	4,860,168	3,528,806	602,428	4,544,358	3,211,214	602,428	4,195,006
7	420	68.2	0.275	0.55	1.08	2,474,496	955,367	3,704,252	2,474,496	847,285	3,587,523	2,361,082	847,285	3,465,036
8	460	79.4	0.223	0.37	0.90	2,677,248	1,112,261	3,410,558	2,677,248	799,904	3,129,436	2,594,700	799,904	3,055,143
9	443	71	0.264	1.70	1.02	2,591,078	994,591	3,657,383	2,591,078	846,788	3,506,623	2,224,009	846,788	3,132,213
10	511	72.9	0.231	0.80	1.16	2,935,757	1,021,207	4,590,077	2,935,757	760,767	4,287,968	2,740,040	760,767	4,060,936
11	415	69.2	0.235	1.17	1.20	2,449,152	969,376	4,102,233	2,449,152	734,660	3,820,574	2,210,360	734,660	3,534,023
12	424	75.1	0.253	0.69	0.80	2,494,771	1,052,025	2,837,437	2,494,771	858,366	2,682,510	2,351,322	858,366	2,567,751
13	273	81.8	0.227	0.04	0.94	1,729,382	1,145,881	2,702,747	1,729,382	838,864	2,414,151	1,723,618	838,864	2,408,733
14	538	77.7	0.256	1.95	0.73	3,072,614	1,088,446	3,037,574	3,072,614	898,614	2,898,997	2,573,315	898,614	2,534,508
15	448	64.9	0.198	0.90	1.06	2,616,422	909,140	3,737,096	2,616,422	580,527	3,388,766	2,420,191	580,527	3,180,760
16	483	73.9	0.242	2.13	1.27	2,793,830	1,035,215	4,862,887	2,793,830	807,927	4,574,232	2,297,926	807,927	3,944,433
17	398	66.1	0.260	1.60	0.92	2,362,982	925,950	3,025,818	2,362,982	776,403	2,888,234	2,047,918	776,403	2,598,375
18	508	61.7	0.245	1.00	1.04	2,920,550	864,313	3,936,258	2,920,550	682,910	3,747,599	2,677,171	682,910	3,494,485
19	387	70	0.299	1.50	0.98	2,307,226	980,582	3,222,052	2,307,226	945,544	3,187,714	2,018,822	945,544	2,905,079
Mean	474.9	71.34	0.246	1.250	1.000	2,753,013	999,383	3,750,603	2,753,013	792,096	3,540,178	2,455,994	792,096	3,243,745
Std. Dev	89.09	7.096	0.026	0.620	0.140	451,564	99,401	671,526	451,564	102,749	624,201	366,740	102,749	538,513
COV	0.188	0.099	0.105	0.496	0.140	0.164	0.099	0.179	0.164	0.130	0.176	0.149	0.130	0.166

Note: 1 psi = 6.89 kPa, 1 ksi = 6.89 MPa, 1 sq in = 6.45 cm^2, 1 in. = 25.4 mm, 1 lb = 4.45 kN

Table 7.6

Statistical Analysis of Shear Wall Using the Barda et. al. Methodology
Aspect Ratio = 2.0 Steel Ratio = .00304

CASE #	Statistical Data					Undegraded Case			20% Loss of Steel			20% Loss of Steel & Cover		
	ft	fy	20% loss of Steel	Loss of Cover	Bsh	Concrete Vc	Steel Vs	Total V=(Vc+Vs)Bsh	Concrete Vc	Steel Vs	Total V=(Vc+Vs)Bsh	Concrete Vc	Steel Vs	Total V=(Vc+Vs)Bsh
	psi	ksi	sq in	in		lbs	lbs	lbs	lbs	lbs	lbs	lbs	lbs	lbs
1	459	72	0.238	1.42	0.96	1,473,638	1,008,599	2,382,948	1,473,638	774,144	2,157,871	1,299,258	774,144	1,990,466
2	677	58.5	0.249	1.81	0.87	2,009,395	819,487	2,461,127	2,009,395	658,063	2,320,689	1,706,311	658,063	2,057,006
3	533	67.1	0.284	2.46	1.00	1,655,501	939,958	2,595,459	1,655,501	860,901	2,516,402	1,316,123	860,901	2,177,024
4	526	86.2	0.217	1.33	1.13	1,638,298	1,207,517	3,215,771	1,638,298	845,044	2,806,176	1,456,720	845,044	2,600,993
5	493	76.3	0.270	1.25	0.84	1,557,197	1,068,835	2,205,867	1,557,197	930,680	2,089,817	1,394,989	930,680	1,953,562
6	628	63.5	0.210	1.08	1.10	1,888,973	889,528	3,056,351	1,888,973	602,428	2,740,541	1,718,965	602,428	2,553,533
7	420	68.2	0.275	0.55	1.08	1,377,792	955,367	2,519,812	1,377,792	847,285	2,403,083	1,314,643	847,285	2,334,882
8	460	79.4	0.223	0.37	0.90	1,476,096	1,112,261	2,329,521	1,476,096	799,904	2,048,400	1,430,583	799,904	2,007,438
9	443	71	0.264	1.70	1.02	1,434,317	994,591	2,477,486	1,434,317	846,788	2,326,727	1,231,122	846,788	2,119,468
10	511	72.9	0.231	0.80	1.16	1,601,434	1,021,207	3,042,263	1,601,434	760,767	2,740,153	1,494,671	760,767	2,616,309
11	415	69.2	0.235	1.17	1.20	1,365,504	969,376	2,801,856	1,365,504	734,660	2,520,197	1,232,367	734,660	2,360,433
12	424	75.1	0.253	0.69	0.80	1,387,622	1,052,025	1,951,718	1,387,622	858,366	1,796,791	1,307,834	858,366	1,732,960
13	273	81.8	0.227	0.04	0.94	1,016,525	1,145,881	2,032,661	1,016,525	838,864	1,744,065	1,013,136	838,864	1,740,880
14	538	77.7	0.256	1.95	0.73	1,667,789	1,088,446	2,012,052	1,667,789	898,614	1,873,474	1,396,773	898,614	1,675,633
15	448	64.9	0.198	0.90	1.06	1,446,605	909,140	2,497,089	1,446,605	580,527	2,148,759	1,338,109	580,527	2,033,754
16	483	73.9	0.242	2.13	1.27	1,532,621	1,035,215	3,261,151	1,532,621	807,927	2,972,496	1,260,581	807,927	2,627,005
17	398	66.1	0.260	1.60	0.92	1,323,725	925,950	2,069,701	1,323,725	776,403	1,932,117	1,147,228	776,403	1,769,741
18	508	61.7	0.245	1.00	1.04	1,594,061	864,313	2,556,709	1,594,061	682,910	2,368,050	1,461,222	682,910	2,229,898
19	387	70	0.299	1.50	0.98	1,296,691	980,582	2,231,728	1,296,691	945,544	2,197,390	1,134,605	945,544	2,038,545
Mean	474.9	71.34	0.246	1.250	1.000	1,512,831	999,383	2,510,593	1,512,831	792,096	2,300,168	1,350,276	792,096	2,137,870
Std. Dev.	89.09	7.096	0.026	0.620	0.140	218,940	99,401	404,317	218,940	102,749	353,445	176,750	102,749	309,551
COV	0.188	0.099	0.105	0.496	0.140	0.145	0.099	0.161	0.145	0.130	0.154	0.131	0.130	0.145

Note: 1 psi = 6.89 kPa, 1 ksi = 6.89 MPa, 1 sq in =.6.45 cm^2, 1 in. = 25.4 mm, 1 lb = 4.45 kN

Table 7.7

Statistical Analysis of Shear Wall Using the Barda et. al. Methodology
Aspect Ratio = 0.5 Steel Ratio = .012

CASE #	Statistical Data					Undegraded Case			20% Loss of Steel			20% Loss of Steel & Cover		
	ft	fy	20% loss of Steel	Loss of Cover	Bsh	Concrete Vc	Steel Vs	Total V=(Vc+Vs)Bsh	Concrete Vc	Steel Vs	Total V=(Vc+Vs)Bsh	Concrete Vc	Steel Vs	Total V=(Vc+Vs)Bsh
	psi	ksi	sq in	in		lbs	lbs	lbs	lbs	lbs	lbs	lbs	lbs	lbs
1	459	72	0.939	1.42	0.96	3,271,450	3,981,312	6,962,651	3,271,450	3,055,832	6,074,190	2,884,328	3,055,832	5,702,553
2	677	58.5	0.983	1.81	0.87	4,661,069	3,234,816	6,869,420	4,661,069	2,597,617	6,315,057	3,958,024	2,597,617	5,703,408
3	533	67.1	1.121	2.46	1.00	3,743,155	3,710,362	7,453,517	3,743,155	3,398,293	7,141,448	2,975,808	3,398,293	6,374,101
4	526	86.2	0.857	1.33	1.13	3,698,534	4,766,515	9,565,506	3,698,534	3,335,700	7,948,685	3,288,614	3,335,700	7,485,474
5	493	76.3	1.066	1.25	0.84	3,488,179	4,219,085	6,474,102	3,488,179	3,673,739	6,016,011	3,124,827	3,673,739	5,710,795
6	628	63.5	0.829	1.08	1.10	4,348,723	3,511,296	8,646,021	4,348,723	2,378,006	7,399,402	3,957,338	2,378,006	6,968,879
7	420	68.2	1.086	0.55	1.08	3,022,848	3,771,187	7,337,558	3,022,848	3,344,545	6,876,784	2,884,301	3,344,545	6,727,153
8	460	79.4	0.880	0.37	0.90	3,277,824	4,390,502	6,901,494	3,277,824	3,157,514	5,791,804	3,176,758	3,157,514	5,700,845
9	443	71	1.042	1.70	1.02	3,169,459	3,926,016	7,237,385	3,169,459	3,342,583	6,642,283	2,720,452	3,342,583	6,184,296
10	511	72.9	0.912	0.80	1.16	3,602,918	4,031,078	8,855,436	3,602,918	3,003,029	7,662,899	3,362,724	3,003,029	7,384,273
11	415	69.2	0.928	1.17	1.20	2,990,976	3,826,483	8,180,951	2,990,976	2,899,973	7,069,139	2,699,356	2,899,973	6,719,194
12	424	75.1	0.999	0.69	0.80	3,048,346	4,152,730	5,760,860	3,048,346	3,388,289	5,149,308	2,873,066	3,388,289	5,009,084
13	273	81.8	0.896	0.04	0.94	2,085,811	4,523,213	6,212,483	2,085,811	3,311,305	5,073,289	2,078,858	3,311,305	5,066,753
14	538	77.7	1.011	1.95	0.73	3,775,027	4,296,499	5,892,214	3,775,027	3,547,161	5,345,198	3,161,585	3,547,161	4,897,385
15	448	64.9	0.782	0.90	1.06	3,201,331	3,588,710	7,197,444	3,201,331	2,291,553	5,822,457	2,961,231	2,291,553	5,567,951
16	483	73.9	0.955	2.13	1.27	3,424,435	4,086,374	9,538,728	3,424,435	3,189,185	8,399,298	2,816,598	3,189,185	7,627,345
17	398	66.1	1.026	1.60	0.92	2,882,611	3,655,066	6,014,663	2,882,611	3,064,748	5,471,570	2,498,263	3,064,748	5,117,970
18	508	61.7	0.967	1.00	1.04	3,583,795	3,411,763	7,275,381	3,583,795	2,695,698	6,530,673	3,285,146	2,695,698	6,220,077
19	387	70	1.180	1.50	0.98	2,812,493	3,870,720	6,549,549	2,812,493	3,732,409	6,414,003	2,460,931	3,732,409	6,069,473
Mean	474.9	71.34	0.971	1.250	1.000	3,373,105	3,944,933	7,311,861	3,373,105	3,126,694	6,481,237	3,008,853	3,126,694	6,117,737
Std. Dev.	89.09	7.096	0.102	0.620	0.140	567,876	392,374	1,156,573	567,876	405,590	955,336	461,874	405,590	853,179
COV	0.188	0.099	0.105	0.496	0.140	0.168	0.099	0.158	0.168	0.130	0.147	0.154	0.130	0.139

Note: 1 psi = 6.89 kPa, 1 ksi = 6.89 MPa, 1 sq in = 6.45 cm^2, 1 in. = 25.4 mm, 1 lb = 4.45 kN

Table 7.8

Statistical Analysis of Shear Wall Using the Barda et. al. Methodology
Aspect Ratio = 1.0 Steel Ratio = .012

CASE #	Statistical Data					Undegraded Case			20% Loss of Steel			20% Loss of Steel & Cover		
	ft	fy	20% loss of Steel	Loss of Cover	Bsh	Concrete Vc	Steel Vs	Total V=(Vc+Vs)Bsh	Concrete Vc	Steel Vs	Total V=(Vc+Vs)Bsh	Concrete Vc	Steel Vs	Total V=(Vc+Vs)Bsh
	psi	ksi	sq in	in		lbs	lbs	lbs	lbs	lbs	lbs	lbs	lbs	lbs
1	459	72	0.939	1.42	0.96	2,672,179	3,981,312	6,387,352	2,672,179	3,055,832	5,498,890	2,355,971	3,055,832	5,195,331
2	677	58.5	0.983	1.81	0.87	3,777,178	3,234,816	6,100,434	3,777,178	2,597,617	5,546,072	3,207,453	2,597,617	5,050,411
3	533	67.1	1.121	2.46	1.00	3,047,270	3,710,362	6,757,632	3,047,270	3,398,293	6,445,563	2,422,580	3,398,293	5,820,873
4	526	86.2	0.857	1.33	1.13	3,011,789	4,766,515	8,789,484	3,011,789	3,335,700	7,172,662	2,677,982	3,335,700	6,795,461
5	493	76.3	1.066	1.25	0.84	2,844,518	4,219,085	5,933,427	2,844,518	3,673,739	5,475,336	2,548,214	3,673,739	5,226,441
6	628	63.5	0.829	1.08	1.10	3,528,806	3,511,296	7,744,113	3,528,806	2,378,006	6,497,494	3,211,214	2,378,006	6,148,142
7	420	68.2	1.086	0.55	1.08	2,474,496	3,771,187	6,745,338	2,474,496	3,344,545	6,284,564	2,361,082	3,344,545	6,162,077
8	460	79.4	0.880	0.37	0.90	2,677,248	4,390,502	6,360,975	2,677,248	3,157,514	5,251,286	2,594,700	3,157,514	5,176,992
9	443	71	1.042	1.70	1.02	2,591,078	3,926,016	6,647,436	2,591,078	3,342,583	6,052,335	2,224,009	3,342,583	5,677,924
10	511	72.9	0.912	0.80	1.16	2,935,757	4,031,078	8,081,529	2,935,757	3,003,029	6,888,991	2,740,040	3,003,029	6,661,959
11	415	69.2	0.928	1.17	1.20	2,449,152	3,826,483	7,530,762	2,449,152	2,899,973	6,418,950	2,210,360	2,899,973	6,132,399
12	424	75.1	0.999	0.69	0.80	2,494,771	4,152,730	5,318,001	2,494,771	3,388,289	4,706,448	2,351,322	3,388,289	4,591,689
13	273	81.8	0.896	0.04	0.94	1,729,382	4,523,213	5,877,439	1,729,382	3,311,305	4,738,246	1,723,618	3,311,305	4,732,827
14	538	77.7	1.011	1.95	0.73	3,072,614	4,296,499	5,379,453	3,072,614	3,547,161	4,832,436	2,573,315	3,547,161	4,467,947
15	448	64.9	0.782	0.90	1.06	2,616,422	3,588,710	6,577,441	2,616,422	2,291,553	5,202,454	2,420,191	2,291,553	4,994,448
16	483	73.9	0.955	2.13	1.27	2,793,830	4,086,374	8,737,860	2,793,830	3,189,185	7,598,430	2,297,926	3,189,185	6,968,631
17	398	66.1	1.026	1.60	0.92	2,362,982	3,655,066	5,536,604	2,362,982	3,064,748	4,993,512	2,047,918	3,064,748	4,703,653
18	508	61.7	0.967	1.00	1.04	2,920,550	3,411,763	6,585,606	2,920,550	2,695,698	5,840,898	2,677,171	2,695,698	5,587,784
19	387	70	1.180	1.50	0.98	2,307,226	3,870,720	6,054,387	2,307,226	3,732,409	5,918,842	2,018,822	3,732,409	5,636,206
Mean	474.9	71.34	0.971	1.250	1.000	2,753,013	3,944,933	6,691,856	2,753,013	3,126,694	5,861,232	2,455,994	3,126,694	5,564,800
Std. Dev	89.09	7.096	0.102	0.620	0.140	451,564	392,374	1,040,919	451,564	405,590	838,726	366,740	405,590	758,921
COV	0.188	0.099	0.105	0.496	0.140	0.164	0.099	0.156	0.164	0.130	0.143	0.149	0.130	0.136

Note: 1 psi = 6.89 kPa, 1 ksi = 6.89 MPa, 1 sq in = 6.45 cm^2, 1 in. = 25.4 mm, 1 lb = 4.45 kN

Table 7.9

Statistical Analysis of Shear Wall Using the Barda et. al. Methodology
Aspect Ratio = 2.0 Steel Ratio = .012

CASE #	Statistical Data					Undegraded Case			20% Loss of Steel			20% Loss of Steel & Cover		
	ft	fy	20% loss of Steel	Loss of Cover	Bsh	Concrete Vc	Steel Vs	Total V=(Vc+Vs)*Bsh	Concrete Vc	Steel Vs	Total V=(Vc+Vs)*Bsh	Concrete Vc	Steel Vs	Total V=(Vc+Vs)*Bsh
	psi	ksi	sq in	in		lbs	lbs	lbs	lbs	lbs	lbs	lbs	lbs	lbs
1	459	72	0.939	1.42	0.96	1,473,638	3,981,312	5,236,752	1,473,638	3,055,832	4,348,291	1,299,258	3,055,832	4,180,886
2	677	58.5	0.983	1.81	0.87	2,009,395	3,234,816	4,562,464	2,009,395	2,597,617	4,008,101	1,706,311	2,597,617	3,744,418
3	533	67.1	1.121	2.46	1.00	1,655,501	3,710,362	5,365,862	1,655,501	3,398,293	5,053,794	1,316,123	3,398,293	4,714,416
4	526	86.2	0.857	1.33	1.13	1,638,298	4,766,515	7,237,438	1,638,298	3,335,700	5,620,617	1,456,720	3,335,700	5,415,434
5	493	76.3	1.066	1.25	0.84	1,557,197	4,219,085	4,852,077	1,557,197	3,673,739	4,393,986	1,394,989	3,673,739	4,257,731
6	628	63.5	0.829	1.08	1.10	1,888,973	3,511,296	5,940,296	1,888,973	2,378,006	4,693,677	1,718,965	2,378,006	4,506,669
7	420	68.2	1.086	0.55	1.08	1,377,792	3,771,187	5,560,898	1,377,792	3,344,545	5,100,124	1,314,643	3,344,545	5,031,923
8	460	79.4	0.880	0.37	0.90	1,476,096	4,390,502	5,279,939	1,476,096	3,157,514	4,170,249	1,430,583	3,157,514	4,129,288
9	443	71	1.042	1.70	1.02	1,434,317	3,926,016	5,467,539	1,434,317	3,342,583	4,872,438	1,231,122	3,342,583	4,665,179
10	511	72.9	0.912	0.80	1.16	1,601,434	4,031,078	6,533,714	1,601,434	3,003,029	5,341,176	1,494,671	3,003,029	5,217,332
11	415	69.2	0.928	1.17	1.20	1,365,504	3,826,483	6,230,385	1,365,504	2,899,973	5,118,572	1,232,367	2,899,973	4,958,808
12	424	75.1	0.999	0.69	0.80	1,387,622	4,152,730	4,432,282	1,387,622	3,388,289	3,820,729	1,307,834	3,388,289	3,756,898
13	273	81.8	0.896	0.04	0.94	1,016,525	4,523,213	5,207,353	1,016,525	3,311,305	4,068,160	1,013,136	3,311,305	4,064,974
14	538	77.7	1.011	1.95	0.73	1,667,789	4,296,499	4,353,930	1,667,789	3,547,161	3,806,914	1,396,773	3,547,161	3,609,072
15	448	64.9	0.782	0.90	1.06	1,446,605	3,588,710	5,337,434	1,446,605	2,291,553	3,962,447	1,338,109	2,291,553	3,847,442
16	483	73.9	0.955	2.13	1.27	1,532,621	4,086,374	7,136,124	1,532,621	3,189,185	5,996,694	1,260,581	3,189,185	5,651,203
17	398	66.1	1.026	1.60	0.92	1,323,725	3,655,066	4,580,487	1,323,725	3,064,748	4,037,395	1,147,228	3,064,748	3,875,018
18	508	61.7	0.967	1.00	1.04	1,594,061	3,411,763	5,206,057	1,594,061	2,695,698	4,461,349	1,461,222	2,695,698	4,323,197
19	387	70	1.180	1.50	0.98	1,296,691	3,870,720	5,064,063	1,296,691	3,732,409	4,928,518	1,134,605	3,732,409	4,769,673
Mean	474.9	71.34	0.971	1.250	1.000	1,512,831	3,944,933	5,451,847	1,512,831	3,126,694	4,621,223	1,350,276	3,126,694	4,458,924
Std. Dev.	89.09	7.096	0.102	0.620	0.140	218,940	392,374	835,803	218,940	405,590	639,064	176,750	405,590	602,634
COV	0.188	0.099	0.105	0.496	0.140	0.145	0.099	0.153	0.145	0.130	0.138	0.131	0.130	0.135

Note: 1 psi = 6.89 kPa, 1 ksi = 6.89 MPa, 1 sq in = 6.45 cm^2, 1 in. = 25.4 mm, 1 lb = 4.45 kN

Table 7.10

Summary of Shear Wall Fragility Based on Barda Methodology

Reinf. Ratio	Height / Width	Undegraded		20 % Steel Loss		20 % Stl Loss + Spall		Spread Sheet	Fragility Curve
		Mean (k)	COV	Mean (k)	COV	Mean (k)	COV		
0.003	0.5	4,371	0.185	4,160	0.184	3,797	0.173	Table 7.4	Fig. 7.16
	1	3,751	0.179	3,540	0.176	3,244	0.166	Table 7.5	Fig. 7.17
	2	2,511	0.161	2,300	0.154	2,138	0.145	Table 7.6	Fig. 7.18
0.012	0.5	7,312	0.158	6,481	0.147	6118	0.139	Table 7.7	Fig. 7.19
	1	6,692	0.156	5,861	0.143	5,565	0.136	Table 7.8	Fig. 7.20
	2	5,452	0.153	4,621	0.138	4,459	0.135	Table 7.9	Fig. 7.21

Note: 1 kip = 4.45 kN

Table 7.11

Summary of ANSYS Shear Wall Capacities
Effect of Degradation for Varying Aspect Ratios

Height(ft)/ Length(ft)	Aspect Ratio	Undegraded kips	20% Loss of Steel Area kips	20% Loss of Steel Area & Spalling kips
20/40	0.5	7,760	7,760	7,460
20/20	1.0	3,860	3,840	3,700
20/15	1.5	3,840	3,190	3,140

Note: 1 ft = 0.3048 m; 1 kip = 0.004448 MN

Based on:
Mean Values of Random Variables
Capacity From Load – Deflection Curves Using 4 X Design Yield Deflection = 0.3 in. (7.62 mm)
Loss of steel area applicable to shear wall and flange walls

8 PERSPECTIVES ON THE ROLE OF STRUCTURAL DEGRADATION ON PLANT SEISMIC RISK AND RESULTING ACCEPTANCE LIMITS

Previous sections of the report have considered the effect of structural degradation on the fragility of individual reinforced concrete members. The effect of these degradations on overall plant risk is considered first in this section. Acceptance limits are then developed so that the increase in plant risk is maintained within tolerable limits. The extent to which the results obtained for seismic loads may be extrapolated to wind loads is described. Finally, the effects of degradation on the structural response of buildings and in-structure response spectra are discussed.

8.1 Plant Risk

In the previous sections of this report, methods for assessing the fragility of degraded and undegraded reinforced concrete structures in NPPs have been presented, and the databases available to support this assessment have been summarized. The evaluation of the impact of structural aging on plant risk must consider a number of factors. First and foremost is the requirement to ensure that aging has not affected the ability of the plant to respond to challenges at or beyond the design envelope and to maintain public safety and health. Beyond this fundamental requirement, however, there are substantial economic and social issues. The utility must be able to meet the regulatory objectives for safe plant operation practically and economically; otherwise the only alternative is to decommission the plant. Nuclear plants are responsible for over 20% of the power currently generated in the United States, and for some utilities the percentage is much higher. The costs and other impacts of decommissioning and power replacement to meet continuing consumer demand may cause economic dislocations in parts of the US if this alternative is widely adopted. Thus, the results of a fragility assessment must be interpreted carefully if used for regulatory purposes. In this section, we identify and discuss some of the key issues related to the use of fragility assessment in risk-informed decision-making.

One question that naturally arises is how the structural deterioration measured by the fragilities in Sections 6 and 7 might impact overall plant risk. The beams and shear walls analyzed in those sections are typical of reinforced concrete structures that might be found in nuclear plants, but were not taken from any one specific plant. To assess the impact on plant risk, then, a specific NPP must be considered.

8.1.1 Impact of Aging on Risk of Zion Unit No. 1

The impact of structural deterioration on fragility and on plant risk (measured by core damage frequency) was assessed for the Zion Plant Unit No. 1 in a previous study (Ellingwood and Song, 1996). This plant was selected because it had been widely reviewed in previous independent risk studies, its plant logic was easily understandable, and the Boolean expressions describing core damage and dominant plant damage state depended on a mix of structural, mechanical and electrical components. Zion Unit No.1 is a PWR with a large dry prestressed concrete containment. Its design-basis earthquake was 0.17g. The Boolean for core damage (CD) is:

$$CD = 4+8+10+14+17+21+9*(12+22+26) \tag{8.1}$$

in which the numbers refer to specific components, the failure of which contribute to core damage, and symbols + and * denote union and intersection, respectively (Zion, 1981). Of these, components 8, 14 and 26 are reinforced concrete structures:

8: Auxiliary building shear wall
14: Pump enclosure cribhouse roof
26: Pressurizer enclosure roof

The fragility parameters for these components are available elsewhere (Zion, 1981; Ellingwood and Song, 1996). Using these component fragilities, a system-level fragility for CD can be determined from Eq. 8.1:

$$\text{Fragility} = P[CD|A = a] \tag{8.2}$$

in which A = effective peak ground acceleration, measured with respect to gravity, g. It might be noted in Eq. 8.1 that the auxiliary building (8) and pump enclosure roof (14) appear in CD as singleton cutsets, while the pressurizer enclosure roof appears in a doubleton (9*26). Because of this, the impact of failure of the pressurizer enclosure roof on CD frequency is likely to be negligible in comparison with the impact of failure of either the auxiliary building shear wall or pump enclosure roof. The mean core damage limit state probability in Eq. 5.1, reproduced here in a slightly different form for convenience, is

$$P[CD] = \int_0^\infty F_R(x)\, dH(x) \tag{8.3}$$

in which $F_R(x)$ is fragility and H(x) is the seismic hazard, defined as the annual probability that earthquake intensities of level x are exceeded.

The changes in fragility or mean core damage probability brought about by postulated structural deterioration are measured with respect to similar risk baselines for the plant in the undegraded condition. These benchmarks have been determined for Zion Unit No. 1 in previously published research (Ellingwood and Song, 1996; Ellingwood, 1998). The mean core damage probability can be estimated from Eqs. 5.5 and 8.1 – 8.3, using the "combined" uncertainty, β_C, for each component fragility. Using this approach, the mean of P[CD] is 9.5×10^{-6}. Similarly, the HCLPF, estimated as the 1.5-percentile of Eq. 5.5, is 0.24g. These metrics, then, serve as the baselines against which the impact of structural degradation can be assessed.

To illustrate the impact of structural deterioration on probability of core damage and seismic safety margin, we consider three severe cases. First, if the median capacity of the auxiliary building shear wall decreases 10% and the logarithmic standard deviations β_R and β_U increase by 10%, the HCLPF for CD decreases from 0.24g to 0.22g (approximately 8%) and the mean core damage probability increases approximately 16% to 1.1×10^{-5}. The HCLPF for CD can be obtained from Eq. 8.2 as the 95% lower confidence limit of the 5 percentile or, equivalently, the 1.5 percentile of Eq. 5.5. Second, if the reinforcement in the pump enclosure roof slab becomes completely ineffective due to corrosion (i.e., no longer contributes to resisting shear of the pump enclosure) and the median capacity is reduced by approximately 35%, the HCLPF for CD decreases to 0.18g (approximately 25%) and P[CD] increases by approximately 79% to 1.7×10^{-5}. Finally, if both shear wall and roof slab degrade the amounts indicated, the HCLPF for CD decreases to 0.17g (approximately 29%) and P[CD] increases by a factor of approximately 2 to 1.9×10^{-5}. Aging of the pressurizer enclosure roof slab was found to have a negligible impact on both HCLPF and P[CD], as expected.

This analysis, documented in more detail elsewhere (Ellingwood and Song, 1996), shows that aging of structural components that appear as singleton cutsets has a minimal impact on core damage probability due to seismic events (less than a factor of 2). Since core damage probabilities of BWR and PWR plants considered in the IPE and IPEEE programs varied by over an order of magnitude, the impact of aging on core damage frequency for Zion Unit No. 1 appears relatively inconsequential in this context for decision analysis purposes. There is a more noticeable impact on the plant-level HCLPF (on the order of 20%).

It should be noted that the postulated deterioration due to corrosion and concrete spalling in the reinforced concrete beams and shear walls modeled in Sections 6 and 7 led to changes in their median capacities,

m_R, that were substantially less than in the severe cases considered above for Zion Unit 1 for illustrative purposes. The maximum decrease in mean flexural strength (Table 6.2) was 18%; with deterioration to 20% loss of steel, it was 16%. Similarly, the maximum decrease in mean shear capacity (Table 7.2) was 6%. Moreover, the logarithmic standard deviation, β_C, remained essentially unchanged in many cases. Accordingly, the impact on HCLPF capacity of structural deterioration that might be of concern from a periodic inspection almost certainly would be less than that described in the preceding paragraph.

8.1.2 Inferences on Risk Due to Structural Aging at Other Plants

The conclusions and inferences above are based on the analysis of Zion Unit No. 1. The plant logic (represented for Zion No. 1 by Eq. 8.1) differs from plant to plant. However, one might expect to arrive at similar conclusions for other plants if key reinforced concrete structural components (designed by ACI Standards 318 and 349 and SRP 3.8.4) appear in the plant logic Booleans as singleton cutsets (cf Eq. 8.1). A review of plant logic for several other plants indicates that this frequently is the case. If the structural component subject to aging appears in the plant logic model as a singleton cutset (cf Eq. 8.1), then a nominal change in its fragility by p-percent generally impacts the safety margin, measured by the plant-level core damage probability or HCLPF capacity by less than p-percent. The only exception to this is if the structural component of concern happens to be the *weakest* component in the plant logic. Seldom is this the case.

Additional perspective on the role of structural degradation and the relative importance of fragility parameters m_R and β_C on seismic risk of NPPs in general can be obtained from an analysis of terms in Eq. 8.3. Over the range of significance to structural safety, the seismic hazard curve can be described, to first approximation, by,

$$\ln H(x) = A - k \ln x \tag{8.4}$$

in which slope k of H(x) plotted on log-log paper is related to the COV in annual extreme ground motion (acceleration). With the fragility described by the lognormal distribution in Eq. 5.5, the limit state probability becomes, approximately,

$$P[LS] = H(m_R) \exp[(k\beta_C)^2/2] \tag{8.5}$$

In other words, the limit state probability equals the seismic hazard evaluated at the median capacity, $H(m_R)$, multiplied by a correction factor. In the Eastern US, the hazard curve is very flat (COV in annual extreme in excess of 100%) and slope k is on the order of 2. Moreover, for most reinforced concrete structures, β_C ranges from about 0.15 to 0.30. Accordingly, this correction factor in Eq. 8.5 usually will be between 1.05 and 1.20 at NPP sites in the Eastern US. This suggests that the logarithmic standard deviation, β_C, has only a marginal impact on seismic risk. One might then assess the impact of structural degradation on plant risk simply by comparing the seismic hazards evaluated at the undegraded and degraded median capacities.

Changes in the failure probability associated with a structural component, P[LS] (or in P[CD] if $F_R(x)$ in Eq. 8.3 is associated with the plant-level fragility) can be estimated as a function of changes in the median fragility, determined from a median-centered finite element analysis or by other means, from Eq. 8.5. Taking derivatives, one finds that,

$$\Delta P[LS] = - k (\Delta m_R/m_R) P[LS] \tag{8.6}$$

With k typically around 2 for most NPP sites in the Eastern US and with most postulated forms of degradation leading to decreases of less than 20% in median plant-level fragility, as noted above, the increase in P[LS] determined from Eq. 8.6 would be less than 40%. In the Western US, where k tends to be somewhat higher (typically about 3), the increase in P[LS] would be less than 60%. Taking into consideration the fact that the structural component is only one of several components of the plant logic model (cf Eq. 8.1) and using the results presented above, the change in P[CD] would be less than ΔP[LS], unless the structural component were to be the weakest singleton cutset in the plant logic; in situations where the structural component appeared in the plant logic as a doubleton, ΔP[CD] would be substantially less than ΔP[LS].

There is, of course, the question of whether increases in core damage frequency of a factor of 2 or decreases in HCLPF on the order of 10 to 20 percent are significant from a risk management viewpoint. As a result of structural aging brought on by operating conditions, aggressive environments and natural phenomena hazards, at some point in its service life the reinforced concrete structure may no longer strictly conform to the original design requirements of ACI Standards 318 or 349 and Standard Review Plan 3.8.4. Nevertheless, the structure may still retain sufficient capacity to withstand challenges from events at or beyond the original prescriptive design basis. This additional margin of safety is due to several factors: material strengths assumed in design are substantially less than the median strengths; design is based on the assumption of elastic behavior, which does not account for additional capacity beyond the elastic range, which is provided by the ductility inherent in properly designed and detailed structures; conservative assumptions are made regarding structural response and "design-basis" limit states of performance; and factors of safety are applied indiscriminately. An existing reinforced concrete structure that has performed well for a service life of 30 to 40 years presents, *ipso facto*, evidence of a minimum level of integrity. Even in a deteriorated condition, that reinforced concrete beam, slab, or shear wall may still satisfy the intent, if not the letter, of the governing Code.

The recently issued Regulatory Guide 1.174 (1998), "An Approach for Using Probabilistic Risk Assessment in Risk-Informed Decisions on Plant-Specific Changes to the Licensing Basis," allows the use of core damage frequency (CDF, or P[CD] in the terminology above) and large early release frequency (LERF) as an acceptable approach to assessing whether increases in risk are small and consistent with the Nuclear Regulatory Commission's Safety Goal Policy Statement. RG 1.174 presents some guidelines for this assessment. For example, when the calculated increase in P[CD] is in the range of 10^{-6} to 10^{-5} per reactor-year, changes are considered in the acceptable range provided that the resulting P[CD] is less than 10^{-4} per reactor-year (Section 2.2.4 of RG 1.174; Region II of Figure 3).

Implementation of the guidelines in RG 1.174 in assessing the impact of aging in a nuclear power plant structure requires, at the minimum, a Level I (or fully coupled) probabilistic safety assessment, in which the probability P[CD] is determined through the convolution of the plant-level fragility (Eqs. 8.1 and 8.2) with a probabilistic description of the hazard, as represented by Eq. 8.3. Moreover, assessment of LERF requires an assessment of various accident sequences leading to significant, unmitigated releases from the containment prior to evacuation of the population proximate to the plant. [Fortuitously, for Zion Unit No. 1, the Boolean expressions describing the logic for CD and LERF are nearly identical, and the point estimates (means) of these events are both 9.5×10^{-6} per year (Ellingwood and Song, 1996).] The focus of the current study (as noted in Section 1) is on fragility modeling procedures for undegraded and degraded reinforced concrete structural components and systems subjected to earthquakes. Thus, only general conclusions and inferences regarding the impact of structural aging and degradation on plant risk in the light of the RG 1.174 Guidelines can be derived from the above risk analysis.

The changes in P[CD] for the postulated states of degradation in Zion Unit No. 1 (noted in the examples within Section 8.1.1) ranged from 1.5×10^{-6} (degradation of the auxiliary building shear wall) to

9.5×10^{-6} (degradation of the auxiliary building shear wall and pump enclosure roof slab). The baseline P[CD] is 9.5×10^{-6}. For other plants with similar baseline mean P[CD] and for typical changes in median fragility of 20 percent or less, ΔP[CD] (using Eq. 8.6) would equal 3.9×10^{-6} for plants in the Eastern US ($k = 2$) and 5.9×10^{-6} for plants in the Western US ($k = 3$). These changes fall within Region II in Figure 3 of RG 1.174, where changes are considered to be "small," but cumulative impacts must be "tracked." Accordingly, changes in median fragility due to degradation of the order indicated above would put the affected plants in a condition where periodic inspection would be required as a condition of continued service, but taking the plant off-line for rehabilitation probably would not be required.

8.1.3 Perspectives and Recommendations for In-Service Fragility Assessment

Structural maintenance and repair invariably are costly, can be invasive and disruptive, may actually cause damage to the structure in some instances, and may not even be feasible in others. A properly constructed and peer-reviewed fragility model, which is periodically revised based on in-service data and other information and is a permanent part of the plant documentation, can provide quantitative evidence that a nominally degraded reinforced concrete structure still can perform its intended function.

The starting point for this assessment must be a benchmark fragility of the structure in the undegraded condition, which should be developed using methods similar to those described in this study. It is recommended that the mean fragility (Eq. 5.5) be used for this purpose. All uncertainties should be evaluated carefully; not all uncertainties are equally significant for risk. Subsequent changes in fragility due to corrosion, cracking, spalling, or other manifestations of degradation then can be identified clearly, and the fragility may be updated periodically during the service life of the plant (or during a period of extended service) following inspection. The fragility analyses of beams and shear walls presented in Sections 6 and 7 indicated that the deterioration mechanisms considered affected the median structural capacity, m_R, but had a negligible impact on logarithmic standard deviation, β_C. Moreover, minor changes in β_C have a negligible impact on limit state probability for seismic events in the Eastern US (cf Eq. 8.5, et seq). Thus, these periodic revisions to structural fragility could be made by performing only one (median-centered) nonlinear structural analysis and assuming that β_C remains unchanged unless a plant walkdown furnished substantial evidence to the contrary. This would lead to a revised estimate, m_R, that would serve as the anchor point of the revised mean fragility curve and would cause it to simply shift horizontally. Changes in the HCLPF due to aging would then be estimated from Eq. 5.4 and could be compared to the review-level event of interest.

The fact that β_C appears to be relatively unimportant in the structural aging analysis makes this fragility updating process relatively straightforward. If the HCLPF capacity is estimated from Eq. 5.5 at the 0.015 fractile of the mean fragility, i.e.,

$$R_k = m_R e^{-2.2\beta_c} \tag{8.7}$$

then the ratio of degraded to undegraded capacity is exactly the ratio of degraded median (or mean) to undegraded median. As noted above, these medians can be determined from one nonlinear finite element analysis, in which the engineering parameters all are set equal to their respective median values. As noted above, changes of p-percent in structural fragility are accompanied by changes of less than p-percent in core damage fragility or mean probability. Accordingly, it would appear that the degradations of the magnitudes determined in Sections 6 and 7 likely would not have a substantial impact on plant margin or risk.

This revised fragility and HCLPF provides a degree of quantitative support for risk-informed decision making that is not possible with conservative design calculations, but the results still must be interpreted

with some care. The absolute numbers obtained may be relatively sensitive to various assumptions made in the analysis. It would, for example, be difficult to attach any statistical significance to differences of 5 to 10 percent in the HCLPF. On the other hand, the rate of change in HCLPF over an extended service interval may be instructive. Changes of 20 percent or more in HCLPF from the benchmark during a service period of 20 years certainly would be cause for concern, and might suggest that a more comprehensive risk assessment be undertaken. Moreover, an increase in the rate of change in HCLPF would indicate the presence of a degradation mechanism, the effect of which was accelerating in time; such a finding would warrant a comprehensive investigation of structural integrity.

Fragility analysis provides a structured framework for identifying aging factors that are potentially significant for continued plant safety, for focusing in-service inspection and repair on a relatively small number of key structural components and systems, and for arriving at risk-informed decisions regarding the suitability of a structure for continued service with or without repair. The fragility analysis process ensures that available information on uncertainties is treated consistently and provides an audit trail for decisions regarding safety of a facility.

8.2 Degradation Acceptance Limits

Acceptance limits that can form the bases for plant inspections are developed in this section of the report. It is useful to first summarize the results obtained in the previous sections of the report that form the basis for the acceptance criteria.

Changes in component fragility resulting from degradation effects are considered in Section 6 for flexural members (beams and slabs) and in Section 7 for shear walls. Both flexural and shear limit states (failure modes) are considered in these analyses. The limit state for flexure was the ultimate capacity of the member while for the shear wall the limit state was defined as the wall drift exceeding four times the drift at yield load. The limit state of four times the drift at yield was selected to represent the potential for damaging equipment and piping systems that may be mounted on or penetrate the wall. The most significant degradation in reinforced concrete members is found to occur as a result of reinforcement corrosion and concrete spalling. Damage to concrete sections that would be readily observable during a visual inspection is found to result in less than a 20% reduction in the member's fragility for both flexural members and shear walls. This suggests that acceptance criteria can be established which could be used during inspections to identify those concrete members which have undergone significant degradation. This is found to be true for the range of member sizes and material characteristics typically found in NPPs.

The effect of this 20% reduction in member capacity on increase in plant risk is discussed in Section 8.1. An existing PRA study for Zion Unit 1 is used to make a qualitative assessment of the effects of this reduction in capacity on core damage frequency (CDF). It is concluded that a 20% reduction in structural capacity would not be expected to cause more than a 20% change in HCLPF capacity and the CDF would rise by less than a factor of 2. This is judged to be a small increase in risk since it is small as compared to the variability in plant core damage frequencies found in the IPE and IPEEE program (an order of magnitude).

Extending the results from the Zion plant to other plants, the change in CDF ranges from 3.9×10^{-6} (for Eastern US plants) to 5.9×10^{-6} (for Western US plants) for a baseline CDF of 9.5×10^{-6} obtained at the Zion plant. To evaluate the significance of these changes, the guidelines presented in the NRC Regulatory Guide 1.174 were utilized. These changes fell into Region II in Figure 3, "Acceptance Guidelines for CDF," of R.G. 1.174. Changes within Region II are considered to be "small" and cumulative impacts are to be "tracked."

The manifestation of structural damage associated with the 20% reduction in capacity is large cracks, staining, and/or major loss of concrete. This damage would be readily observable during an inspection and forms the basis for the development of acceptance criteria discussed below.

Most reinforced concrete structures contain cracks. It is important during an inspection to distinguish between cracks that are primarily cosmetic and cracks that are structurally significant or of importance to aging. Some level of cracking is therefore to be expected and does not imply any degradation of the component. The recommended degradation acceptance limits are based on levels of degradation that would have to occur to significantly increase plant risk. These limits correspond to severe levels where significant degradation has likely occurred. In this context, degradation resulting in more than a 20% reduction in a component's capacity has been defined as excessive.

8.2.1 Flexural Members

Acceptance criteria are developed for three cases: loss of steel area and concrete spalling, loss of steel area (without concrete spalling), and concrete spalling (without loss of steel area). Additional acceptance criteria are provided following these three cases to ensure that flexural failure rather than shear failure would govern. The additional criteria provided to preclude shear failure would apply to each of the three cases that are presented below.

Loss of Steel Area and Concrete Spalling

The acceptance limits are based on crack sizes associated with a given loss of steel area and loss of concrete outside of the reinforcement. For flexural members, when the steel area loss is combined with a total loss of concrete outside of the reinforcement cage, the steel area loss must be less than 20%. The amount of steel area loss is restricted so that the degradation of the member's fragility curve is less than 20%.

Experimental data is discussed in Section 3.1.2 relating loss of steel area with crack width. Based on these data (Alonso, Andrade, Rodriguez, and Diez, 1998), the crack size (w) associated with a given loss of reinforcing bar radius (Δr_b) is taken to be:

$$w = \Delta r_b / 300 \qquad \text{for } c/d_b < 2$$

$$w = 0.3 + (0.7/200)(\Delta r_b - 100) \qquad \text{for } c/d_b > 2 \tag{8.8}$$

where, w is in mm
Δr_b is in μm
c is concrete cover
d_b is bar diameter

These equations are used together with Eq. 6.25 to obtain restrictions on the depth of a flexural member based on observed crack sizes. For a given crack size, Eqs. 8.8 are used to determine the rebar radius loss. This radius loss is easily converted to steel area loss. Equation 6.25 is then used to evaluate the member depth required to restrict the degraded strength to be at least 80% of the undegraded strength. The results of these calculations are given in Table 8.1 for slabs [19.1 mm (3/4 in.) cover], interior beams [38.1 mm (1-1/2 in.) cover], and exterior beams [76.2 mm (3 in.) cover]. The depths listed in the tables are minimum depths required for the given crack size to apply. For example if a slab is reinforced with # 5 bars, the crack width acceptance limit is 0.79 mm (1/32 in.), 1.59 mm (1/16 in.), and 2.38 mm (3/32 in.) if the slab depth is greater than 15.9 cm (6.25 in.), 21.6 cm (8.5 in.), and 63.5 cm (25 in.) respectively.

Entries in Table 8.1 containing a star indicate that the depths of the flexural members are beyond the range commonly found in NPPs.

Loss of Steel Area (Without Concrete Spalling)

Generalization of the beam results presented in Section 6.4 indicates that a 20% loss of steel area (without concrete spalling) would result in less than a 20% reduction in the member capacity. The same relationships between crack widths and loss of steel area described above in Eqs. 8.8 are used to calculate the acceptable crack widths. The crack acceptance limits for this case are presented in Table 8.2. In this case the crack acceptance criteria are not dependent on the depth of the flexural member for depths normally found in NPPs.

Concrete Spalling (Without Loss of Steel Area)

For the condition of complete concrete spalling outside the reinforcement cage (without loss of steel area), Section 6.4 concluded that the reduction in member strength is less than 20% for the following member depths:

Interior slabs	> 12.7 cm (5 in.) deep
Interior beams	> 25.4 cm (10 in.) deep
Exterior flexural members	> 45.7 cm (18 in.) deep

These parameters fall within the range of those found at most plants operating in the U.S.

Criteria to Preclude Shear Failure

The ACI Code provisions are set so that if failure were to occur, flexural failure rather than shear failure would develop. As discussed in Section 6.4, it is unlikely that the failure mode will change from flexure to shear as a result of degradation. It is possible, however, that the failure mode can change if there is corrosion of the shear reinforcement (stirrups). Corrosion of the stirrups will be manifested by stains and cracks in the flexural member that follow the orientation of the stirrups (perpendicular to the axis of the beam on the outside surfaces). The crack sizes that would indicate significant loss of steel area are the same as the cracks discussed above for flexural members. Stirrups are usually # 5 bars or smaller. Therefore, the acceptance criterion to ensure that shear capacity is not significantly reduced is that crack widths following the orientation of the stirrups should be less than 3.0 mm (1/8 in.) This shear criterion is applicable to each of the three flexural cases presented above.

8.2.2 Shear Walls

For shear walls, the combined effect of a 20% loss of steel area and loss of all concrete outside of the reinforcement cage is found to result in less than a 20% loss of shear wall strength. Therefore, acceptable crack widths for a shear wall are based on a 20% steel area loss in combination with a loss of concrete outside of the reinforcing cage. Using the same relationships between crack widths and loss of steel area described above for flexural members (Eqs. 8.8), the acceptable crack widths are presented in Table 8.3. The above conclusions are applicable to reinforced concrete shear walls with aspect ratios 0.5 to 2.0 and reinforcement ratios up to 0.012. These parameters fall within the range of those found at most plants operating in the U.S.

8.2.3 Conditions for the Use of Acceptance Limits

The above crack limits apply regardless of the number and orientation of the cracks. If any cracks are identified which exceed these limits, then corrective actions should be taken which would include identifying the cause, eliminating the source/cause of the degradation, and repairing the reinforced concrete member.

It should be noted that although it is difficult to define a precise relationship between loss of steel area and crack width, the exact numerical values as defined above are not crucial. If crack widths are found to be greater than these tabulated values, repairs should be made; conversely, if crack widths are less (but larger than normally encountered for undegraded members), an evaluation must be performed to determine if indeed a problem exists which will require corrective action. Therefore, in neither case are cracks ignored; rather, the methodology which addresses them is different. The acceptance limits are not to be used for design basis calculation, qualification, or disposition but only to provide guidance for inspection of reinforced concrete members to determine what further actions are warranted when concrete degradation is encountered. In addition, since the guidance provided herein is based on a probabilistic risk assessment methodology, the acceptance limits cannot be used for NRC licensing activities such as license renewal (10 CFR Part 54) which rely on the current licensing basis of nuclear power plants.

The above limits are applicable to benign environments (e.g., not continuously exposed to high humidity, aggressive chemicals, water/fluids, radiation, etc.). It is expected that repairs would be made prior to reaching these size cracks or spalling of the concrete cover because further degradation could occur in a relatively short time period.

8.3 Extrapolation of Results to Wind Loads

The extent to which the above conclusions may be applicable to wind loading is considered next. In the design of NPPs, seismic and wind loadings are not considered to occur simultaneously. For most NPPs, seismic loading controls and therefore, for these plants the results and conclusions reached in this report would be applicable to wind loads as well. It should be noted that tornado missile damage is not considered here and the seismic analyses shed no light on the missile impact loading case. The following discussion addresses those plants where wind loadings may control over seismic loading.

Seismic and wind loads are similar in that they both require the structural frame to transmit horizontal shear loads down to the foundation. Reinforced concrete members are subjected to uniform loads resulting from either seismic induced accelerations or wind-induced pressures. There is a difference in that the imposed deformations from seismic effects are directly proportional to the seismic accelerations while the wind pressures are proportional to the square of the velocity. Therefore, the seismic capacity (expressed in terms of peak acceleration) of a structure that has been degraded by 20% is 80% of the capacity of the undegraded structure. However, the wind velocity that the degraded structure can withstand is proportional to the square root of 0.8 which is equal to 89% of the capacity of the undegraded structure, assuming that the structural response is essentially elastic in nature. Another difference between the seismic and wind problem lies in the distributions selected to model the problem. The probability distribution of concrete strength was selected to include the effects of rate of loading which is different for the two problems. This is expected to have a minor influence on the results. Therefore it is concluded that the fragility results presented in Sections 6 and 7 are directly applicable to wind loading on the basis that the wind velocity capacities are reduced in proportion to the square root of the degraded capacity.

The use of the fragility data to extend the conclusions to core damage frequency depends, among other factors, on the hazard curve for the initiating event (seismic or wind). The discussions of core damage frequency cannot be extended from seismic to wind since the hazard curves used in this report are based

on a seismic demand. Therefore for those plants where wind loadings control over seismic loadings, the results of this study cannot be extended to wind without further evaluation. However, the methodology developed in this report can be utilized to evaluate this particular concern if it does arise.

8.4 Effects of Degradation on Building Response and Response Spectra

Although not within the scope of this research effort, the effect of degradation on the overall response of NPP plant structures and on floor response spectra has been a concern. It should be noted that degradation that occurs in one or several individual members are not expected to significantly affect the overall response of a structure which typically contains numerous beams, slabs, and walls.

The issue described above has been addressed to some extent in NRC documents, industry standards, and past studies. The development of floor response spectra is discussed in NRC NUREG-0800 (Standard Review Plan) which references NRC Regulatory Guide 1.122, Rev. 1. This regulatory guide provides recommendations for smoothing and broadening floor response spectra to account for uncertainties in the structural frequencies due to uncertainties in the material properties of the structure and soil, and to approximations in the modeling techniques.

Industry standards ASCE 4-86 and ASCE 4-98 also provide guidance on this issue. These standards describe how floor response spectra should be broadened to account for uncertainties in the supporting structure frequencies and soil-structure interaction analysis. For example, ASCE 4-86 specifies that the minimum broadening shall be + and - 15% at each frequency in the amplified response region.

The variation in stiffness properties for concrete resulting from cracks is discussed in the ASCE 4-86 and ASCE 4-98 standards. Section C3.1.3 of ASCE 4-98 references the findings of the ASCE Working Group on the Stiffness of Concrete Shear Wall Structures of ASCE Dynamic Analysis Committee. The Working Group reviewed experimental data available in the open literature on large-scale model tests of shear walls. The results of this review are reported in the ASCE publication "Stiffness of Low Rise Reinforced Concrete Shear Walls." The report concluded that the review of experimental data demonstrated that differences between measured stiffness values and those calculated by common industry methods exist. Therefore, a consensus on how to calculate the stiffness of low aspect ratio reinforced concrete shear walls was developed. The recommendation is to use two concrete in-plane stiffness estimates to bound the effects on in-structure response spectra due to lateral loading. The upper bound stiffness is based on 1.25 X Young's modulus and shear modulus, and the lower bound stiffness is based on 0.75 X Young's modulus and shear modulus.

A research study which provides some insight into the effect of degraded shear wall stiffnesses on seismic plant risk and seismic design loads is described in NUREG/CR-5407. The report describes the results for the reevaluation of the seismic risk for three nuclear power plants: Peach Bottom, Zion, and Arkansas Nuclear One (ANO-1). In the study, shear wall stiffness degradations on the order of 75% and more [for shear stresses above 1,034 kPA (150 psi)] were considered. Increases in core damage frequencies at (1) Peach Bottom were 25 to 30%, (2) ANO-1 were 10%, and (3) Zion were essentially unchanged. An evaluation was also made for deterministic "design-like" structural dynamic calculations with and without the shear stiffness reductions. The loads typically increased in the range of 10 to 20%.

Although the above address reductions in concrete stiffnesses resulting primarily from concrete cracking due to loadings or concrete curing, it is believed that the findings would also encompass age-related cracking as long as the age-related cracking is not significant and as noted earlier occurs in only one or several isolated members of a building structure.

Table 8.1
Flexural Members
Probability-Based Crack Acceptance Limits
Considering Loss of Steel Area and Concrete Spalling

Slabs (3/4 in. Cover)

Minimum Slab Depth (in.)				Acceptable Crack Width
#4 Reinf	#5 Reinf	#6 & #7 Reinf	> #8 Reinf	(in.)
6.5	6.25	6	5.75	1/32
12.75	8.5	7.25	6.5	1/16
*	25	12.75	7.75	3/32
*	*	77	13	1/8
*	*	*	33	5/32

Interior Beams (1-1/2 in. Cover)

Minimum Beam Depth (in.)				Acceptable Crack Width
#4 Reinf	#5 & #6 Reinf	#7 & #8 Reinf	> #9 Reinf	(in.)
13	12.25	12	11.5	1/32
20	15.25	13.5	12.75	1/16
*	29	19	14.5	3/32
*	*	39	20	1/8
*	*	*	35	5/32

Exterior Beams (3 in. Cover)

Minimum Beam Depth (in.)				Acceptable Crack Width
#4 Reinf	#5 & #6 Reinf	#7 & #8 Reinf	> #9 Reinf	(in.)
26	24.5	23.5	23	1/32
40	30.5	26.25	25	1/16
*	58	32.5	27.5	3/32
*	*	50.5	33.5	1/8
*	*	*	47	5/32

*Depth is beyond the range for members commonly found in NPPs
Note: 1 in. = 25.4 mm

Table 8.2

Flexural Members
Probability-Based Crack Acceptance Limits
Without Concrete Spalling

Bar Size	Acceptable Crack Width	
	(mm)	(in.)
#5 or smaller	3.0	1/8
#6 and #7	4.1	5/32
#8 or larger	4.7	3/16

The crack acceptance limits are applicable to all depths of flexural members.

Table 8.3

Shear Walls
Probability-Based Crack Acceptance Limits
Considering Loss of Steel Area and Concrete Spalling

Bar Size	Acceptable Crack Width	
	(mm)	(in.)
#5 or smaller	3.0	1/8
#6 and #7	4.1	5/32
#8 or larger	4.7	3/16

9 SUMMARY, CONCLUSIONS, AND RECOMMENDATIONS

9.1 Summary

The overall objective of this phase of the research program was to develop analytical methods and acceptance limits for degradation of NPP reinforced concrete structures based on considerations of acceptable risk. This was achieved by investigating condition assessment techniques, performing structural analyses of degraded reinforced concrete components, developing probabilistic models for parameters affecting structural performance, conducting fragility and risk evaluation of degraded concrete components, and developing probability-based degradation acceptance limits. In meeting the objective, background information/data and analytical techniques were developed for use in improving and developing methods to assess the effects of age-related degradation on the performance of NPP reinforced concrete structures, including fragility evaluations.

Factors that can lead to age-related degradation of reinforced concrete structures were identified and described. Corrosion of embedded steel reinforcement and concrete spalling (resulting from steel corrosion or freeze-thaw effects) were identified as the primary degradation factors of concern. The relationships between structural performance and concrete cracking and corrosion were investigated. Prior research on the performance of structures degraded by corrosion was summarized. Methods used to assess and quantify the effects of age-related degradation were reviewed. Considerations for development of an in-service inspection program were identified. Finally, criteria were provided for the classification and assessment of concrete degradation, based primarily on visual indicators.

Analytical techniques were developed for use in performing deterministic analyses of reinforced concrete structures including the effects of age-related degradation. These methods include closed-form analysis methods and nonlinear finite element methods. These methods were validated by comparison to alternate analytical methods and experimental test data on reduced scale specimens. The analyses were performed for statically indeterminate reinforced concrete flexural members (beams and slabs) and for shear walls. The relationships between the structural characteristics (strength, stiffness, and ductility) and basic properties (concrete compressive strength, concrete area, steel reinforcement area, and bond strength) were investigated.

To evaluate the effect of age-related degradation of reinforced concrete components on plant risk, fragility analyses were performed for concrete flexural members and shear walls. Fragility curves were developed first for undegraded members to serve as benchmarks, and subsequently for members subjected to postulated states of structural degradation. Random variables included in the fragility analysis are concrete compressive strength, concrete tensile strength, steel yield strength, concrete initial tangent modulus, loss of steel cross-sectional area, loss of concrete area, component dimensions, and structural modeling uncertainty. The limit state for flexural members is based on the ultimate capacity in flexure, while for shear walls the limit state is based on a drift criteria corresponding to four times the yield deflection. Using the reduction in fragility due to age-related degradation of the reinforced concrete components, an estimate is made of the effect that degradation has on overall plant risk.

Based on the reduction in fragility curves and the effect on plant risk, degradation acceptance criteria are developed. These criteria identify the maximum level of degradation that can reasonably be expected to occur and whether such degradation would affect overall plant risk. The level of degradation (change in compressive strength, loss of steel area, loss of concrete area, and loss of bond) is related to levels of degradation that would be observed during a plant walkdown. With this information, individuals who may observe degradation such as cracks in concrete or spalling of concrete will be able to make an informed engineering judgement as to the significance of the noted degradation to plant risk.

9.2 Conclusions

9.2.1 Condition Assessment and Experimental Data

The performance of reinforced concrete structures in NPPs has been good, with the majority of problems being identified and corrected during construction. However, as these structures age, incidences of degradation due to environmental stressor effects are likely to increase the potential threat to their functionality and durability. The most commonly observed form of degradation has been concrete cracking. The degradation factor of primary concern that can potentially impact structural margins of reinforced concrete structures is corrosion of steel reinforcement due to carbonation of the concrete or ingress of chloride ions.

Although it is difficult to define a strong relationship between surface crack width and magnitude of corrosion, as the crack width increases, the probability of corrosion will increase as well as corrosion occurrence. Crack widths $\geq$ 0.15 mm (0.0059 in.) are capable of accelerating the onset of corrosion. As the number of cracks increases, the corrosion risk also increases. Codes furnish limiting crack widths in an attempt to provide corrosion protection.

The ratio of concrete cover to reinforcement bar diameter (C/d) is a significant corrosion parameter. After generation of a crack, the increase in crack width shows a linear relationship to corrosion. Corrosion can reduce the cross-sectional area and ductility of the steel reinforcement. Although test results are limited, evaluations of the performance of reinforced concrete structures (i.e., beams, walls, and columns) indicate that in general the performance of these structures improves with occurrence of corrosion, up to the point of concrete cracking and, depending on conditions, possibly up to the point where spalling occurs provided adequate development length is maintained. Performance has been noted to improve at corroded area ratios up to 20% of the surface area (i.e., bond between concrete and steel reinforcement). The improvement in performance has been attributed to increases in surface roughness of the corroded reinforcement (improved mechanical interlock) and confining forces transverse to the reinforcement developed due to expansion of the corrosion products. As the amount of corrosion increases beyond this point, however, there is a reduction in stiffness, ductility, and strength of the member. Fatigue behavior appears to be most affected by corrosion as the steel can fail prematurely or as a breakdown in the bond between concrete and steel reinforcement occurs. These reductions increase significantly after spalling of the concrete. Also the mode of failure can be affected by cracks resulting from corrosion. Cracks that coincide with the loading direction and cracks that are parallel to the reinforcement are most significant with respect to structural margins. Some data are available from tests in which surface crack widths are related to loss of rebar section, but it is difficult to establish a precise relationship.

In the performance of structural evaluations using visible indicators for guidance, the critical parameter is the occurrence of cracks along (parallel to) the steel reinforcement due to corrosion. At this point in all likelihood there will have been no degradation in structural capacity and sufficient time will remain to implement a repair strategy. Sufficient structural capacity can still remain at the onset of concrete spalling due to corrosion, if adequate development length remains. However, the time period from onset of spalling to loss of structural margins may be relatively short.

Methods for the conduct of condition assessments of reinforced concrete structures are fairly well established and generally start with a visual examination of the structure's surfaces. Guidance is presented in Section 4 for use in development of an in-service inspection program for NPP reinforced concrete structures. Acceptance criteria using both a visual-based as well as a degradation-based approach are provided. In the visual-based approach these criteria are based on surface observations and presented in terms of three levels of acceptance: acceptance without further evaluation, acceptance after review, and additional evaluation required. The degradation-based approach is based on the concept that degradation

of a component is manifested in physical evidence or signs and that these signs can be categorized or classified into distinct stages or conditions in accordance with their potential impact on performance. Concrete cracking and surface defects, and corrosion are addressed by this approach. Establishing a limiting state at which steel corrosion is sufficient to decrease structural margins based on visual indicators is difficult and has been attempted without success by several researchers. As discussed below, surface manifestations (concrete spalling, cracking, and staining) are prominent at levels of degradation resulting in small increases in plant risk.

9.2.2 Flexural Members

The following conclusions resulted from the deterministic structural evaluation and fragility analysis performed on degraded and undegraded beams and slabs:

1. The ANSYS program (with concrete finite elements) was used to predict the response of a typical beam. Very good agreement was found between the ANSYS and analytic solutions for the beam subjected to static monotonically increasing loads.

2. As a result of the very good agreement between the finite element solution and the analytical solution, evaluations of flexural members to age-related degradation can be made using the analytical solution methodology described in Section 6, provided that actual strengths (rather than design strengths) are used in the evaluation. In some instances, this may require in-situ sampling of structural concrete or reinforcement.

3. Degradation mechanisms of corrosion of the reinforcement and concrete spalling resulting from steel corrosion, freeze-thaw effects, or scouring action were found to be potentially significant depending on the level of degradation. Degradation of concrete compressive strength is shown to have little effect on safety margins in flexure, especially since concrete strength generally increases with time thereby compensating for some of the potential losses in strength or effective area due to degradation. Degradation of bond strength is likely to have little effect when adequate detailing is provided.

4. The beam fragility curves shift to lower values of strength as the beam properties degrade. For a 20% loss of steel cross-sectional area (without concrete spalling) or complete spalling of concrete cover (without loss of steel area) the strength of the degraded beam decreases by less than 20%. These levels of degradation are manifested by sizable cracks and staining or spalling. For the case of loss of steel area in combination with complete concrete spalling the loss of steel area must be restricted to be less than 20% in order to maintain the same level of reduction in fragility curves. It is concluded that for all of the cases discussed above, damage to the beam would readily be observable before large strength degradation occurs and that based on the observed damage, it is expected that the beam would be repaired prior to reaching this level of degradation.

5. The beam fragility curves remain almost parallel to each other as beam properties degrade. This implies that the effects of degradation on beam strength at any given conditional probability of failure can be estimated, to first approximation, by considering the impact of degradation on its median capacity, determined by assuming all parameters take on their median values.

6. Generalization of the beam results indicates that the above conclusions apply to all beams and slabs. For the condition of complete concrete spalling, the above conclusions are true for the following:

Interior slabs	> 12.7 cm (5 in.) deep
Interior beams	> 25.4 cm (10 in.) deep
Exterior flexural members	> 45.7 cm (18 in.) deep

9.2.3 Shear Walls

1. Predictions obtained with an ANSYS finite element model of a shear wall are compared with experimental data obtained from a wall with the same design. Both the measured load-deflection and crack patterns compare well with the predictions obtained with the finite element model. Thus the ANSYS program can be used to generate reliable estimates of shear wall behavior when the wall is subjected to a monotonically increasing load.

2. The behavior of a wall typical of those found in NPPs is studied with an ANSYS finite element model of the wall. The wall has a 1:1 aspect ratio, a reinforcement ratio equal to 0.003, and is subjected to an axial load resulting in an axial stress equal to 2.07 MPa (300 psi). Solutions are obtained for the wall in both the undegraded and degraded states. Two degradation states are considered: loss of steel cross-sectional area resulting from corrosion and loss of steel cross-sectional area plus concrete spalling. The mean capacity of the wall is found to decrease by 6% as a result of a 20% loss of steel area and complete concrete spalling. The capacity of the wall at a 2% probability of failure is found to decrease by 7%, indicating (as with flexural members above) that the undegraded and degraded fragility curves are almost parallel. This decrease is not likely to have significant consequences on the plant risk. It is also associated with rather severe corrosion so that a simple inspection of the plant would indicate that there were corrosion problems that should be addressed.

3. The degradation mechanisms that were important for flexural members were also found to be important for shear walls.

4. An analytical model (Barda et al., 1977) developed from structural tests of low-rise shear walls is also used to evaluate the behavior of a wider range of shear walls (with aspect ratios of 0.5, 1, and 2 and reinforcement ratios of 0.003 and 0.012). This range should include most shear walls in NPPs. The closed-form model permits a much simpler solution than the ANSYS solution so that it is feasible to consider a wider range of wall parameters. On the other hand, because of the nature of the supporting structural tests, only the ultimate load capacity rather than maximum deformation can be identified from this analytical model. This model yields a reduction of mean strength of 13% (as compared to 6% with ANSYS) and at a 2% probability of failure, the strength of the wall is reduced by 11% (as compared to 7% with ANSYS). While the results are not directly comparable, since the limit states are different, solutions obtained from the simpler model represent trends as the wall parameters vary, and the quantitative predictions made with the model are likely to be conservative as compared with ANSYS.

   The maximum mean strength degradation obtained with the simpler model is found to be 18% for the case of both loss of steel and concrete spalling. This occurs for the higher reinforcement ratio (0.012) and the highest aspect ratio (2.0). The degradation at the 2% probability of failure point is found to be 19%, again indicating that the undegraded and degraded fragility curves are nearly parallel, suggesting (as before) that it may be sufficient to use the median fragility in the degraded condition (from an evaluation with all parameters at their median values) to anchor the fragility curve. This level of degradation is associated with readily observable cracking and staining of the concrete. It is expected that at these levels (20% reduction in strength), the effects of degradation would be quite severe and would lead to repairs when significant cracking and/or staining is observed. It should be

noted that the modeling uncertainty associated with the prediction of either deformation or capacity of short walls in shear is relatively large in comparison to other parameter uncertainties.

9.2.4 Degradation Effects on Plant Risk

The potential impact of the structural degradation on plant level HCLPF and probability of core damage frequency (CDF) was addressed based on the results of a study of the Zion Plant Unit No. 1. It was shown that a 10% degradation of median shear wall strength and 10% increase in the logarithmic standard deviation results in an 8% decrease in HCLPF and 16% increase in CDF. It was also shown that a 35% reduction in mean strength of a flexural member resulted in a 25% reduction in HCLPF and a 79% increase in CDF. When shear wall and roof slab degradation were considered simultaneously, the HCLPF decreased by 29% and CDF increased 100%. Both statistical measures of degradation (decrease in median; increase in logarithmic standard deviation) are more severe than those found in the current study. It should also be noted that IPEEE studies found an order of magnitude difference in CDF between plants so that a 100% increase (factor of 2) should not be considered very significant.

Based on the conclusions reached from the analysis of the Zion plant, inferences on the change in CDF at other plants were made. To evaluate the significance of the change in CDF, the guidelines presented in the NRC Regulatory Guide 1.174 were utilized. The changes in CDF fell into Region II in Figure 3, "Acceptance Guidelines for CDF," of R.G. 1.174. Changes within Region II are considered to be "small" and cumulative impacts are to be "tracked."

9.2.5 Probability-Based Acceptance Limits for Degraded Reinforced Concrete Components

Based on the results of this study, levels of degradation that are observable and most likely would be repaired would have to occur to increase plant risk significantly. As an example, a 20% loss of steel cross-sectional area and loss of concrete cover were shown in this study to be acceptable limits for age-related degradation of reinforced concrete shear walls. Although, the loss of steel area beyond 20% could be tolerated for its effect on overall plant risk, cracks resulting from such degradation would be very obvious and it would be expected that the plant would make repairs under these conditions.

The acceptance limits developed in this research can be used during plant inspections to evaluate whether age-related degradation of the concrete and reinforcement potentially has a significant effect on plant risk. Since the results of this research were developed using a probabilistic risk assessment methodology, the acceptance limits may be used to determine whether more detailed inspections and evaluations are warranted but should not be used as a "design basis" for acceptance of a degraded condition or for NRC licensing activities such as license renewal (10 CFR Part 54) which rely on the current licensing basis of NPPs.

Degradation acceptance limits have been developed based on levels of degradation that would have to occur to significantly increase plant risk. These degradation acceptance limits correspond to a reduction in fragility of 20%. A detailed description of the acceptance limits and the conditions for their use is presented in Section 8.2 for degraded reinforced concrete flexural members and shear walls. The acceptance limits for these concrete members are summarized as follows:

Flexural Members
Probability-Based Crack Acceptance Limits
Considering Loss of Steel Area and Concrete Spalling

Slabs (3/4 in. Cover)

Minimum Slab Depth (in.)				Acceptable Crack Width
#4 Reinf	#5 Reinf	#6 & #7 Reinf	> #8 Reinf	(in.)
6.5	6.25	6	5.75	1/32
12.75	8.5	7.25	6.5	1/16
*	25	12.75	7.75	3/32
*	*	77	13	1/8
*	*	*	33	5/32

Interior Beams (1-1/2 in. Cover)

Minimum Beam Depth (in.)				Acceptable Crack Width
#4 Reinf	#5 & #6 Reinf	#7 & #8 Reinf	> #9 Reinf	(in.)
13	12.25	12	11.5	1/32
20	15.25	13.5	12.75	1/16
*	29	19	14.5	3/32
*	*	39	20	1/8
*	*	*	35	5/32

Exterior Beams (3 in. Cover)

Minimum Beam Depth (in.)				Acceptable Crack Width
#4 Reinf	#5 & #6 Reinf	#7 & #8 Reinf	> #9 Reinf	(in.)
26	24.5	23.5	23	1/32
40	30.5	26.25	25	1/16
*	58	32.5	27.5	3/32
*	*	50.5	33.5	1/8
*	*	*	47	5/32

* Depth is beyond the range for members commonly found in NPPs.
Note: 1 in. = 25.4 mm

Flexural Members
Probability-Based Crack Acceptance Limits
Without Concrete Spalling

Bar Size	Acceptable Crack Width	
	(mm)	(in.)
#5 or smaller	3.0	1/8
#6 and #7	4.1	5/32
#8 or larger	4.7	3/16

The crack acceptance limits are applicable to all depths of flexural members.

Flexural Members
Concrete Spalling Without Loss of Steel Area

Complete concrete spalling outside the reinforcement cage (without loss of steel area) was found to be acceptable for the following member depths:

Interior slabs	> 12.7 cm (5 in.) deep
Interior beams	> 25.4 cm (10 in.) deep
Exterior flexural members	> 45.7 cm (18 in.) deep

These parameters fall within the range of those found at most plants operating in the U.S.

Criteria to Preclude Shear Failure in Degraded Flexural Members

To ensure that shear failure would not govern, cracks in degraded flexural members that follow the orientation of stirrups (perpendicular to the axis of the beam on the outside surfaces) should be less than 3.0 mm (1/8 in.). This shear criterion is applicable to all three flexural cases presented above.

Shear Walls
Probability-Based Crack Acceptance Limits
Considering Loss of Steel Area and Concrete Spalling

Bar Size	Acceptable Crack Width	
	(mm)	(in.)
#5 or smaller	3.0	1/8
#6 and #7	4.1	5/32
#8 or larger	4.7	3/16

9.3 Recommendations for Possible Future Research

Although the results and conclusions reached in this research effort are considered valid, recommendations for additional studies are provided which could be used to remove some of the conservatisms and/or confirm some of the engineering judgements made in the course of the work reported herein.

9.3.1 Condition Assessment and Experimental Data

Additional research on the performance of degraded concrete structures is available in other countries, including Japan and Spain, which may better relate the observed degradation state to expected structural performance (e.g., structural margins). Also, there are activities funded by the Commission of European Communities that address residual service life of reinforced concrete members (e.g., Project 4062) and condition assessment and maintenance strategies (e.g., Project 4213). It is recommended that this information be obtained and evaluated to determine if a more quantitative relationship between degradation and performance can be developed.

To satisfy the needs of licensing activities such as license renewal (which cannot utilize probability-based acceptance criteria at this time) it would be useful to develop acceptance criteria for concrete degradation on a deterministic basis. This deterministically-based acceptance criteria would ensure that the current licensing basis at NPPs is maintained. The acceptance criteria would specify limits for the significant types of concrete degradation (e.g., cracking and spalling) that are normally encountered at NPPs. Quantitative limits for the aging effects would include location, size, orientation, and number of such defects within a given concrete member.

Although basic approaches are available for conducting condition assessments of reinforced concrete structures, a systematic approach for use by NRC personnel performing plant inspections does not exist. The information contained in this report can be used to develop such a guidance document to quickly assess the potential impact of a degraded condition. Such a document would be most useful if it included the deterministically-based acceptance criteria (discussed above) and the probability-based acceptance criteria (already developed in this report). If the deterministically-based criteria were satisfied then no further evaluation or corrective action would be warranted. If the degradation exceeds the deterministically-based criteria but less than the probability-based criteria, then further evaluation would be needed. If the degradation exceeds the probability-based criteria, then corrective actions such as repair or replacement would be required.

If greater understanding of the degraded condition is desired or needed by the NRC inspector or reviewer, then a more detailed condition assessment approach could be developed. This information would be in the form of a recommended procedure and contain guidelines for use in identifying different types of distress, as well as the cause(s), and documentation of the results. Flow diagrams and charts would be identified and/or developed to aid in the identification and in-depth assessment of degradation. With advances in computer hardware technology and software development, a knowledge-based approach could be utilized that would enable incorporation of pictures, drawings, databases, guides, and computational tools. Some work has already been done in this area at the National Institute of Standards and Technology (Kaetzel et al., 1993) and in France (Petre-Lazar et al., 1988).

9.3.2 Analysis of Flexural Members and Shear Walls

Extending the analytical effort in several areas would validate some of the engineering judgements made in this research effort. These efforts might include:

1. Cyclic loading (non-dynamic) to capture the hysteretic response of the degraded concrete components and to assess the impact, if any, on fragility curves.

2. Dynamic loading rather than static loading to determine whether any significant change in fragility occurs as a result. This would include the dynamic characteristics of the beam and wall (e.g., frequency, dynamic material properties).

3. Additional analysis to demonstrate that, the loss of steel area would govern rather than loss of bond for properly designed steel reinforcement anchorages..

The beam and wall designs/configurations studied in this research effort were selected to be representative of most NPPs operating in the U.S. Variations of some important parameters were investigated. However, some plants may not fall within the range of the design parameters and configurations studied. Therefore, it is recommended that the analysis be expanded to address a wider range of parameters. The analysis could include a wider range of aspect ratios and higher reinforcement ratios. For wall evaluations with aspect ratios greater than 2, moment behavior should be included since it would have some effect on the limit state. The analysis should also consider walls in which the vertical and horizontal reinforcement ratios are different; the walls studied in this research effort had equal steel reinforcement ratios. Additional analyses could be performed to determine the effect of varying design dimensions. For example, smaller wall thicknesses may be more critical for some plants. Other reinforced concrete configurations such as deep beams and columns could also be evaluated.

9.3.3 Application of Methodologies to an Actual Plant

To test the methodologies developed in this research program, it is recommended that these methods be applied to an actual plant. This trial case would also be useful to refine the methods if deemed necessary. The trial case could consist of selecting a representative nuclear plant, which currently has known cases of concrete degradation. This could be either an operating plant or a decommissioned plant where accessibility is easier and limited destructive testing could be performed if needed. Alternatively, it may be possible to get information from actual known cases of degradation which have occurred in the past at nuclear power plants. To test the methodologies and results, some or preferably all of the approaches developed in this research effort could be implemented.

The application of the methodologies could be done in a cost-effective way. For example, the proposed fragility evaluation methodology could be applied to a representative plant for which a PRA study has already been performed in the past. Therefore, most of the existing analysis results may be utilized to calculate the effect of degradation on the reduction in fragilities and the effect on overall plant risk.

10 REFERENCES

Abe, M., Kikuta, S., Masuda, Y., and Tomozawa, F. (1989). "Experimental Study On Mechanical Behavior of Reinforced Concrete Members Affected by Alkali-Aggregate Reaction." *8th International Conference on Alkali-Aggregate Reaction*, Edited by Okada, pp. 691-696, Nishibayashi, and Kawamura, Elsevier Applied Science, London, England.

ACI Committee 201 (1968). "Guide for Making a Condition Survey of Concrete in Service." ACI 20101R-68, American Concrete Institute, Farmington Hills, Michigan.

ACI Committee 201 (1987). "Guide to Durable Concrete." ACI 201.2R-77. American Concrete Institute, Farmington Hills, Michigan.

ACI Committee 201 (1968). "Guide for Making a Condition Survey of Concrete in Service." ACI 201.1R-68. American Concrete Institute, Farmington Hills, Michigan.

ACI Committee 207 (1979). "Practices for Evaluation of Concrete in Existing Massive Structures for Service Conditions." ACI 207.3R-79. American Concrete Institute, Farmington Hills, Michigan.

ACI Committee 210 (1993). "Erosion of Concrete Hydraulic Structures." American Concrete Institute, Farmington Hills, Michigan.

ACI Committee 215 (1974). "Considerations for Design of Concrete Structures Subjected to Fatigue Loading." ACI 215R. American Concrete Institute, Farmington Hills, Michigan.

ACI Committee 222 (1999). "Protection of Metals in Concrete Against Corrosion." ACI 222R-9X (draft). American Concrete Institute, Farmington Hills, Michigan.

ACI Committee 224 (1984). "Causes, Evaluation, and Repair of Cracks in Concrete Structures." Report No, 224R-84. *Journal of the American Concrete Institute* 81(3), pp. 211-230, American Concrete Institute, Farmington Hills, Michigan.

ACI Committee 224 (1990). "Control of Cracking in Concrete Structures." ACI 224R. *Manual of Concrete Practice*, Part 3, American Concrete Institute, Farmington Hills, Michigan

ACI Committee 228 (1989). "In-Place Methods for Determination of Strength of Concrete." ACI 228.1R-89. American Concrete Institute, Farmington Hills, Michigan.

ACI Committee 228 (1999). "Nondestructive Test Methods for Evaluation of Concrete in Structures." ACI 228.2R-99. American Concrete Institute, Farmington Hills, Michigan.

ACI Committee 311 (1988). "Guide for Concrete Inspection." ACI311.4R-88. American Concrete Institute, Farmington Hills, Michigan.

ACI Committee 318 (1995). "Building Code Requirements for Reinforced Concrete." ACI Standard 318. American Concrete Institute, Farmington Hills, Michigan.

ACI Committee 318 (1999). "Building Code Requirements for Reinforced Concrete." ACI Standard 318. American Concrete Institute, Farmington Hills, Michigan.

ACI Committee 349 (1985). "Code Requirements for Nuclear Safety Related Concrete Structures." ACI 349-85. American Concrete Institute, Farmington Hills, Michigan.

ACI Committee 349 (1991). "Reinforced Concrete Design for Thermal Effects on Nuclear Power Plant Çoncrete Structures." ACI 349.1R. American Concrete Institute, Farmington Hills, Michigan.

ACI Committee 349 (1996). "Evaluation of Existing Nuclear Safety-Related Concrete Structures." ACI 349.3R. American Concrete Institute, Farmington Hills, Michigan.

ACI Committee 359 (1989). "Code for Concrete Reactor Vessels and Containments." ACI 359-89. American Concrete Institute, Farmington Hills, Michigan.

ACI Committee 364 (1993). "Guide for Evaluation of Concrete Structures Prior to Rehabilitation." ACI 364.1R. *ACI Materials Journal* 90(5), American Concrete Institute, Farmington Hills, Michigan.

ACI Committee 515 (1985). "A Guide to the Use of Waterproofing, Dampproofing, Protective, and Decorative Barrier Systems for Concrete." ACI 515.1R. American Concrete Institute, Farmington Hills, Michigan.

AISC (1980). "Manual of Steel Construction." 8th Edition, pp. 6.4-6.6, American Institute of Steel Construction, Chicago, Illinois.

Akiyama, H., Sakano, K., and Yamanobe S. (1987). "Shear Strength and Deformation for Reinforced Concrete Beams with Latticed Through Cracks." Annual Report of Kajima Institute of Construction Technology, Vol. 35, pp. 57-62, (in Japanese), Japan.

Allen, R. T. L. and Forrester, A. (1983). "The Investigation and Repair of Damaged Reinforced Concrete Structures." *Corrosion of Reinforcement in Concrete Construction*, Society of Chemical Industry, Chichester, Ellis Horwood, England.

Almusallam, A. A., Al-Gahtani, A. S., Aziz, A. R., Dakhil, F. H., and Rasheeduzzafar (1996). "Effect of Reinforcement Corrosion on Flexural Behavior of Concrete Slabs." *Journal of Materials in Civil Engineering* 8(3), pp. 123-127, American Society of Civil Engineers, New York, New York, August.

Alonso, C., Andrade, c., Rodriguez, J, and Diez, J. M. (1998). "Factors Controlling Cracking of Concrete Affected by Reinforcement Corrosion." *Materials and Structures* 31(211), pp. 435-441, RILEM, Cachan, France.

Al-Sulaimani, G. J., Kaleemullah, M., Basunbul, I. A., and Rasheeduzzafar (1990). "Influence of Corrosion and Cracking on Bond Behavior and Strength of Reinforced Concrete Members." *ACI Structural Journal* 87(2), pp. 220-231, American Concrete Institute, Farmington Hills, Michigan.

Amleh, l. and Mirza, S. (1999). "Corrosion Influence on Bond Between Steel and Concrete." *ACI Structural Journal* 96(3), 415-423, American Concrete Institute, Farmington Hills, Michigan.

Andrade, C., Alonso, C., González,J. A., and Rodríguez, J. (1989). "Remaining Service Life of Corroding Structures." *Proceedings of IABSE Symposium on Durability of Structures*, pp. 359-363, International Association of Bridge and Structural Engineers, Zurich, Switzerland.

Andrade, C., Alonso, C., and Molina, F. J. (1993). "Cover Cracking as a Function of Bar Corrosion: Part 1 – Experimental Test." *Materials and Structures* 26(162), pp. 453-464, RILEM, Cachan, France.

ANS (1985). "Guidelines on the Nuclear Analysis and Design of Concrete Radiation Shielding for Nuclear Power Plants." ANSI/ANS-6.4-1985. American Nuclear Society, La Grange Park, Illinois.

ANSI/ASCE (1990). "Guidelines for Structural Condition Assessment of Existing Buildings." ANSI/ASCE 11-90. American Society of Civil Engineers, New York, New York.

ANSYS. Finite Element Computer Code. ANSYS Rev. 5.4, ANSYS, Inc., Canonsburg, PA.

Arya, C. and Wood, L. A. (1995). "The Relevance of Cracking in Concrete to Corrosion of Reinforcement." Technical Report No. 44, Concrete Society, Slough, Berkshire, England.

Arya, C. (1995). "When Cracks Start to Show." *Concrete*, November/December.

Ashar, H. and Bagchi, G. (1995). "Assessment of Inservice Conditions of Safety-Related Nuclear Power Plant Structures." NUREG-1522. U. S. Nuclear Regulatory Commission, Washington, D.C.

Ashar, H. and Bagchi, G. (1999). "Monitoring Age-Related Degradations of Concrete Structures in U.S. Nuclear Power Plants." *International Conference on Life Prediction and Aging Management of Concrete Structures*, pp. 347-355, EXPERTCENTRUM, Bratislava, Slovakia.

ASCE (1994) Publication. "Stiffness of Low Rise Reinforced Concrete Shear Walls." American Society of Civil Engineers, New York.

ASME (1995). "Requirements for Class CC Concrete Components of Light-Water Cooled Plants." Section XI, ASME Boiler and Pressure Vessel Code. American Society of Mechanical Engineers, New York, New York.

ASTM (1990). "ASTM Protective Coatings Standards for Use in Nuclear Power Plants." American Society for Testing and Materials, West Conshohocken, Pennsylvania.

ASTM (1990a). "Manual on Maintenance of Coatings in Nuclear Power Plants." Manual MNL 8. American Society for Testing and Materials, West Conshohocken, Pennsylvania.

ASTM C 803. "Standard Test Method for Probe Penetration Resistance of Hardened Concrete." American Society for Testing and Materials, West Conshohocken, Pennsylvania.

ASTM C 805. "Standard Test Method for Rebound Number of Hardened Concrete." American Society for Testing and Materials, West Conshohocken, Pennsylvania.

ASTM C 856. "Standard Practice for Petrographic Examination of Hardened Concrete." American Society for Testing and Materials, West Conshohocken, Pennsylvania.

ASTM C 597. "Test Method for Pulse Velocity Through Concrete." American Society for Testing and Materials, West Conshohocken, Pennsylvania.

ASTM C 856. "Standard Recommende Practice for Petrographic Examination of Hardened Concrete." American Society for Testing and Materials, West Conshohocken, Pennsylvania.

ASTM C 876. "Standard Test Method for Half Cell Potentials of Reinforcing Steel in Concrete." American Society for Testing and Materials, West Conshohocken, Pennsylvania.

ASTM C 900. "Standard Test Method for Pullout Strength of Hardened Concrete." American Society for Testing and Materials, West Conshohocken, Pennsylvania.

ASTM C 1152. "Test Method for Acid-Soluble Chloride in Mortar and Concrete." American Society for Testing and Materials, West Conshohocken, Pennsylvania.

ASTM C 1218. "Test Method for Water-Soluble Chloride in Mortar and Concrete." American Society for Testing and Materials, West Conshohocken, Pennsylvania.

ASTM D 4580. "Practice for Measuring Delaminations in Concrete Bridge Decks by Sounding." American Society for Testing and Materials, West Conshohocken, Pennsylvania.

ASTM D 4788. "Test Method for Detecting Delaminations in Bridge Decks Using Infrared Thermography." American Society for Testing and Materials, West Conshohocken, Pennsylvania.

Barda, F., Hanson, J. M., and Corley, W. G. "Shear Strength of Low-Rise Walls with Boundary Elements." Reinforced Concrete Structures in Seismic Zones, ACI SP-53, American Concrete Institute, 1977.

Beeby, A. W. (1978). "Corrosion of Reinforcing Steel in Concrete and Its Relation to Cracking." *The Structural Engineer* 56A(3), pp. 77-81, London, England, March.

Beeby, A. W. (1978a). "Cracking and Corrosion." *Concrete In the Oceans*, Technical Report No. 1, Cement and Concrete Association, Slough, England.

Beeby, A. W. (1979). "Corrosion of Reinforcement and Crack Widths." Proceedings of International Symposium, *Offshore Structures*, pp. 1.47-1.60, Rio de Janeiro, Brazil, Pentech Press, Plymouth, England.

Beeby, A. W. (1979a). "The Prediction of Crack Width in Hardened Concrete." *The Structural Engineer* 57A(1), pp. 9-17, London, England, January.

Beeby, A. W. (1979b). "Cracking and Corrosion." Concrete in the Oceans, Technical Report No. 1, Construction Industry Research and Information Association/Cement and Concrete Association, 77 pp., London, England.

Beeby, A. W. (1983). "Cracking, Cover, and Corrosion of Reinforcement." *Concrete International* 5(2), pp. 35-40, American Concrete Institute, Farmington Hills, Michigan.

Bensted, J. (1994). "Efflorescence – A Visual Problem on Buildings." *Construction Repair*, pp. 47-49, January/February.

Bertero, V. V. and Polivka, M. (1972). "Influence of Thermal Exposure on Mechanical Characteristics of Concrete." SP-34, *Concrete for Nuclear Reactors*, Paper 28, American Concrete Institute, Farmington Hills, Michigan.

Braun, K. (1987). "Prediction and Evaluation of Durability of Reinforced Concrete Elements and Structures." *Proceedings of 4th Conference on durability of Building Materials and Components*, pp. 383-388, Singapore.

Braverman, J. I., et al., (2000). "Assessment of Age-Related Degradation of Structures and Passive Components for U.S. Nuclear Power Plants." NUREG/CR-6679. Brookhaven National Laboratory, Upton, N.Y.

BRITE/EURAM (1995). "The Residual Service Life of Reinforced Concrete Structures." BREU-CT92-0591, Project 4062, BRITE/EURAM Programme, Commission of European Communities, Brussels, Belgium.

BRE (1982). "The Durability of Steel in concrete: Part 2 – Diagnosis and Assessment of Corrosion-Cracked Concrete." *Building Research Establishment Digest* 264, Building Reasearch Station, Garston, Watford, England.

Browne, R. D., Geoghegan, M. P., and Baker, A. F. (1983). "Corrosion of Reinforcement in Concrete Construction." Chapter 13, pp. 193-222, A. P. Crane Editor, SCI Publisher, London, England.

Browne, R. D. (1988). "Durability of Reinforced Concrete Structures." Pacific Concrete Conference, vol. 3, Auckland, New Zealand, November.

BS8110 (1985). "Structural Use of Concrete, Part 1: Code of Practice for Design and Construction." British Standards Institution, London, England.

Bungey, J. H. (1996). "Testing of Concrete in Structures." Third Edition, Surrey University Press, London, England.

Butler, T.A. and L.E. Fugelso (1982). "Response of the Zion and Indian Point Containment Buildings to Severe Accident Pressures." NUREG/CR-2569.

Cady, P. D. and Weyers, R. E. (1984). "Deterioration Rates of Concrete Bridge Decks." *Journal of Transportation Engineering* 110(1), pp. 35-44, American Society of Civil Engineers, New York, New York.

Campbell-Allen, D. and Lau, B. (1978). "Cracks in Concrete Bridge Decks." *University of Sydney School of Civil Engineering Research Report R313*, January.

CEB (1983). "Assessment of Concrete Structures and Design Procedures for Upgrading." Bulletin d'Information No. 162, Comite Euro-Internationale du Beton, Thomas Telford Services, Ltd., London, England.

CEB-FIP (1986). Federation International de la Precontrainte, "Inspection and Maintenance of Reinforced and Prestressed Concrete Structures." Published by Thomas Telford Services, Ltd., London, England, reprinted with permission of *fib*, Federation Internationale du Beton (CEB-FIB).

CEB (1992). "Durable Concrete Structures – Design Guide." Comite Euro-Internationale du Beton, Thomas Telford Services Ltd., London, England.

Chan, S. Y. N., Peng, G-f, and Chan, J. K. W. (1996). "Comparison Between High Strength Concrete and Normal Strength Concrete Subjected to High Temperature." *Materials and Structures* 29, pp. 616-619, RILEM, Cachan, France.

Chana, P. and Korobokis, G. A.(1991). "Bond Strength of Reinforcement in Concrete Affected by ASR," Contractor Report No. 233. Transport and Road Research Laboratory, London, England.

Christensen, J. A. (1990). "NPAR Approach to Controlling Aging in Nuclear Power Plants." NUREG/CP-0105. *Proceedings of the 17th Water Reactor Safety Information Meeting* 3, Washington, D.C.

CIB (1989). "Repairability of Fire-Damaged Structures." Report No. 111. International Council for Building Research Studies and Documentation, Rotterdam, The Netherlands.

Clifton, J. R. (1991). "Predicting the Remaining Service Life of Concrete." NISTIR 4712. U.S. Department of Commerce, National Institute of Standards and Technology, Gaithersburg, Maryland.

Concrete Society (1990). "Assessment and Repair of Fire-Damaged Concrete Structures." Technical Report No. 33. London, England.

Concrete Society (1992). "Non-Structural Cracks in Concrete." Technical Report No. 22. London, England.

Cowen, A. and Nichols, R. W. (1968). "Effect of Irradiation on Steels Used in Pressure Vessels. *Prestressed Concrete Pressure Vessels*, Marilyn S. Udell Editor, Group D, Paper 20, PP. 229-235, The Institution of Civil Engineers, London, England

Cruz, C. R. (1966). "Elastic Properties of Concrete at High Temperature." *Journal Portland Cement Association – Research and Development Laboratories*, 8(1), pp. 37-45, Skokie, Illinois.

CSA (1990). "Concrete Materials and Methods of Concrete Structures." CAN/CSA – A23.1, Appendix B, Canadian Standards Association, Toronto, Canada.

Danish Ministry of Transport Directorate (1986). "Load Carrying Capacity of Bridges Subjected to Alkali-Silica Reactions. - The Shear Strength of Concrete Beams Subjected to Alkali-Silica Reactions." Interim Report I, MoT, Copenhagen, Denmark.

Danish Ministry of Transport Directorate (1990). "Load Carrying Capacity of Structural Members Subjected to Alkali-Silica Reactions." Copenhagen.

Darwin, D. (1985). "Debate: Crack Width, Cover and Corrosion." *Concrete International Design and Construction* 7(5), pp. 20-35.

Day, R.L. (1992). "The Effect of Secondary Ettringite Formation on the Durability of Concrete: A Literature Analysis." Research and Development Bulletin RD108T. Portland Cement Association, Skokie, Illinois.

Edwards, W. T. and Gamble, W. L. (1986). "Strength of Grade 60 Reinforcing Bars After Exposure to Fire Temperatures." *Concrete International* 8(10), pp. 17- 19, October.

Ellingwood, B. (1978). "Reliability Basis of Load and Resistance Factors for Reinforced Concrete Design." Building Science Series No. 110. National Bureau of Standards, Washington, DC.

Ellingwood, B. and T.V. Galambos (1982). "Probability-Based Criteria for Structural Design." Structural Safety 1(1):15-26.

Ellingwood, B. (1983). "Probabilistic Descriptions of Resistance of Safety-Related Nuclear Structures." Report NUREG/CR-3341, (BNL-NUREG-51681), Brookhaven National Laboratory.

Ellingwood, B. and H. Hwang (1985). "Probabilistic Descriptions of Resistance of Safety-Related Structures in Nuclear Plants." Nuclear Engineering and Design 88(2):169-178.

Ellingwood, B. (1990). "Validation Studies of seismic PRAs." Nuclear Engineering & Design, 123(2):189-196.

Ellingwood, B. (1994). "Validation of Seismic Probabilistic Risk Assessments of Nuclear Power Plants." Report NUREG/GR-0008. US Nuclear Regulatory Commission, Washington, DC.

Ellingwood, B. R. and Mori, Y. (1994a). "Maintaining Reliability of Concrete Structures I: Role of Inspection/Repair." *Journal of Structural Engineering* 120(3), pp. 824-845, American Society of Civil Engineers, New York, New York.

Ellingwood, B. R. and Mori, Y. (1994b). "Maintaining Reliability of Concrete Structures II: Optimum Inspection/Repair Strategies." *Journal of Structural Engineering* 120(3), pp. 846-862, American Society of Civil Engineers, New York, New York.

Ellingwood, B. R. and Song, J. (1996). "Impact of Structural Aging on Seismic Risk Assessment of Reinforced Concrete Structures in Nuclear Power Plants." NUREG/CR-6425, U. S. Nuclear Regulatory Commission, Washington, D.C.

Ellingwood, B. R. (1998). "Issues Related to Structural Aging in Probabilistic Risk Analysis of Nuclear Power Plants." *Journal of Reliability Engineering and System Safety*, 62(3), pp. 171-183.

El-Nesr, O. (1995). "Diagnosis and Repair of Buildings Damaged by Fire Exposure." *Extending the Lifespan of Structures*, IABSE Symposium San Francisco, International Association of Bridge and Structural Engineers, Zurich, Switzerland.

Elsener, B., Wojtas, H., and Bohni, H. (1994). "Galvanostatic Pulse Measurements - Rapid On Site Corrosion Monitoring." Proc. of Int'l Conf. held at the University of Sheffield, England on 24-28 July.

EPRI (1998). "Guideline on Nuclear Safety-Related Coatings." EPRI TR-109937. Electric Power Research Institute, Palo Alto, California, April.

Erlin, B. and Verbeck, G. J. (1975). "Corrosion of Metals in Concrete – Needed Research." *Corrosion of Metals in Concrete*, SP-49. American Concrete Institute, Farmington Hills, Michigan.

FEMA 273. "NEHRP Guidelines for the Seismic Rehabilitation of Buildings." Federal Emergency Management Agency, October 1997.

Flis, J. et al., (1993). "Electrochemical Measurements of Bridges for Evaluation of Reinforcement Corrosion Rates." *Corrosion* 49, pp. 601-613.

Foley, R. T. (1975). "Complex Ions and Corrosion." *Journal of the Electrochemical Society* 122(11), pp. 1493-1549.

Francois, R. and Arliguie, G. (1991). "Reinforced Concrete: Correlation Between Cracking and Corrosion." SP 126, *Durability of Concrete – Second International Conference*, Montreal, Canada, pp. 1221-1238, American Concrete Institute, Farmington Hills, Michigan.

Francois, R. and Arliguie, G. (1999). "Effect of Microcracks and Cracking on the Development of Corrosion in Reinforced Concrete Members." *Magazine of Concrete Research* 51(2), pp. 143-150, London, England.

Freskakis, G. N. et al., (1979). "Strength Properties of Concrete at Elevated Temperature." *Civil Engineering Nuclear Power*, Vol. 1, ASCE National Convention, Boston, April.

Fujii et al., (1987). "The Static and Dynamic Behavior of Reinforced Concrete Beams with Cracking Due to Alkali-Silica Reactions." *8th International Conference on Alkali-Aggregate Reaction*, Edited by Grattan-Bellew, pp. 126-130, Noyes Publications, Newark, New Jersey

Gonzalez, J. A., Alonso, C. and Andrade, C. (1983). "Corrosion Rate of Reinforcements During Accelerated Carbonation of Mortar Made From Different Types of Cement." *Corrosion of Reinforcement in Concrete Construction*, Society of Chemical Industry, pp. 159-174Chichester, Ellis Horwood, England.

González, J. A., Feliu, S., Rodríguez, P., W., Ramírez, E., and Andrade, C. (1996). "Some Questions on the Corrosion of Steel in Concrete – Part 1: When, How and How Much Steel Corrodes." *Materials and Structures* 29, pp. 40-46, January-February.

González, J. A., Feliu, S., Rodríguez, P., López, W., Ramírez, E., Alonso, C. and Andrade, C. (1996a). "Some Questions on the Corrosion of Steel in Concrete – Part II: Corrosion Mechanism and Monitoring Service Life Prediction and Protection Methods." *Materials and Structures* 29, pp. 97-104, March.

González, J. A., Otero, E., Feliu, S., Bautista, A., Ramírez, E., and Rodríguez, P. (1998). "Some Considerations on the Effect of Chloride Ions on the Corrosion of Steel Reinforcement Embedded in Concrete Structures." *Magazine of Concrete Research* 50(3), pp. 189-199, London, England.

Gou, P.F. and J.E. Love (1982). "Pressure Carrying Capability of the Containment Structural System of the Mark III Standard Plant." NUREG/CP-0033.

Haavik, D. J. (1990). "Evaluating Concrete Cracking by Measuring Crack Width." *Concrete Construction* 35(6), pp. 553-556, Aberdeen Group, Addison, Illinois, June.

Halvorsen, G. T. (1987). "Requirements for Crack Control." *Lewis H. Tuthill International Symposium on Concrete and Concrete Construction*, SP-124, pp. 275-322, American Concrete Institute, Farmington Hills, Michigan.

Halvorsen, U. A. (1966). "Corrosion and Leaching of Lime in Cracks." Division of Building Technology, Lund Institute of Technology, Bulletin 1, Lund, Sweden.

Hilsdorf, H. K., Kropp, J, and Koch, H. J. (1978). "The Effects of Nuclear Radiation on the Mechanical Properties of Concrete." ACI SP-55. *Douglas McHenry International Symposium on Concrete and Concrete Structures*, American Concrete Institute, Farmington Hills, Michigan.

Hobbs, D. W. (1988). "Alkali- Silica Reaction in Concrete." Thomas Telford Ltd., London, England.

Hookham, C. J. (1991). "Structural Aging Assessment Methodology for Concrete Structures in Nuclear Power Plants." ORNL/NRC/LTR-90/17. Oak Ridge National Laboratory, Oak Ridge, Tennessee.

Hookham, C. J. (1995). "In-Service Inspection Guidelines for Concrete Structures in Nuclear Power Plants." ORNL/NRC/LTR-95/14. Oak Ridge National Laboratory, Oak Ridge, Tennessee.

Hwang, H., S. Kao and M. Reich (1982). "Probabilistic Models for Materials Used in a Reinforced Concrete Containment." NUREG/CR-3041.

Hwang, H. et al., (1985). "Probability-Based Load Combinations for the Design of Concrete Containments." Nuclear Engineering. & Design, 86(3):327-339.

Hope, B. B. and Ip, A. K. (1985). "Corrosion and Electrical Impedance in Concrete." Cement and Concrete Research 15, pp. 525-534.

Houston, J., Atimtay, E., and Ferguson, P. M. (1972). "Corrosion of Reinforcing Steel Embedded in Structural Concrete." Research Report No. 112-1-F. Center for Highway Research, University of Texas, Austin.

Hussain, S. E., Al-Gantani, and Rasheeduzzafar (1996). "Chloride Threshold for Corrosion of Reinforcement in Concrete." ACI Materials Journal 93(6), pp.535-548,

IAEA (1998). "Assessment and Management of Ageing of Major Nuclear Power Plant Components Important to Safety: Concrete Containment Buildings." IAEA-TECDOC-1025. International Atomic Energy Agency, Vienna, Austria.

Imam, R.L. and W.J. Conover (1980). "Small Sample Sensitivity Analysis Techniques for Computer Models With an Application to Risk Assessment." Comm. in Stat. Part A- Theory and Methods A9(17):1749-1842.

Ingvarsson, H. (1987). "Non-Destructive Condition Assessment of Concrete." *Monitoring of Large Structures and Assessment of Their Safety*, pp. 65-81, International Association for Bridge and Structural Engineering, Zurich, Switzerland.

Inoue, S., Fujii, M., Kobayashi, K., and Nakano, K. (1989). "Structural Behaviors of Reinforced Concrete Beams Affected by Alkali-Silica Reaction." *8th International Conference on Alkali-Aggregate Reaction*, Edited by Okada, Nishibayashi, and Kawamura, pp. 727-732, Elsevier Applied Science, London, England.

JCI (1998). "Integrated Design of Concrete Structures." JCI TC 961 Committee, Japan Concrete Institute, Tokyo, Japan.

Jones, A. E. K. and Clark, L. A. (1998). "The Effects of ASR on the Properties of Concrete and the Implications for Assessment." *Engineering Structures*, 20(9), pp. 785-791, Elsevier Science Ltd., London, England.

Jung, J. (1984). "Ultimate Strength Analysis of the Watts Bar, Maine Yankee and Bellefonte Containments." NUREG/CR-3724.

Kaetzel, L. J., Clifton, J. R., Klieger, P. and Snyder, K. (1993). "Highway Concrete (HWYCON) Expert System User Reference and Enhancement Guide." NISTIR 5184. National Institute of Standards and Technology, Gaithersburg, Maryland, May.

Kawamura, M., Takemoto, K. and Ichise, M. (1989). "Influences of the Alkali-Silica Reaction on Steel Reinforcement in Concrete." *8th International Conference on Alkali-Aggregate Reaction*, Edited by Okada, pp. 115-120, Nishibayashi, and Kawamura, Elsevier Applied Science, London, England.

Kawamura, A., Maruyama, K. Yoshida, A., and Masuda, T. (1999). "Residual Capacity of Concrete Beams Damaged By Salt." Private Communication, Nagaoka University of Technology, Japan.

Kaplan, M. F. (1989). "Concrete Radiation Shielding." Concrete Design and Construction Series, Longman Scientific and Technical, Essex, England.

Klinghoffer, O. (1995). "In-Situ Monitoring of Reinforcement Corrosion by Means of Electro-Chemical Methods." *Nordic Concrete Research* 95(1).

Kobayashi, K., Suzuki, K., and Uno, Y. (1990). "Carbonation of Concrete Structures and Decomposition of C-S-H." Cement and Concrete Research 24(1), pp. 619-622.

Krauss, P. D. (1994). "Repair Materials and Techniques for Concrete Structures in Nuclear Power Plants." ORNL/NRC/LTR-93/28. Martin Marietta Energy Systems, Inc., Oak Ridge National Laboratory, Oak Ridge, Tennessee.

Krawinkler, H. and Seneviatna, G. D. (1998). "Pros and Cons of Pushover Analysis in Seismic Performance Evaluation." *Engineering Structures*, 20(4), pp. 452-464.

Lee, H. S., Tomosawa, F. and Noguchi, T. (1996). "Effects of Rebar Corrosion on the Structural Performance of Singly Reinforced Beams." *Durability of Building Materials and Components 7*, Vol. 1, C. Sjöström Editor, E.&F. N Spon., London, England.

Lew, H.S. (1988). "Nondestructive Testing." SP-112. American Concrete Institute, Farmington Hills, Michigan.

Litzner, H. –U. and Becker, A. (1999). "Design of Concrete Structures for Durability and Strength to Eurocode 2." *Materials and Structures* 32(219), pp. 323-330, RILEM, Cachan, France, June.

MacGregor, J.G., S.A. Mirza and B.Ellingwood (1983). "Statistical Analysis of Resistance of Reinforced and Prestressed Concrete Members." Journal American Concrete Institute, 80(3):167-176.

Majlesi, Y. (1994). "A Laboratory Investigation Into Structural Performance and Mechanical Properties of Plain and Reinforcing Concrete Elements Affected by ASR." PhD Thesis, QMW – University of London, England.

Malhotra, H. L. (1956). "The Effect of Temperature on Compressive Strength of Concrete." *Magazine of Concrete Research*, 8(23), pp. 85-94, London, England.

Malhotra, H. L. (1982). "Design of Fire-Resistant Structures." pp. 67, 73, and 78, Chapman and Hall, New York, New York.

Malhotra, V.M. and Carino, N.J. (1991). "Handbook of Nondestructive Testing of Concrete." CRC Press, Boca Raton, Florida.

Mangat, P. S. and Elgarf, M. S. (1996). "Bond Characteristics of Corroding Reinforcement in Concrete Beams." *Materials and Structures* 32(216), pp. 89-97, RILEM, Cachan, France.

Manning, D. G. (1985). "Debate: Crack Width, Cover, and Corrosion." Concrete International Design and Construction 7(5), pp. 20-35, American Concrete Institute, Farmington Hills, Michigan.

Maruyama, K. Shimomura, T., and Hamada, H. (1999). "Degradation Model for Reinforced Concrete Structures Under Salt Attack Environment." *Private Communication*, Nagaoka University of Technology, Japan.

Maruyama, K. and Shimomura, T. (1999). "Effect of Rebar Corrosion on the Structural Capacity of Concrete Structures." *Private Communication*, Nagaoka University of Technology, Japan.

Mather, B. (1979). "Concrete Need Not Deteriorate." *Journal of the American Concrete Institute* 1(9), P. 33, American Concrete Institute, Farmington Hills, Michigan, September.

Martin, H. and Schiessl, P. (1969). "The Influence of Cracks on the Corrosion of Steel in Concrete." Preliminary Report of RILEM *International Symposium on the Durability of Concrete*, Vol. II, Prague, Slovakia.

Mehta, P.K. (1986). "Concrete – Structure, Properties and Materials." Prentiss Hall Inc., Englewood Cliffs, N. J.

Mehta, P. K. and Gerwick, Jr., B.C. (1982). "Cracking – Corrosion Interaction in Concrete Exposed to Marine Environment." *Concrete International* 4(10), American Concrete Institute, Farmington Hills, Mich., October , pp. 45-51.

Meinheit, D. F. and Heidbrink, F. D. (1985). "Behavior of Drilled-In Expansion Anchors." Concrete International 7(4), pp. 62-66, American Concrete Institute, Farmington Hills, Michigan.

Meyers, T. A. et al., (1990). "Application of Structural Reliability and Risk Assessment to the Management of Aging. " NUREG/CP-0100. *Proceedings of International Nuclear Power Plant Aging Symposium*, Washington, D.C.

Mielenz, R. C., Marusin, S. L., Hime, W. G., and Jugovic, Z. T. (1995). "Investigation of Prestressed Concrete Railway Tie Distress." *Concrete International*, 17(12), American Concrete Institute, Farmington Hills, Michigan.

Mindress, S. and Young, J. F. (1981). "Concrete." Prentice-Hall, Inc., Englewood Cliffs, New Jersey.

Mirza, S.A. and J.G. MacGregor (1979). "Variations in Dimensions of Reinforced Concrete Members." Journal Structural Division, ASCE 105(4):751-766.

Misra, S. and Uomoto, T. (1991). "Reinforcement Corrosion Under Simultaneous Diverse Exposure Conditions." SP 126. *Durability of Concrete – Second International Conference*, Montreal, Canada, pp. 423-441, American Concrete Institute, Farmington Hills, Michigan.

Mohammed, T. U., Otsuki, N. and Hisada, M. (1999). "Corrosion of Steel Bars with Respect to Orientation in Concrete." ACI Materials Journal 96(2), pp. 154-159, American Concrete Institute, Farmington Hills, Michigan.

Mori, Y. and Ellingwood, B. (1993). "Methods for reliability-based condition assessment - application to concrete structures in nuclear plants." NUREG/CR-6052. U.S. Nuclear Regulatory Commission.

Morinaga, S. (1988). "Prediction of Service Lives of Reinforced Concrete Buildings Based on Rate of Corrosion of Reinforcing Steel." *Special Report of Institute of Technology Shimizu Corporation* 23, Japan, June.

Morinaga, S. (1990). "Prediction of Service Lives of Reinforced Concrete Buildings Based on the Corrosion Rate of Reinforcing Steel." *Durability of Building Materials and Components*, E.&F. N Spon., London, England.

Morinaga, S. (1999). *Private Communication*, Kyushu Tokai University, Kumamoto-ken, Japan, April 16, 1999.

Natesaiyer, K. and Hover, K. (1992). "Cornell's Gel Fluorescence Test Identifies ASR Products in Concrete." *Concrete Technology Today*, 13(2), Portland Cement Association, Skokie, Illinois.

Naus, D. J., Oland, C. B. and Ellingwood, B. R. (1996). "Report on Aging of Nuclear Power Plant Reinforced Concrete Structures." NUREG/CR-6424. U. S. Nuclear Regulatory Commission, Washington, D.C.

Naus, D. J. (1999). "Report of Foreign Travel of D. J. Naus of Engineering Technology Division to Visit Japanese Utilities and Research Organizations to Obtain Information on Aging of Concrete Structures and Components," ORNL Foreign Trip Report 102249. Oak Ridge National Laboratory, Oak Ridge, Tennessee, May 10.

Newton, C.J., and Sykes, J. M. (1988). "A Galvanic Pulse Technique for Investigation of Steel Corrosion in Concrete." *Corrosion Science* 28, pp. 1051-1073.

Nielsen, A. (1978). "How Wide is a Crack in Reinforced Concrete Allowed to be?" *Miscellaneous Papers in Civil Engineering*, Dialog 77, pp. 199-212, Danish Engineering Academy, Lyngby.

NRC Regulatory Guide 1.174 (1998). "An Approach for Using Probabilistic Risk Assessment in Risk-Informed Decisions on Plant-Specific Changes to the Licensing Basis," July.

NRC "Standard Review Plan for the Review of Safety Analysis Reports for Nuclear Power Plants." NUREG-0800, U.S. Nuclear Regulatory Commission, Office of Nuclear Reactor Regulation.

Okada, K., Kobayashi, K., and Miyagawa, T. (1988). "Influence of Longitudinal Cracking Due to Reinforcement Corrosion on Characteristics of Reinforced Concrete Members." *ACI Structural Journal* 58(2), pp. 134-140, American Concrete Institute, Farmington Hills, Michigan, March-April.

O'Neill, E. F. (1980). "Study of Reinforced Concrete Beams Exposed to Marine Environment." *Concrete in Marine Environment*, SP-65, American Concrete Institute, Farmington Hills, Michigan.

Ono, K. (1988). "Damaged Concrete Structures in Japan Due to Alkali Silica Reaction." *International Journal of Cement Composites and Lightweight Concrete*, 10(4), p. 247.

Park, R. and T. Paulay (1975). "Reinforced Concrete Structures." John Wiley & Sons, New York.

Park, Y. (1988). "Effects of Aging Degradation on Seismic Performance of Reinforced Concrete Structures: Summary of Japanese Literature in Related Areas." Private Communication, Brookhaven National Laboratory, Upton, New York, June.

Paull, R. (1987). "Inspection of Concrete Structures for Steel Reinforcement Corrosion." *Presentation at Meeting of Institution of Engineers*, Malaysia, October 17.

Parrott, L. J. (1990). "Damage Caused by Carbonation of Reinforced Concrete." *Materials and Structures* 23(135), pp. 230-234, RILEM, Cachan, France.

PCA (1997). "Concrete Slab Surface Defects: Causes, Prevention, Repair." PCA R&D Serial No. 2155, Portland Cement Association, Skokie, Illinois.

Perenchio, W. F. (1989). "The Condition Survey." *Concrete International* 11(1), pp. 59-62, American Concrete Institute, Farmington Hills, Michigan.

Petre-Lozar, I., Gerard, B., Marchand, J. and Beaudouin, J. (1988). "LEO 1.0 – A Computer Software Based Maintenance Strategy for Reinforced Concrete Structures Undergoing Rebar Corrosion." *International Congress on Corrosion of Concrete Structures*, Orlando, Florida, December 7-11.

Pinjarkar, S. G. (1984). "Field Condition Survey for Strength Evaluation of Existing Buildings." *ACI Symposium on Evaluation of Existing Concrete Buildings*, ACI Spring Convention, held in Phoenix, Arizona, American Concrete Institute, Farmington Hills, Michigan, March 4-9.

Poston, R. W., Whitlock, A. R., and Kesner, K. E. (1995). "Condition Assessment Using Nondestructive Evaluation." *Concrete International* 17 (7), pp. 36-42, American Concrete Institute, Farmington Hills, Michigan.

Pullar-Strecker, P. (1987). "Corrosion Damaged Concrete Assessment and Repair." CIRIA, Butterworths, London, United Kingdom.

Raphael, M. and Shalon, R. (1971). "A Study of the Influence of Climate on Corrosion of Reinforcement." Proceedings RILEM International Symposium on Concrete and Reinforced Concrete in Hot Countries, pp. 77-96, Technion, Israel Institute of Technology, Haifa

Rasheeduzzafar, Al-Saadoun, S. S., and Al-Gahtani, A. S. (1992). "Corrosion Cracking In Relation to Bar Diameter, Cover, and Concrete Quality." *Journal of Materials in Civil Engineering* 4(4), pp. 327-341, American Society of Civil Engineers, New York, New York, November.

Rehm, G. and Moll, H. (1964). "Versuche zum Studium des Einflusses der Rissbriete auf die Rostbilding an der Bewehrung von Stahlbeton-Bauteilen." Heft 169, Deutscher Ausschuss fur Stahlbeton, Berlin, Germany.

Reis, E. E., Mozer, J. D., Bianchini, a. D. and Kesler, C. E. (1965). "Causes and Control of Cracking in Concrete Reinforced with High-Strength Steel Bars: A Review of Research." Engineering Experiment Station Bulletin No. 479, University of Illinois, Urbana.

Richardsen, M. G. (1987). "Cracking in Reinforced Concrete Buildings." *Concrete International* 9(1), pp. 21-23, American Concrete Institute, Farmington Hills, Michigan.

RILEM/CEB/FIP (1973). "Bond Test for Reinforcing Steel." *Materials and Structures* 6(32), Cachan, France.

RILEM (1988). "Measurement of Hardened Concrete Carbonation Depth." RILEM Recommendation CPC-18, *Materials and Structures* 21(126), pp. 453-455, Cachan,France.

RILEM (1988a). *Feedback from Practice of Durability Data (Draft),* Joint CIB/RILEM Committee W80/100-TSL. "Prediction of the Service Life of Building Materials and Components." Cachan, France, December.

RILEM (1994). "Draft Recommendations for Damage Classification of Concrete Structures." *Materials and Structures* 27(170), RILEM, Cachan, France, July.

Roberts, M. H. (1981). "Carbonation of Concrete Made with Dense Natural Aggregates." Information Paper 6/81, Building Research Establishment, Glasgow, Scotland.

Robery. P. (1990). "Now you See It – Radar, Vibration, and Thermography as Investigative Tools for Structures." *Construction Maintenance & Repair*, pp. 120 124, May/June.

Rodriguez, J., Ortega, L. M., and Casal, J. (1995). "Load Carrying Capacity of Concrete Structures with Corroded Reinforcement." *International Conference on Structural Faults and Repairs*, London, England, July.

Rodriguez, J., Ortega, L. M., Casal, J. and Diez, J. M. (1996). "Corrosion of Reinforcement and Service Life of Concrete Structures." *7th International Conference on the Durability of Building Materials and Components*, Stockholm, Sweden.

Roper, H. and Baweja, D. (1991). "Carbonation-Chloride Interactions and Their Influence on Corrosion Rates of Steel in Concrete." SP 126. *Durability of Concrete – Second International Conference*, Montreal, Canada, pp. 295-315, American Concrete Institute, Farmington Hills, Michigan.

Sarkar, A., Godbole, P. N., and Chakrabarti, S. C. (1996). "Potential for Expert Systems in the Assessment and Repair of Fire Damaged Buildings in India." *Building Research and Information*, 24(1).

SAIC (1977). "Study of Radiation Dosage to Structural Components in Nuclear Reactors." EPRI NP-152. Electric Power Research Institute, Palo Alto, California.

Schiessl, P. (1975). "Admissible Crack Width In Reinforced Concrete Structures." *Inter-Association Colloquium on the Behaviour of In Service Concrete Structures*, Contribution II 3-17, Preliminary Report Vol. 1, Liege, Belgium.

Schiessl, P. (1976). "Zur Frage der Zulassigen Rissbreite und der Enforderlichen Betondeckung im Stahlbeton unter Besonderer Berucksichtigung der Karbonatisierung des Betons." Bulletin No. 255, 175 pp., Deutscher Ausschuss fur Stahlbeton, Berlin, Germany.

Schneider, U. et al., (1981). "Effect of Temperature on Steel and Concrete for PCPVs." *Nuclear Engineering and Design* 67, Elsevier Science, The Netherlands, pp. 245-258.

Shimmura, T. (1999). "Simulation of Time-Dependent Performance Change of RC Structures Subjected to Salt Attack." *International Conference on Life Prediction and Aging Management of Concrete Structures*, pp. 128-133, EXPERTCENTRUM, Bratislava, Slovakia.

Shunmugavel, P. and T.E. Johnson (1982). "Internal Pressure Capacity of Prestressed Concrete Containments for Nuclear Power Plants." NUREG/CP-0033.

Sims, I. (1994). "The Assessment of Concrete for Carbonation." *Concrete*, pp. 33-38, November/December.

Smith, P. (1978). "Resistance to High Temperatures." *Significance of Tests and Properties of Concrete and Concrete-Making Materials*, STP 169B, American society for Testing and Materials, West Conshohocken, Pennsylvania.

Stark, D. (1991). "How to Evaluate the State of Alkali-Silica Reactivity (ASR) in Concrete." Publication #R910104. Aberdeen Group, Addison, Illinois.

Stuzman, P. E. (1991). "Characterization of Field Concrete." NISTIR: 4516, National Institute of Standards and Technology, Gaithersburg, Maryland, January.

Suprenant, B. A. (1997). "Evaluating Fire-Damaged Concrete." Publication #R970020. *Concrete Repair Digest*, The Aberdeen Group, Addison, Illinois.

Swamy, R. N. (1989). "Structural Implications of Alkali Silica Reaction." *Proc. of 8th International Conference on Alkali-Aggregate Reaction*, Kyoto, Japan, Elsevier Applied Science, London ,England.

Swenson, E. G. (1999). "Concrete in Sulphate Environments." CBD-136. *Canadian Building Digest*, National Research Council, Canada, September.

Tremper, B. (1947). "The Corrosion of Reinforced Steel in Cracked Concrete." *Journal of the American Concrete Institute*18, June.

Tucker, D. M. and Read, R. E. H. (1981). "Assessment of Fire Damaged Structures." IP 24/81. Building Research Establishment, Glasgow, Scotland.

Tuutti, K. (1982). "Corrosion of Steel in Concrete." Swedish Cement and Concrete Research Institute," Stockholm.

Uddin, T. and Culver, C. G. (1975). "Effects of Elevated Temperature on Structural Materials." *Journal of Structural Division*, 101(7), American Society of Civil Engineers, New York, New York.

Uomoto, T. and Misra, S. (1988). "Behavior of Concrete Beams and Columns in Marine Environment When Corrosion of Reinforcing Bars Takes Place." SP 109. *Concrete in Marine Environment –Second International Conference*, St. Andrews by-the-Sea, Canada, pp. 127-146, American Concrete Institute, Farmington Hills, Michigan.

U.S. Army Corps of Engineers (1986). "Evaluation and Repair of Concrete Structures." EM-1110-2-2003. Washington, D.C.

Wang, C-K, and Salmon, C. G. (1979) "Reinforced Concrete Design" Third Edition, Harper & Row Publishers, New York.

Wallback, E. J. (1989). "The Performance of Concrete in Bridges – A Survey of 200 Highway Bridges." HMSO, Department of Transport, London, England.

Wesley, D. A., and Hashimoto, P. S. "Seismic Structural Fragility Investigation for the Zion Nuclear Power Plant." NUREG/CR-2320. U.S. Nuclear Regulatory Commission, October 1981.

Wiberg, U. (1993). "Material Characterization and Defect Detection in Concrete by Quantitative Ultrasonics." KTH, TRITA-BKN, Bulletin 7, Sweden.

Woodham, D. B. and Schuller, M. P. (1999). "Tomographic Imaging for Investigation of Concrete Structures." *International Conference on Life Prediction and Aging Management of Concrete Structures*, pp. 88-93, EXPERTCENTRUM, Bratislava, Slovakia.

Yamakawa, T. (1995). "An Experimental Study on Deterioration of Aseismatic Behavior of R/C Structural Walls Damaged by Electrolytic Corrosion Testing Method." *Concrete Under Severe Conditions: Environment and Loading*, Proceedings of the International Conference on Concrete Under Severe Conditions held in Sapporo, Japan, Volume Two, pp. 1521-1530, Edited by K. Sakai, N. Banthia, and O. E. Gjorv, published by E & FN Spon, London, England.

Yamakawa, T. (1998). "Seismic Behavior of R/C Columns Damaged Under Exposure Test." *Concrete Under Severe Conditions: Environment and Loading*, Proceedings of the International Conference on Concrete Under Severe Conditions CONSEC '98 held in Tromso, Norway, June 21-24, 1998, Volume Two, pp. 897-908, Edited by O. E. Gjorv, K. Sakai, and N. Banthia, published by E & FN Spon, London, England.

Yamamoto, A., Motohashi, K., Misra, S., and Tsutsumi, T. (1995). "Proposed Durability Design for RC Marine Structures." *Concrete Under Severe Conditions: Environment and Loading*, Volume One, pp. 544-553, Edited by K. Saki,N. Banthia, and Gjorv, E.&F. N. Spon, London, England.

Yoda, A. and Yokomuro, T. (1987). "Durability Survey of 60 Year Old Reinforced Concrete Office Building." Annual Meeting, Architectural Institute of Japan, Tokyo.

Yokota, M. et al., (1994). "Steel Corrosion and Load Carrying Capacity of Cracked Concrete Beams." *48th Annual Meeting of Japan Cement Association*, pp. 621-625.

"Zion Probabilistic Safety Study (1981)." Commonwealth Edison Company, Chicago, IL.

NRC FORM 335
(2-89)
NRCM 1102,
3201, 3202

U.S. NUCLEAR REGULATORY COMMISSION

BIBLIOGRAPHIC DATA SHEET

(See instructions on the reverse)

1. REPORT NUMBER
(Assigned by NRC, Add Vol., Supp., Rev., and Addendum Numbers, if any.)

NUREG/CR-6715
BNL-NUREG-52618

2. TITLE AND SUBTITLE

Probability-Based Evaluation of Degraded Reinforced Concrete Components in Nuclear Power Plants

3.DATE REPORT PUBLISHED

MONTH	YEAR
April	2001

4. FIN OR GRANT NUMBER
W-6684

5. AUTHOR(S)

Braverman, J.I. (BNL), Miller, C.A. (BNL), Ellingwood, B.R. (GIT), Naus, D.J. (ORNL), Hofmayer, C.H. (BNL), Shteyngart, S. (BNL), Bezler, P. (BNL)

6. TYPE OF REPORT

7. PERIOD COVERED *(Inclusive Dates)*

8. PERFORMING ORGANIZATION - NAME AND ADDRESS *(if NRC, provide Division, Office or Region, U.S. Nuclear Regulatory Commission, and mailing address; if contractor, provide name and mailing address.)*

Brookhaven National Laboratory (BNL)
Energy Sciences and Technology Department
Bldg. 130 / P.O. Box 5000
Upton, NY 11973-5000

Georgia Institute of Technology (GIT)
School of Civil & Environmental Engineering
790 Atlantic Drive
Atlanta, GA 30332-0355

Oak Ridge National Laboratory (ORNL)
P.O. Box 2009, Bldg. 9204-1
Oak Ridge, TN 37831-8056

9. SPONSORING ORGANIZATION - NAME AND ADDRESS *(if NRC, type "Same as above"; if contractor, provide NRC Division, Office or Region, U.S. Nuclear Regulatory Commission, and mailing address.)*

Division of Engineering Technology
Office of Nuclear Regulatory Research
U.S. Nuclear Regulatory Commission
Washington, DC 20555-0001

10. SUPPLEMENTARY NOTES

T.Y. Chang, Project Manager

11. ABSTRACT *(200 words or less)*

This report describes the research performed to address concerns related to aging degradation of reinforced concrete structures at nuclear power plants (NPPs). The aging effects due to reinforced concrete degradation mechanisms are studied in order to develop analytical methods and degradation acceptance limits for concrete flexural and shear wall members. The focus of this phase of the research program is to perform a probability-based evaluation of degraded reinforced concrete members. The research effort develops fragility modeling procedures for undegraded and degraded reinforced concrete structural components subjected to earthquake ground motions. These quantitative methods provide a basis for evaluating reinforced concrete structures in nuclear plants for continued service and for providing guidelines for in-service inspection and repair. The probability-based degradation acceptance limits that are developed can be used as a tool for making risk-informed decisions regarding degradation of reinforced concrete members.

This study is being conducted under Phase II of a multi-year research program sponsored by the Nuclear Regulatory Commission (NRC) to assess age-related degradation of structures and passive components for U.S. NPPs. A full description of the Phase I effort, which has identified reinforced concrete members and other components for further research in Phase II, is presented in NUREG/CR-6679.

12 KEY WORDS/DESCRIPTORS *(List words or phrases that will assist researchers in locating the report.)*

concrete, beams, shear walls, degradation, aging, corrosion, cracking, fragility, nuclear power plants, finite element analysis, risk, seismic

13. AVAILABILITY STATEMENT

Unlimited

14. SECURITY CLASSIFICATION
(This Page)

Unclassified
(This Report)

Unclassified

15. NUMBER OF PAGES

16. PRICE

NRC FORM 335 (2-89)

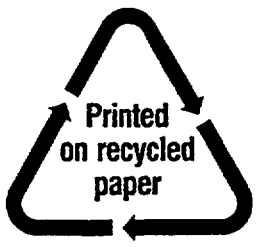

Federal Recycling Program

UNITED STATES
NUCLEAR REGULATORY COMMISSION
WASHINGTON, DC 20555-0001

OFFICIAL BUSINESS
PENALTY FOR PRIVATE USE, $300